AD-A171 050 DEVELOPMENT OF INSTRUMENTATION TO MEASURE SOUND SPEED AND FLOW DIRECTION I..(U) NTS ENGINEERING LONG BEACH CA D G HONEGGER 11 NOV 85 85-1502 DNA-TR-85-369 1/2

UNCLASSIFIED DNA001-84-C-0441 F/G 18/4 NL

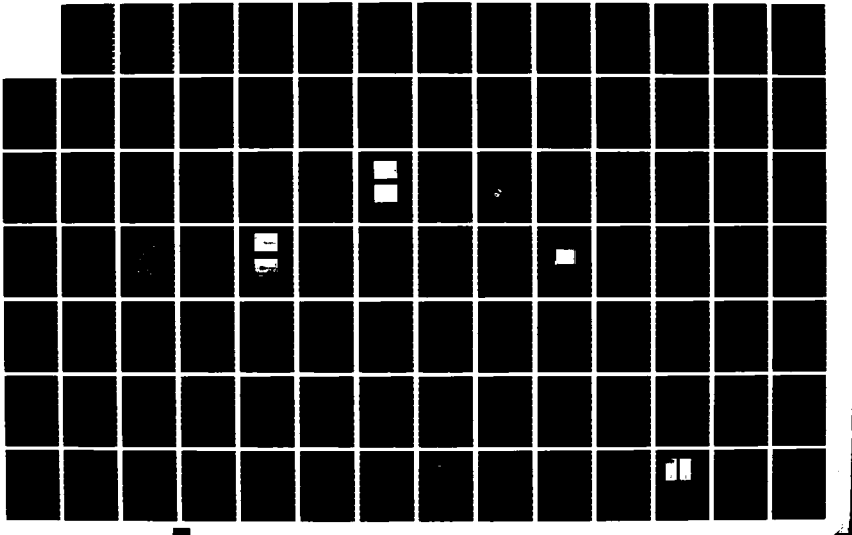

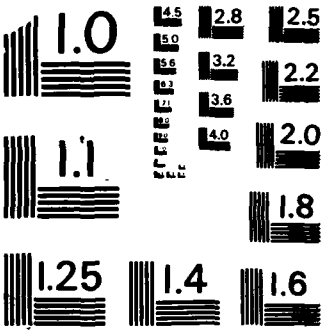

MICROCOPY RESOLUTION TEST CHART
NATIONAL BUREAU OF STANDARDS-1963-A

DNA-TR-85-369

DEVELOPMENT OF INSTRUMENTATION TO MEASURE SOUND SPEED AND FLOW DIRECTION IN DUSTY FLOW FIELDS

Douglas G. Honegger
NTS Engineering
J. H. Wiggins Co., Inc.
6695 East Pacific Coast Highway
Long Beach, CA 90803

11 November 1985

Technical Report

CONTRACT No. DNA 001-84-C-0441

THIS WORK WAS SPONSORED BY THE DEFENSE NUCLEAR AGENCY
UNDER RDT&E RMSS CODE X342084469 Q93QMXAG00041 H2590D.

Prepared for
Director
DEFENSE NUCLEAR AGENCY
Washington, DC 20305-1000

UNCLASSIFIED
SECURITY CLASSIFICATION OF THIS PAGE

AD-A171050

REPORT DOCUMENTATION PAGE

Form Approved
OMB No. 0704-0188
Exp. Date: Jun 30, 1986

1a. REPORT SECURITY CLASSIFICATION UNCLASSIFIED	1b. RESTRICTIVE MARKINGS
2a. SECURITY CLASSIFICATION AUTHORITY N/A since Unclassified	3. DISTRIBUTION/AVAILABILITY OF REPORT Approved for public release; distribution is unlimited.
2b. DECLASSIFICATION/DOWNGRADING SCHEDULE N/A since Unclassified	
4. PERFORMING ORGANIZATION REPORT NUMBER(S) 85-1502	5. MONITORING ORGANIZATION REPORT NUMBER(S) DNA-TR-85-369
6a. NAME OF PERFORMING ORGANIZATION NTS Engineering 6b. OFFICE SYMBOL (If applicable)	7a. NAME OF MONITORING ORGANIZATION Director Defense Nuclear Agency
6c. ADDRESS (City, State, and ZIP Code) J. H. Wiggins Co., Inc. 6695 East Pacific Coast Highway Long Beach, CA 90803	7b. ADDRESS (City, State, and ZIP Code) Washington, DC 20305-1000
8a. NAME OF FUNDING/SPONSORING ORGANIZATION 8b. OFFICE SYMBOL (If applicable)	9. PROCUREMENT INSTRUMENT IDENTIFICATION NUMBER DNA 001-84-C-0441
8c. ADDRESS (City, State, and ZIP Code)	10. SOURCE OF FUNDING NUMBERS PROGRAM ELEMENT NO: 62715H; PROJECT NO: Q93QMXA; TASK NO: G; WORK UNIT ACCESSION NO: DH251400

11. TITLE (Include Security Classification)
DEVELOPMENT OF INSTRUMENTATION TO MEASURE SOUND SPEED AND FLOW DIRECTION IN DUSTY FLOW FIELDS

12. PERSONAL AUTHOR(S)
Honegger, Douglas G.

13a. TYPE OF REPORT	13b. TIME COVERED	14. DATE OF REPORT (Year, Month, Day)	15. PAGE COUNT
Technical	FROM 841001 TO 850930	851111	108

16. SUPPLEMENTARY NOTATION
This work was sponsored by the Defense Nuclear Agency under RDT&E RMSS Code X342084469 Q93QMXAG00041 H2590D.

17. COSATI CODES			18. SUBJECT TERMS (Continue on reverse if necessary and identify by block number)	
FIELD	GROUP	SUB-GROUP		
20	3		Dusty Gas Flow	Mach Flow Measurements
			Electrolytic Cell	Piezoelectric Transducer
8	7		Flow Direction	Piezoresistive Transducer

19. ABSTRACT (Continue on reverse if necessary and identify by block number)

To support the simulation effort associated with the evaluation of the Hardened Mobile Launcher basing concept, a flow-field instrumentation development program has been undertaken. Specific items targeted for investigation were dusty gas sound speed and flow orientation within a simulated precursed flow regime. The investigation has included laboratory tests in a small shock tube facility as well as field testing in the MINI SCALE 2 high explosive simulation event. Evaluation of the ultrasonic system has indicated that the use of such a system for monitoring dusty gas sound speed during a high explosive test is achievable. Results from a prototype flow direction gage using a spherical drag body correlated well with pressure records and precurser flow structure observed during high explosive simulation. Recommendations are made for further investigative efforts regarding flow direction measurement. Such measurements allow a means to aid in the evaluation of models, blast-wing measurement devices and quality of the simulator.

20. DISTRIBUTION/AVAILABILITY OF ABSTRACT	21. ABSTRACT SECURITY CLASSIFICATION
☐ UNCLASSIFIED/UNLIMITED ☒ SAME AS RPT ☐ DTIC USERS	UNCLASSIFIED
22a. NAME OF RESPONSIBLE INDIVIDUAL Betty L. Fox	22b. TELEPHONE (Include Area Code) (202) 325-7042
	22c. OFFICE SYMBOL DNA/STTI

DD FORM 1473, 84 MAR

83 APR edition may be used until exhausted
All other editions are obsolete

SECURITY CLASSIFICATION OF THIS PAGE
UNCLASSIFIED

18. SUBJECT TERMS (Continued)

Precursed Flow Measurement
Sound Speed Measurement
Soil Pressure
Ultrasonic Transducer Sensor

PREFACE

Several individuals were especially important to the development effort reported herein. Mr. Charles Wood and Mr. Bob Barth of OPTITRON provided essential assistance in the design of electronic components and fabrication of components for field testing. We would like to thank Dr. V.J. Kulkarny and Mr. John Novak of TRW for their assistance in conducting tests at the TRW four-inch shock tube facility. Finally, thanks is due to Ms. Julie Bredehorn and Ms. Patricia Irvin for facilitating the preparation of this document.

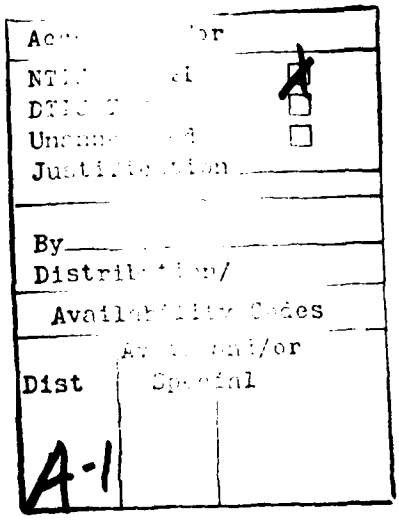

CONVERSION TABLE

Conversion factors for U.S. Customary to metric (SI) units of measurement.

MULTIPLY → TO GET	BY → BY	TO GET ← DIVIDE
angstrom	1.000 000 X E -10	meters (m)
atmosphere (normal)	1.013 25 X E +2	kilo pascal (kPa)
bar	1.000 000 X E +2	kilo pascal (kPa)
barn	1.000 000 X E -28	meter^2 (m^2)
British thermal unit (thermochemical)	1.054 350 X E +3	joule (J)
calorie (thermochemical)	4.184 000	joule (J)
cal (thermochemical)/cm^2	4.184 000 X E -2	mega joule/m^2 (MJ/m^2)
curie	3.700 000 X E +1	giga becquerel (GBq)*
degree (angle)	1.745 329 X E -2	radian (rad)
degree Fahrenheit	$T_K=(t°f+459.67)/1.8$	degree kelvin (K)
electron volt	1.602 19 X E -19	joule (J)
erg	1.000 000 X E -7	joule (J)
erg/second	1.000 000 X E -7	watt (W)
foot	3.048 000 X E -1	meter (m)
foot-pound-force	1.355 818	joule (J)
gallon (U.S. liquid)	3.785 412 X E -3	meter^3 (m^3)
inch	2.540 000 X E -2	meter (m)
jerk	1.000 000 X E +9	joule (J)
joule/kilogram (J/kg) (radiation dose absorbed)	1.000 000	Gray (Gy)**
kilotons	4.183	terajoules
kip (1000 lbf)	4.448 222 X E +3	newton (N)
kip/inch^2 (ksi)	6.894 757 X E +3	kilo pascal (kPa)
ktap	1.000 000 X E +2	newton-second/m^2 (N-s/m^2)
micron	1.000 000 X E -6	meter (m)
mil	2.540 000 X E -5	meter (m)
mile (international)	1.609 344 X E +3	meter (m)
ounce	2.834 952 X E -2	kilogram (kg)
pound-force (lbf avoirdupois)	4.448 222	newton (N)
pound-force inch	1.129 848 X E -1	newton-meter (N·m)
pound-force/inch	1.751 268 X E +2	newton/meter (N/m)
pound-force/foot^2	4.788 026 X E -2	kilo pascal (kPa)
pound-force/inch^2 (psi)	6.894 757	kilo pascal (kPa)
pound-mass (lbm avoirdupois)	4.535 924 X E -1	kilogram (kg)
pound-mass-foot^2 (moment of inertia)	4.214 011 X E -2	kilogram-meter^2 (kg·m^2)
pound-mass/foot^3	1.601 846 X E +1	kilogram/meter^3 (kg/m^3)
rad (radiation dose absorbed)	1.000 000 X E -2	Gray (Gy)**
roentgen	2.579 760 X E -4	coulomb/kilogram (C/kg)
shake	1.000 000 X E -8	second (s)
slug	1.459 390 X E +1	kilogram (kg)
torr (mm Hg, 0°C)	1.333 22 X E -1	kilo pascal (kPa)

* The becquerel (Bq) is the SI unit of radioactivity; 1 Bq = 1 event/s.
**The Gray (Gy) is the SI unit of absorbed radiation.

TABLE OF CONTENTS

TABLE OF CONTENTS (CONTINUED)

TABLE OF CONTENTS (CONCLUDED)

LIST OF ILLUSTRATIONS

LIST OF ILLUSTRATIONS (CONTINUED)

LIST OF ILLUSTRATIONS (CONCLUDED)

LIST OF TABLES

SECTION 1
INTRODUCTION

Current technology related to high yield nuclear weapons and the increased targeting accuracy with which such weapons can be directed has given rise to the Hardened Mobile Launcher (HML) concept of basing small ballistic missiles. The Defense Nuclear Agency (DNA) along with several other agencies has been performing testing programs aimed at better defining the thermal precursor environment to which an HML could be exposed. Explosive simulation tests conducted by DNA include MINI SCALE 1 and 2 and, subsequently MINOR SCALE. These tests were designed to simulate the airblast and ground motion environment related to a nuclear explosion.

To support the simulation effort, National Technical Systems (NTS) engaged in a flow-field instrumentation development program sponsored by DNA under contract DNA-001-84-C-0441. Specific flow-field quantities of interest included sound speed, flow velocity and flow angle. Much of the effort focussed on the development of an ultrasonic system to measure sound speed. As a result of the expected configuration of the system it was felt that simultaneous measurements of flow velocity and flow angle could also be obtained. In addition to the ultrasonic system, attention was given to the design of a novel three-dimensional flow direction gage and the development of a rugged pressure transducer capable of surviving in the blast-generated flow environment.

All of these concepts were developed as much as possible over a four month period leading up to installation of prototype models in the MINI SCALE 2 field test in late February. The results of the development effort and the MINI SCALE 2 test are presented in this report.

1.1 HISTORICAL BACKGROUND.

Interest in the measurement of sound speed and flow orientation date back to investigations of surface effects related to the detonation of nuclear weapons in the mid 1950's. The general goal of the early studies was to provide information on how different surface conditions affect the formation of a thermal layer and an associated precursed pressure waveform. Some brief background information pertaining to past performance on early instrumentation is presented below.

1.1.1 Sound and Flow Speed.

Measurements of sound and wind speed were attempted with a SWASSI gage (Sonic Wind And Sound Speed Indicator) developed by Sandia Corporation in operations TUMBLER-SNAPPER, IVY and UPSHOT-KNOTHOLE (Reference 1). The device consisted of a speaker-microphone system with electronics that enabled the measurement of transit times in two opposite directions; the average being the acoustic pulse travel time and the difference being twice the travel time of a flow disturbance.

The second source was a rotor-stator type pulsed siren with a typical pulse duration of 400 msec. Timing signals to mark the emission of each pulse were produced by a stator-mounted coil and a rotor-mounted magnet.

The devices installed on operations TUMBLER-SNAPPER and IVY performed poorly as a result of the inability of the sound source to overcome shock-generated noise. This problem was caused by the need to transmit a sound pulse close to the ringing frequency of the receiver in order to obtain the desired sensitivity. Modification to the devices on operation UPSHOT-KNOTHOLE consisted of a more powerful siren capable of obtaining the necessary received signal levels at a frequency approximately equal to half the ringing frequency of the receiver. The modification apparently solved the noise problem but difficulties related to the physical mounting of the siren, line voltage delivered to siren motor and the electromagnetic transient associated with the nuclear detonation prevented the measurement of data following shock arrival.

1.1.2 Flow Direction.

1.1.2.1 Vane Device. A vane-type flow direction gage developed by J.W. Wistor of Sandia Corporation was fielded on operations TUMBLER-SNAPPER and TEAPOT (Reference 2). The gage consisted of a small vane mounted on a damped torque shaft. The shaft was supported by two sealed bearings. Connection of the torque shaft to small potentiometer allowed variations in vane orientation to be read directly as voltage changes. Reorientation of the vane required 3 to 7 msec depending upon vane size, dynamic pressure level and amount of reorientation required.

Poor results in the field on operation TUMBLER-SNAPPER led to a sturdier design on operation TEAPOT. Except for gages eliminated by the zero-time transient, all of

the gages were judged to have performed satisfactorily on operation TEAPOT. A cross-sectional drawing of the gage is provided in Figure 1.

1.1.2.2 Drag Body Acceleration. A device to measure flow direction utilizing multiple, internally mounted accelerometers within a metal sphere was proposed by Systems, Science and Software Inc. in a study to review airblast instrumentation (Reference 3). A development project to design a dynamic pressure gage utilizing the same approach (accelerometer mounted in a spherical body) was only partially successful.

One of the most difficult problems encountered in the project involved avoiding resonance between the accelerometer and one of the natural frequencies of the sphere. Minimization of the effects of spherical vibrations resulted in a complex composite sphere construction. Prototype gages also exhibited variations in rise times of their response. This problem was most likely related to the characteristics of the elastically-mounted accelerometer.

1.2 REPORT ORGANIZATION.

A description of the development and testing effort leading up to the design of an ultrasonic gage to measure sound speed, flow velocity and flow angle is presented in Section 2. Section 3 provides a summary of the concepts that formed the basis for the design of the NTS flow direction gage. A brief description of an electrolytic pressure gage under development at NTS is given in Section 4. The three gage designs described in Sections 2, 3 and 4 were fielded in MINI SCALE 2. The results of this test are reported in Section 5. Following MINI SCALE 2, additional research was undertaken to harden the ultrasonic receivers againt the combined effects of shock wave passage and particle impacts. This effort is described in Section 6. Finally, in Section 7, conclusions are drawn concerning the success of the development program and recommendations are made regarding future areas of investigations.

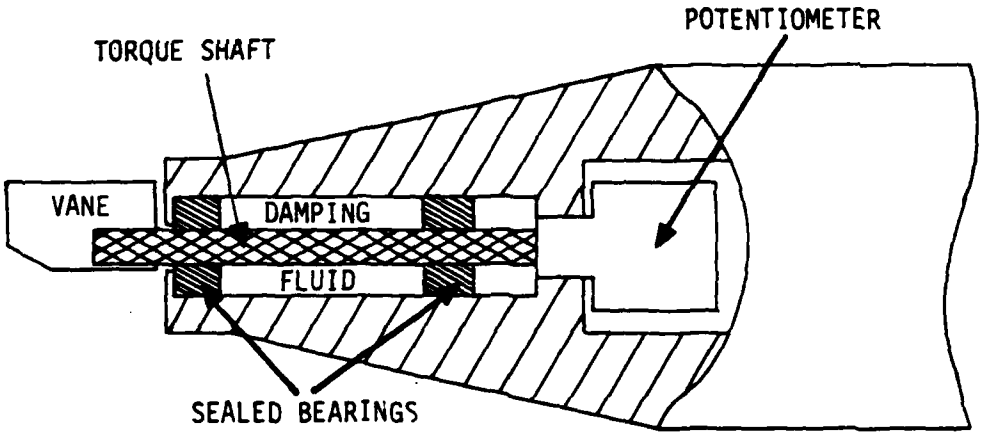

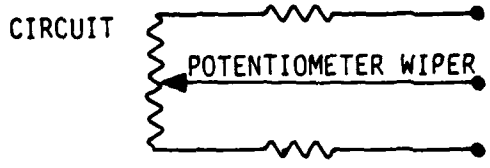

Figure 1. Cross-section of flow direction gage installed on operation TEAPOT, 1955.

SECTION 2
DUSTY GAS SOUND SPEED AND FLOW VELOCITY

The approach taken in the development of instrumentation to measure sound speed and flow velocity was based on theoretical evaluations of the propagations of an acoustic disturbance within the flow. The basic system considered consisted of an ultrasonic transmitter and an array of receivers as shown in Figure 2. In the operation of the system, a pulse is assumed to be sent from the transmitter at a known time, t_o, and received by the cross-flow receivers, R_1, R_2, R_3 and R_4, at respective times t_1, t_2, t_3 and t_4 with respective peak amplitudes A_1, A_2, A_3 and A_4. The determination of pulse transit time and received signal amplitude is a function of path length, local flow velocity, local sound speed, flow angle, transmitter beam profile and transmitted pulse characteristics (frequency, duration, amplitude, impedence). In general, the method of reducing data obtained by such a system is dependent upon the profile of the transmitted pulse wave front. Theoretical data reduction equations are developed in this section for planar and spherical wave fronts.

The remainder of Section 2 presents the results of the ultrasonic sound speed and flow velocity gage development effort. Theoretical data reduction relationships are derived in Section 2.1 for pulses with planar and spherical wave fronts. Detailed investigations into the characteristics of the transmitter and receiver chosen for evaluation are summarized in Section 2.2. Operation of the system in a low velocity flow environment is reported in Section 2.3 for flow in clean air and in a dusty mixture of air and flour. Finally, the design of the ultrasonic device, as installed in MINI SCALE 2 is contained in Section 2.4.

2.1 THEORETICAL DATA REDUCTION EQUATIONS.

Derivation of theoretical relations for interpretation of ultrasonic data records is dependent on the wave front propagation characteristics of the ultrasonic pulse.

In this study, the wave front is assumed to be either spherical or planar. A spherical wave is typically assumed to result from a point source although cylindrical ring piezoelectric crystals can also generate waves that approach a spherical shape within several cylinder diameters. Planar wave fronts are generally produced by transmitters that can generate many point sources over a planar area large in comparison to the transmitted wavelength. The shape of the ultrasonic field can be

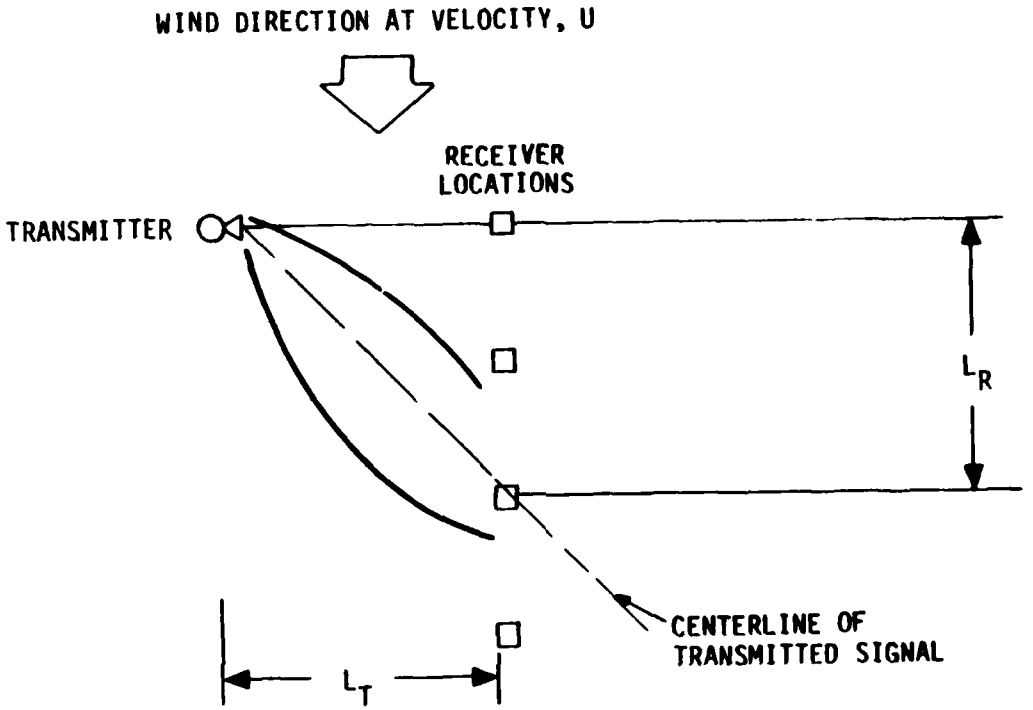

- TRANSMITTER SENDS PLANAR WAVEFRONT ULTRASONIC TONE BURST AT TIME T_1
- RECEIVER RECEIVES TONE BURST AT TIME T_2
- ACOUSTIC VELOCITY IS GIVEN BY

$$C = \frac{L_T}{T_2 - T_1}$$

- DISTANCE TO RECEIVER RECEIVING STRONGEST SIGNAL AMPLITUDE, L_R DETERMINES WIND VELOCITY,

$$U = \frac{L_R}{T_2 - T_1}$$

Figure 2. General configuration of ultrasonic measurement system.

computed using Huygen's principle which provides a means of accounting for the interaction of the many spherical sources generated on a plane at any point some distance away from the plane. Generally, this results in a specific minimum range of distances from the transmitter face, between which the wave front is planar. As the distance from the transmitter is increased beyond this range, the wave front becomes more spherical until, at large distances, it is indistinguishable from a point source.

2.1.1 Theoretical Data Reduction for Planar Wave Fronts.

The general approach to the interpretation of ultrasonic receiver data for planar transmitter pulses is shown in Figure 3. In the figure, the flow behind the blast wave is assumed to be parallel to the alignment of the four receivers. A more general condition will be discussed later. It is assumed that there is no flow disturbance related to the details of the flow behind the blast wave or the blast shield structure housing the ultrasonic transmitter and receivers.

As shown in Figure 3 for one-dimensional flow between the blast wings, a planar acoustic pulse emitted at the transmitter produces a local pressure disturbance in the flow between the blast wings. This disturbance propagates across the blast wing space, D, at the speed of sound of the flow medium, c. However, the fact that the medium is in motion causes the disturbance to migrate in the flow direction. The average flow velocity, u, can be calculated by dividing the downstream ultrasonic beam displacement, Z, by the transit time, Δt, needed by the pulse to travel the distance D. The downstream beam location is determined from the ratios of the receiver signal amplitudes and knowledge of the transmitted beam profile. Two received signals are required to locate the displaced pulse.

Extension of the data reduction methodology to two-dimensional flow conditions between the blast wings is straightforward provided that a sufficient number of receivers are present to track the deflected beam. Also, the addition of another dimension necessitates the use of a three-dimensional transmitted beam profile in order to accurately determine the location of the center of the transmitted pulse. This theoretical approach to data reduction is shown in Figure 4.

In this case, there is a vertical compoonent of flow with a velocity calculated by dividing the vertical displacement distance Δv, by the transmit time, Δt, of the ultrasonic pulse.

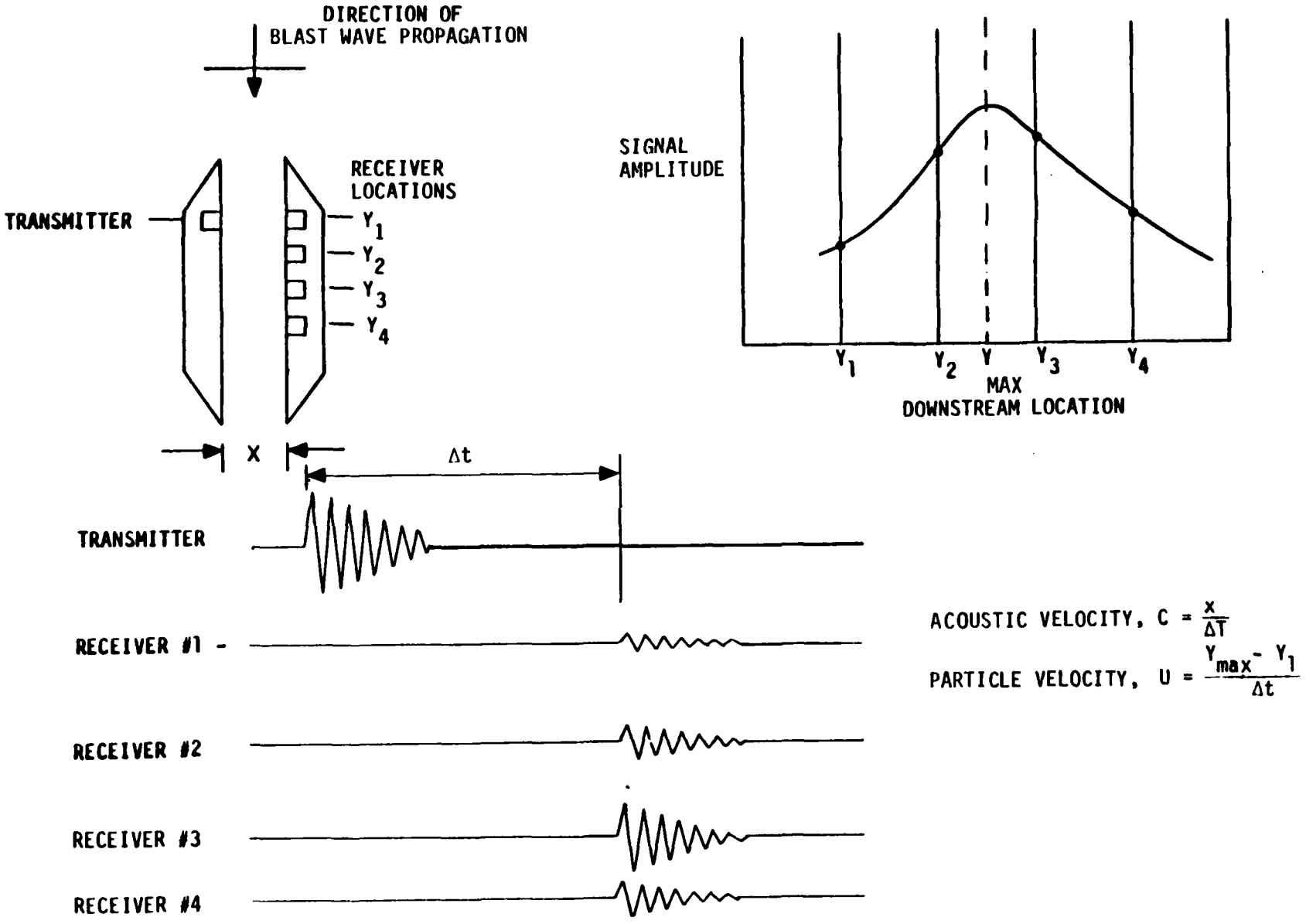

ACOUSTIC VELOCITY, $C = \frac{X}{\Delta T}$

PARTICLE VELOCITY, $U = \frac{Y_{max} - Y_1}{\Delta t}$

Figure 3. Data reduction using plane waves.

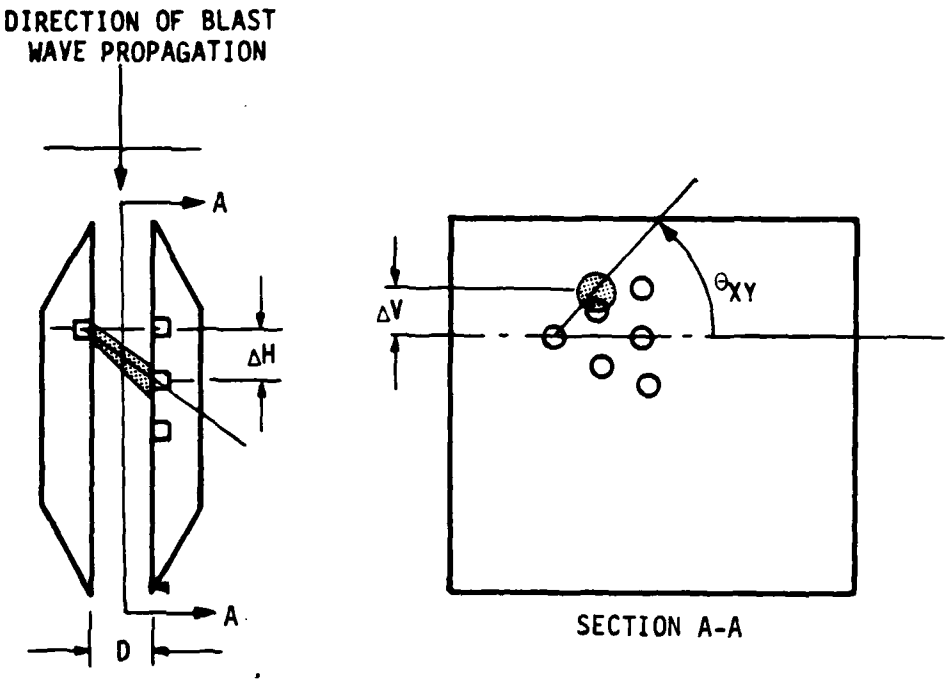

- PULSE TRANSMITTED AT TIME, T_1, RECEIVED AT TIME, T_2
- ΔH AND ΔV DETERMINED FROM COMPARISON OF RECEIVED SIGNAL AMPLITUDES WITH KNOWN BEAM AMPLITUDE PROFILE
- FLOW ANGLE = $\frac{\Delta V}{\Delta H}$
- FLOW VELOCITY = $\frac{\sqrt{\Delta V^2 + \Delta H^2}}{(T_2 - T_1)}$
- SOUND SPEED = $\frac{D}{(T_2 - T_1)}$

Figure 4. Determination of flow parameters for two-dimensional receiver array.

2.1.2 Theoretical Data Reduction for Spherical Wave Fronts.

The data reduction procedure for ultrasonic pulses with spherical ultrasonic wave fronts differs from that for planar wave fronts in that amplitude information must be used to determine both the local speed of sound and the flow velocity. The reason for this is demonstrated in Figure 5. The minimum transit time for the pulse is determined from the arrival of a signal at a single location on the receiving face. If the pulse arrival location does not correspond to a receiver position then the relative amplitudes of the received signals, as well as the time of arrival of those signals, must be used to determine the minimum transit time.

If the ultrasonic wave front is perfectly spherical, two leading edges, one travelling upstream and the other travelling downstream, of the pulse will progress along the face of the transmitting wing. The upstream traveling edge will propagate at c-u and the downstream traveling edge will propagate at c + u. Once the pulse has travelled the distance D, a similar condition will exist on the receiving wing. As indicated in Figure 5, the wave front will propagate in an upstream and downstream direction from the point of first contact at rates v_u and v_d, where

$$v_u = c\sqrt{1 - \left(\frac{D}{ct}\right)^2} - u \qquad (1)$$

$$v_d = v_u + 2u \qquad (2)$$

For flow conditions in which the local Mach number is greater than 1.0 ($u > c$) there is no upstream propagation velocity. To further illustrate the effect of Mach numbers, a plot of arrival times versus location on the receiver face for Mach numbers ranging from 0.5 to 2.0 is provided in Figure 6.

The use of spherical waves, in a blast wing configuration as previously discussed, necessitates an alternate type of data reduction. As shown in Figure 7, if the time difference between the transmission of a pulse and reception of a pulse is plotted as a function of the receiver location, a minimum point can be estimated. This point has, as its abscissa, the location on the receiver wing of the initial pulse arrival. The ordinate of this same point represents the travel time of the leading edge of the pulse center line to the receiving side. Once these two quantities are known, the calculation of acoustic velocity and flow velocity is straightforward as is indicated in the figure.

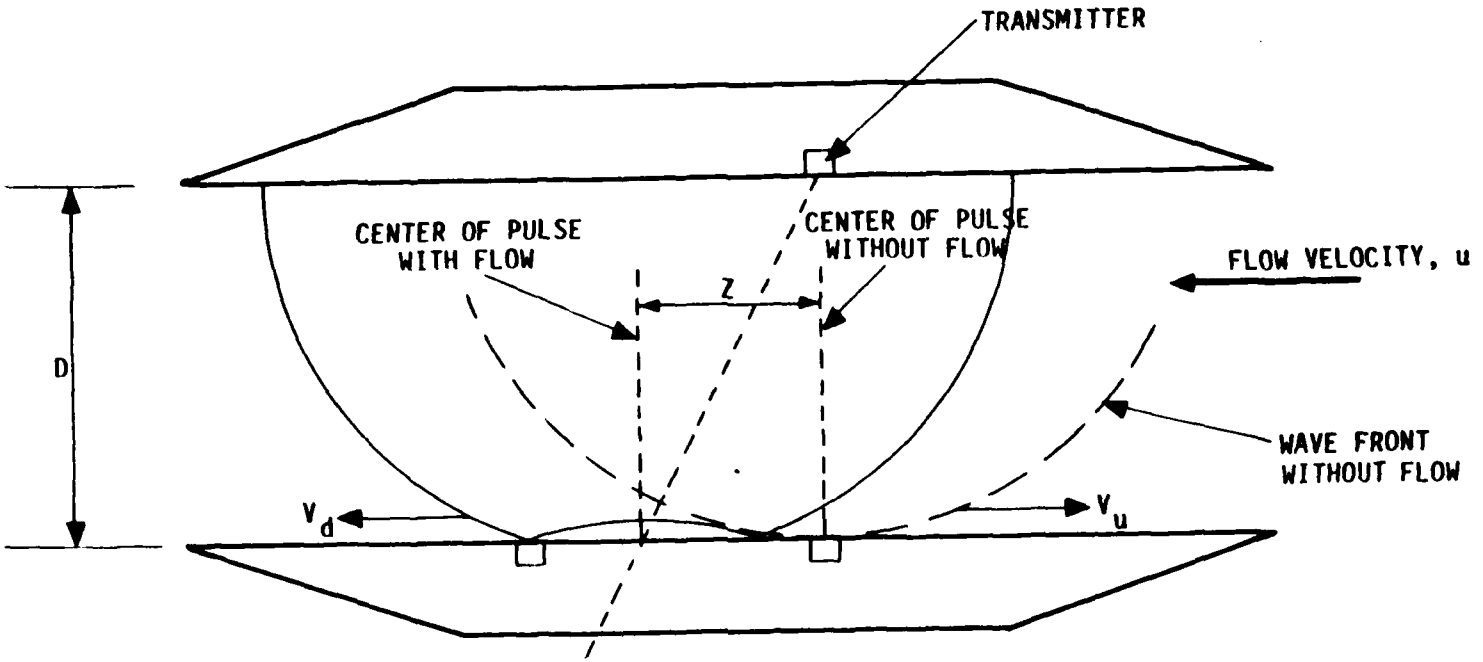

V_d = DOWNSTREAM PROPAGATION VELOCITY ON RECEIVER FACE

V_u = UPSTREAM PROPAGATION VELOCITY ON RECIEVER FACE

$$V_u = c\sqrt{1 - \left(\frac{D}{ct}\right)^2} - u$$

$$V_d = V_u + 2u$$

Figure 5. Theoretical wave front propagation.

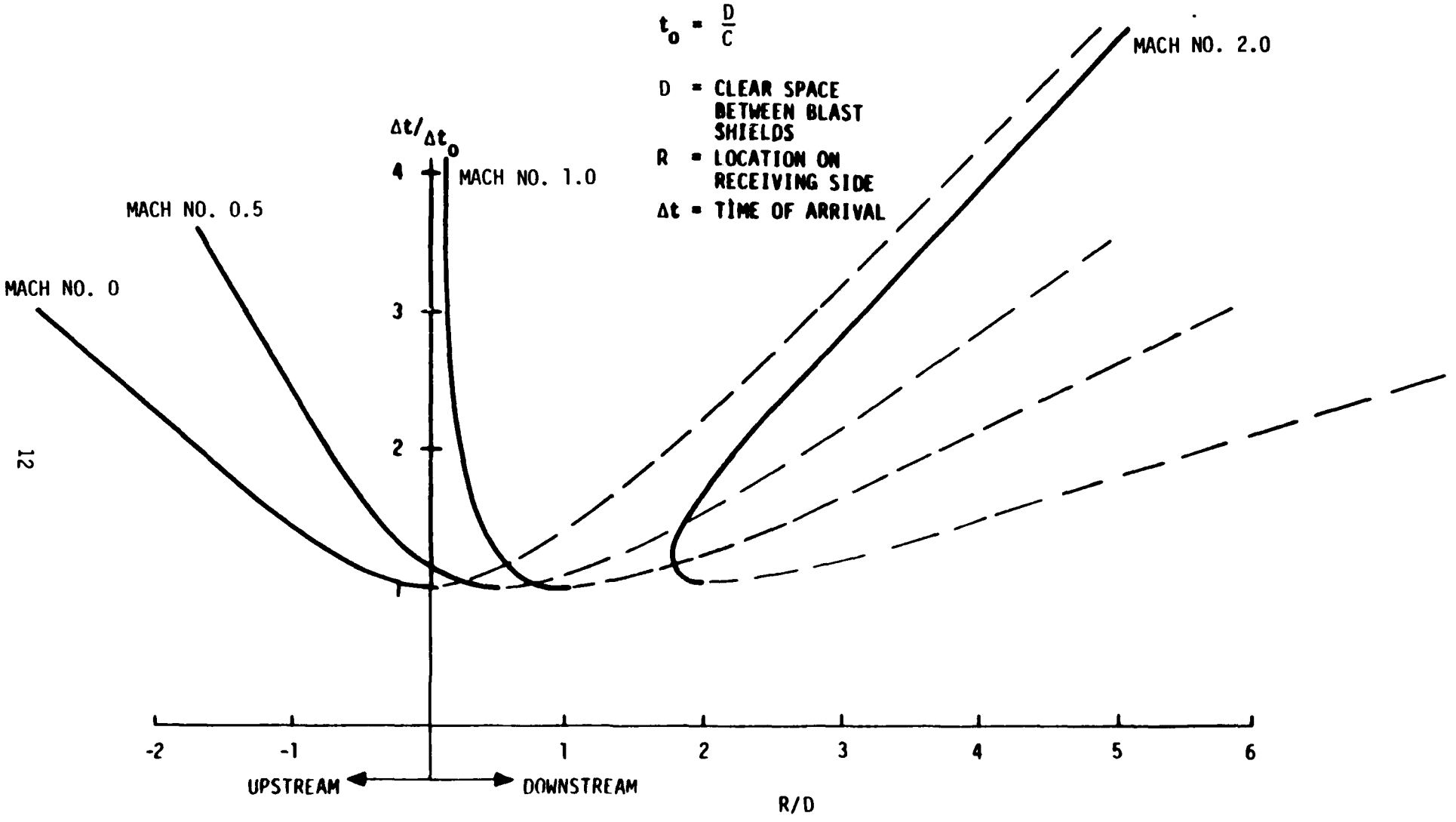

Figure 6. Spherical wave arrival times at receivers for several flows.

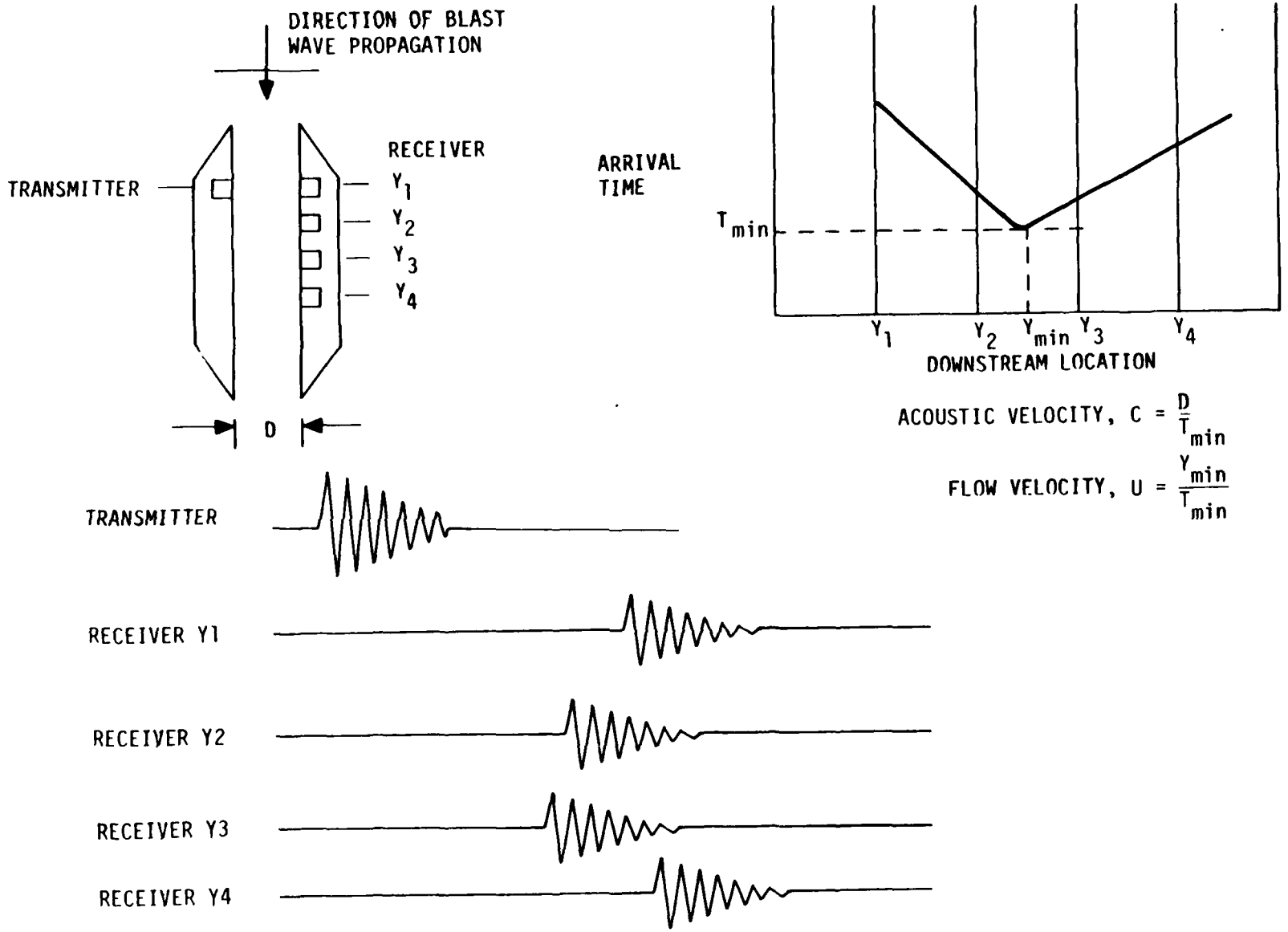

Figure 7. Data reduction using spherical waves.

Extension of the spherical data reduction equations to accommodate a two-dimensional receiver array is straightforward In addition to a plot of arrival time versus downstream receiver location, Y, a plot of arrival time versus vertical receiver location, Z, is needed. The minima associated with these two curves allow the calculation of the downstream and vertical flow components. The minimum ordinate of either curve can be used to determine the sound speed as the minimum travel time must be the same for the Y and Z axes.

2.2 INVESTIGATION OF TRANSMITTER AND RECEIVER CHARACTERISTICS.

After considerable review of the numerous types of ultrasonic transducers readily available, several candidate receivers were selected. The choice of transmitter was dictated by the requirement that output power be maximized to aid in overcoming blast generated noise. Receiver selection was governed by size and response frequency considerations. The transmitter chosen was a Par-Sonics 4012 B and the receiver selected was a Massa Products Corporation Model TR-89/B Series. Sketches showing the relative sizes of these two transducers along with some of the more pertinent specifications are shown in Figures 8 and 9. Both of these transducers utilize piezoelectric crystals as the primary active element.

In order to better understand the physical characteristics of the ultrasonic transmitter, several tests were undertaken to investigate the spatial variations in beam power and phase. Measurements for the sensitivity experiments were conducted with the Massa Corp. receivers so that the results could be used directly in developing the configuration of future blast wing test structures and in providing information on received pulse profiles for data reduction purposes.

Initial efforts in the development of the ultrasonic system were directed towards a resonant system in which the transmitter and receiver operated at a single frequency that was close to their respective resonant frequencies. However, the response bandwidth of the receiver was widened to enable filtering of frequencies other than those of interest. It was hoped that the efficiencies in energy transmission of such a system would alleviate many of the signal noise problems related to blast effects and shock-wave passage.

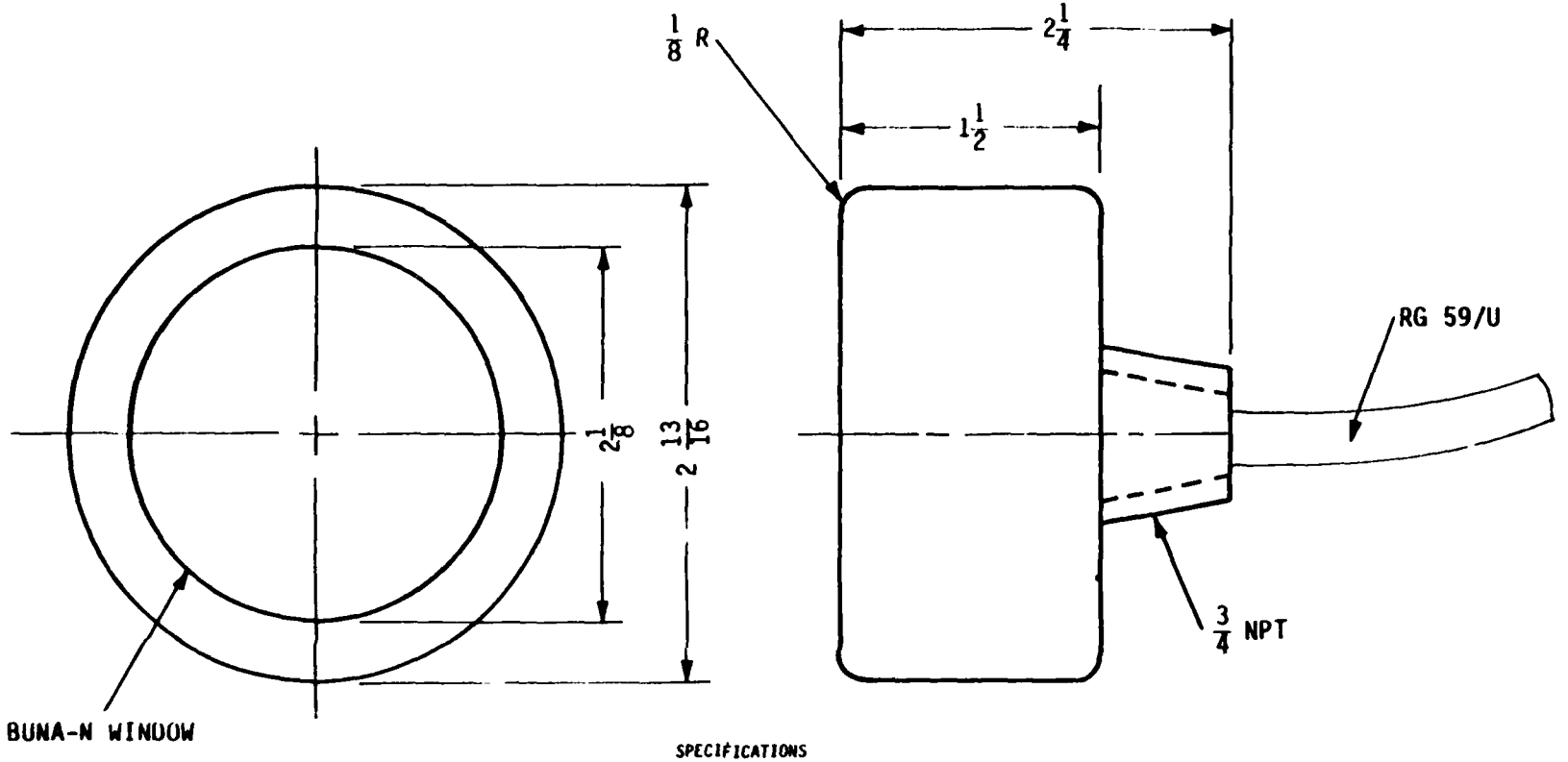

SPECIFICATIONS

Frequency, ± 2 KHz	40
Impedence (ohms)	210-J250
Sensitivity	
Transmit: db/v re 1 microbar (15")	14
Receive: dbv/microbar	-91
Insertion Loss (db)	77
Capacitance (pfd)	7500
Temperature Limits (°F, max/min	165/-40
Max. Drive Volts	450 p-p

Figure 8. Parsonics 4012.B transmitter.

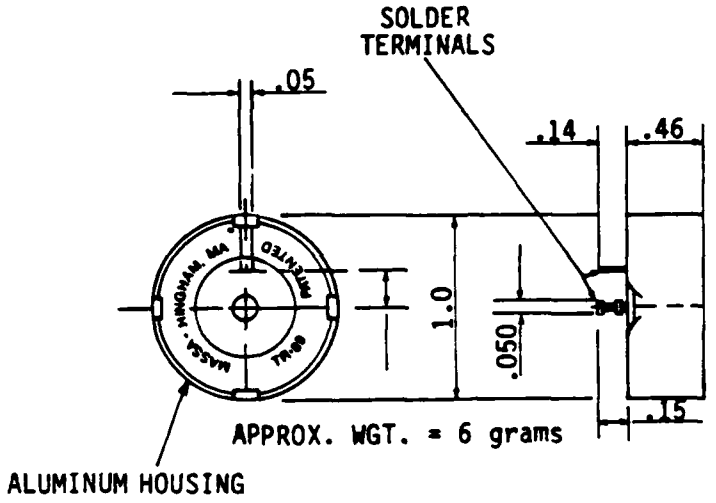

SPECIFICATIONS

Frequency	40 kHz
Bandwidth	
Tuned	10 kHz
Untuned	0.5 kHz
Transmitting Sensitivity dB vs 1 bar per volt at 1 foot (Untuned)	+22
Receiving Sensitivity dB vs 1 volt/ bar (Untuned)	-50
Rated Power or Voltage	200mW
Total Beam Angle (-3dB)	20°
Weight	0.2 oz

Figure 9. MASSA TR-89/B receiver.

2.2.1 Profile of Received Signal Amplitude.

In order to ascertain the power profile of the transmitter, a simple experiment was performed to measure the variation is received signal strength with increasing off-axis receiver placement. The experimental arrangement and plot of signal strength versus distance from the centerline of the transmitter is presented in Figure 10. As can be seen in the figure, the signal strength is maximized when the centerlines of the receiver and transmitter are aligned. Signal strength decreases to approximately half of maximum value after an off-axis movement of 1.0 inches. At an off-axis distance of 2.0 inches, the signal strength is reduced to only 10% of the maximum value.

The results indicated that the beam being transmitted was very narrow, having nearly all of its signal confined to the limits of the 2.125-inch diameter BUNA-N window (refer to Figure 8). Of course, this is not a true profile because of the fact that a 1.00-inch receiver was used to sense the signal. Pin-like sensing probes are generally used for accurate profile determination. However, as mentioned earlier, the profile obtained was indicative of anticipated field data. The same signal strength profile was measured for different transmitters and for the same transmitter rotated 90° in its mount in 15° to 20° increments. The uniformity of the results indicated that separate calibration efforts to determine optimum orientation for each transmitter would not be necessary.

Another piece of information gained during these tests related to the maximum received signal amplitudes that might be attainable. The transmitter was excited by a 3V peak-to-peak sine wave with a frequency equal to the transmitter's resonance frequency. The peak signal received was 2mV. Scaling this value up to the maximum 450V peak-to-peak excitation cited in the specifications revealed that maximum received signal amplitude could be on the order of 300mV.

2.2.2 Profile of Received Signal Phase.

Following the investigation of signal power profile, the same test arrangement was used to measure the variation in received phase with distance off the transmitter centerline. This measurement was very important because it determines the degree of planarity of the transmitted beam and thus provided an indication of which data reduction scheme was most appropriate. The separation distance between the faces of

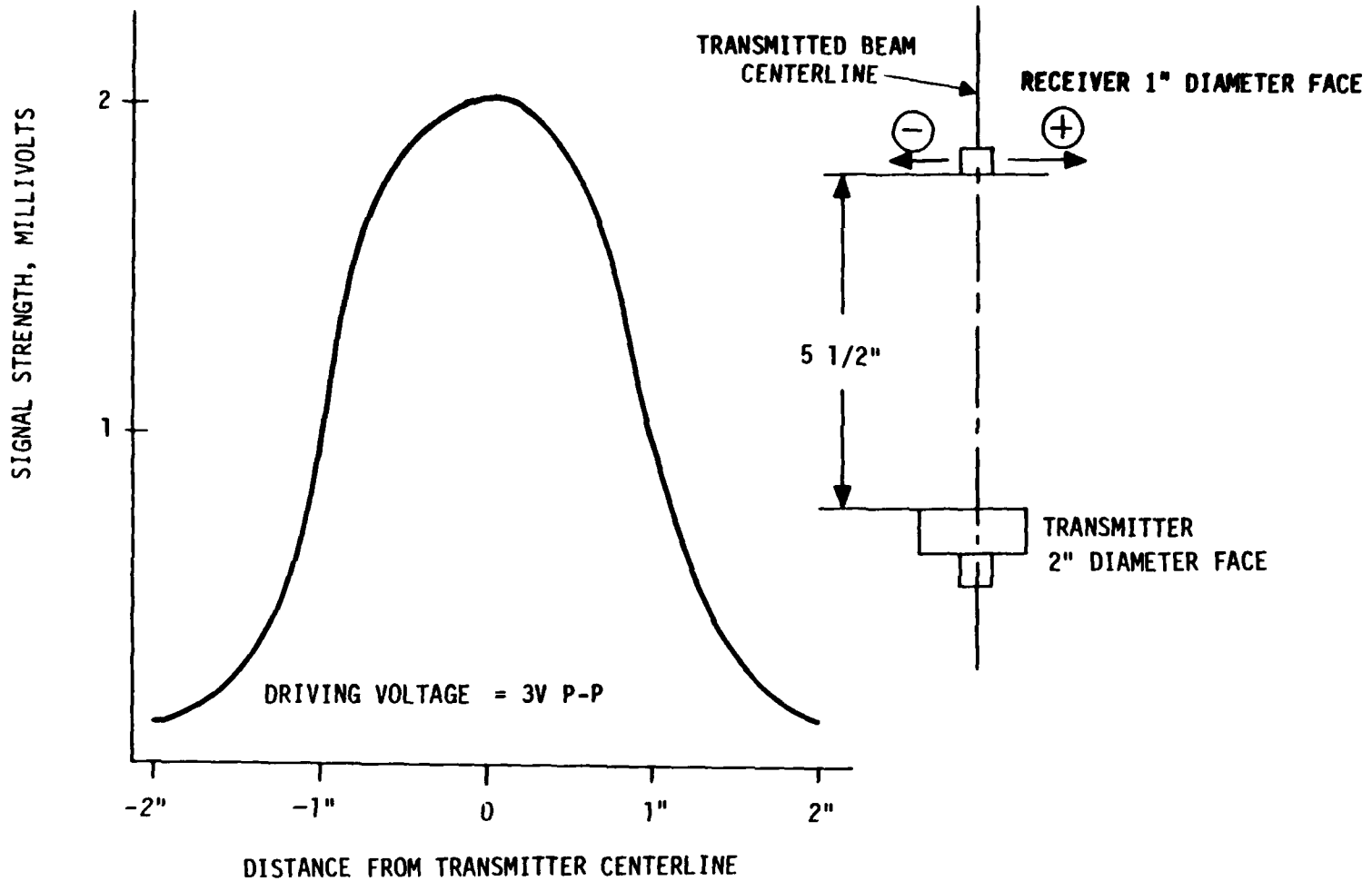

Figure 10. Ultrasonic transmitter beam power profile.

the transmitter and the receiver was set at 6 inches. The results of these measurements, presented in Figure 11, indicated that the wave front was very planar within an off-centerline distance of approximately $\pm$ 1.0 inch. Beyond this off-axis excursion the transmitted beam exhibited a shift in phase that was nearly proportional to the distance moved in excess of 1.0 inches.

Using this information, along with that provided by the received signal profile, it was concluded that the structural configuration of a system using these transducers would be based on a 2-inch diameter cylindrical beam with signal strength at its centerline equal to twice that of its outer most points.

2.2.3 Development of Optimal Pulse Profile.

The next tests in the investigations of general beam characteristics were directed at producing a pulse from the transmitter that would meet the operational requirements of the proposed ultrasonic system. The three critical aspects of pulse generation that were focussed upon were pulse rise time, pulse duration and decay time. The goal of these tests was to minimize rise time and decay time while precisely controlling the pulse duration.

Several problems became immediately apparent during initial efforts related to the shape of the received pulse obtained by driving the transmitter with one single electrical pulse.

This approach was not very successful primarily due to the fact that the pulse was of long duration and did not possess any characteristics that would make it easily recognized in even a minimal noise environment. An example of such a waveform is presented in Figure 12a. The low rise time of approximately 30 to 35 cycles (0.75 msec to 0.88 msec) makes identification of the pulse arrival time highly dependent upon ambient noise levels. Once the pulse had reached its maximum signal level, and remained at that level for approximately 0.25 msec, an exponential decay was observed. The total pulse duration was close to 1.6 msec.

This wave shape was improved upon significantly by making two changes in the manner the transmitting crystal was excited. First, to improve rise time characteristics, the driving voltage was applied for two cycles at intervals equal to half the natural period of the crystal so as to drive the crystal in its expanding mode and also

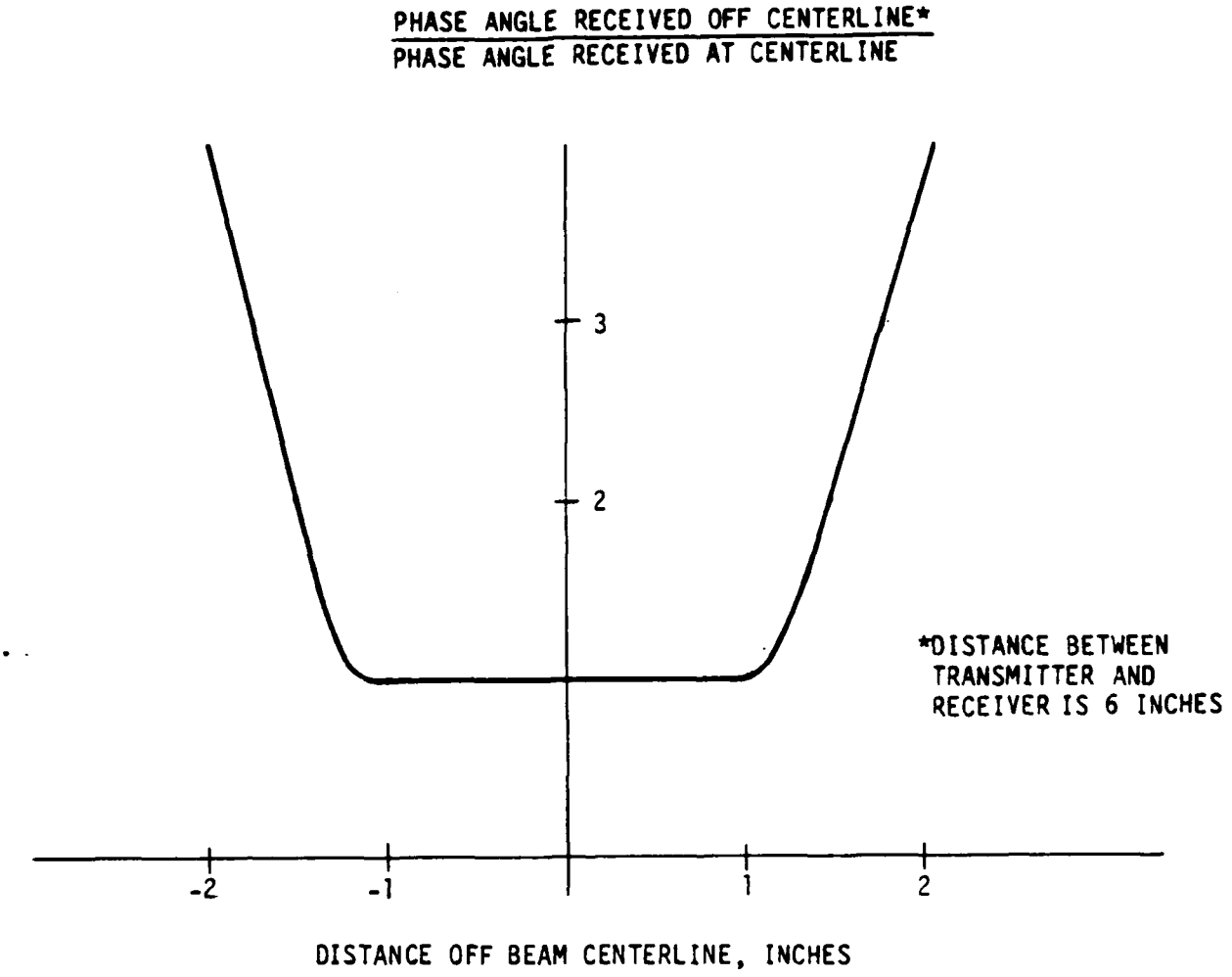

Figure 11. Par-sonics 4012.B transmitter beam phase angle profile.

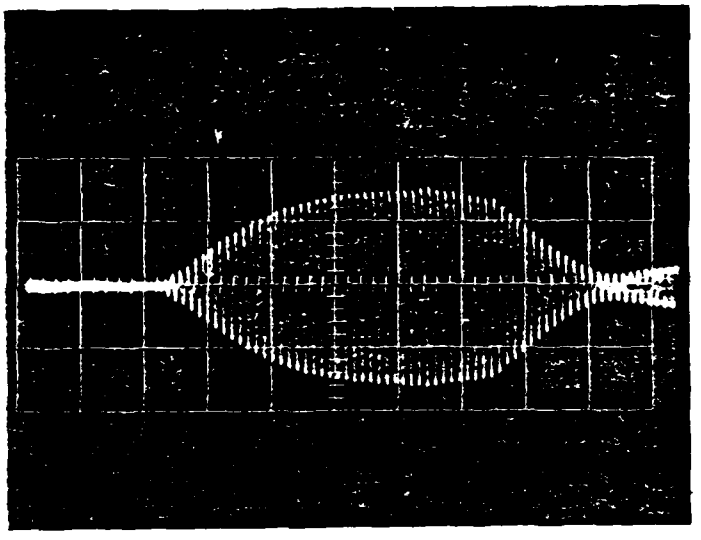

a. PULSE SHAPE FROM SINGLE PULSE, NO DECAY ENHANCEMENT
(0.2 msec/cm, 5mV/cm)

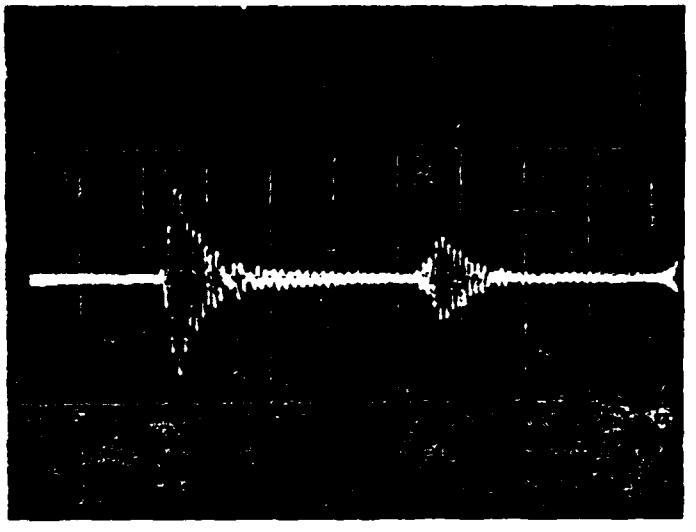

b. PULSE SHAPE FROM TWO PULSES AT NATURAL FREQUENCY,
FEEDBACK-DRIVEN DELAY CIRCUIT
(0.2 msec/cm, 5 mV/cm)

Figure 12. Enhancement of driven ultrasonic waveform.

in its contracting mode. Secondly, to decrease the decay time, a feedback circuit was added to provide electronic damping of the ringing oscillations. The final pulse shape is shown in Figure 12b.

2.3 SENSITIVITY OF SIGNAL TRANSMISSION TO PRESSURE AND DENSITY.

As the goal of this development effort was to produce a system capable of operating in a helium-generated precursor environment with a nominal 30 psi overpressure, tests were performed in a small, pressurized, anechoic chamber to investigate the effects of pressure and helium concentration on transmission characteristics. A sketch of the experimental apparatus is shown in Figure 13. Twenty tests were conducted with four different gas mixtures (0%, 33%, 67% and 100% helium) and five different pressures (0, 5, 10, 20 and 30 psig). Measurements were made of received signal strength and pulse travel time. The results of these tests are tabulated in Table 1.

It is apparent from the data in Table 1 that the introduction of a helium atmosphere into the anechoic chamber can greatly decrease the received signal strength. The calculated change in sound speed with helium concentration, based upon the measured travel time and a 20cm separation distance, is plotted in Figure 14. The shaded region on the plot does not reflect an effect of pressure on measured sound speed. Rather, it is an indication of the error in the measurement when the amplitude of the received signals is very low. The amplitude of the received signal, as has been shown by the results in Table 1, is highly dependent upon the helium content. This dependence can be partly explained by considering the mechanism for imparting energy from the crystal to the gas. The efficiency of energy transmission depends upon the degree of mismatch in the mechanical impedances of the gas and the piezoelectric crystal. Mechanical impedance, R_m, is defined as

$$R_m = \sqrt{E\rho} \qquad (3)$$

where

E = bulk modules of the material

ρ = material density

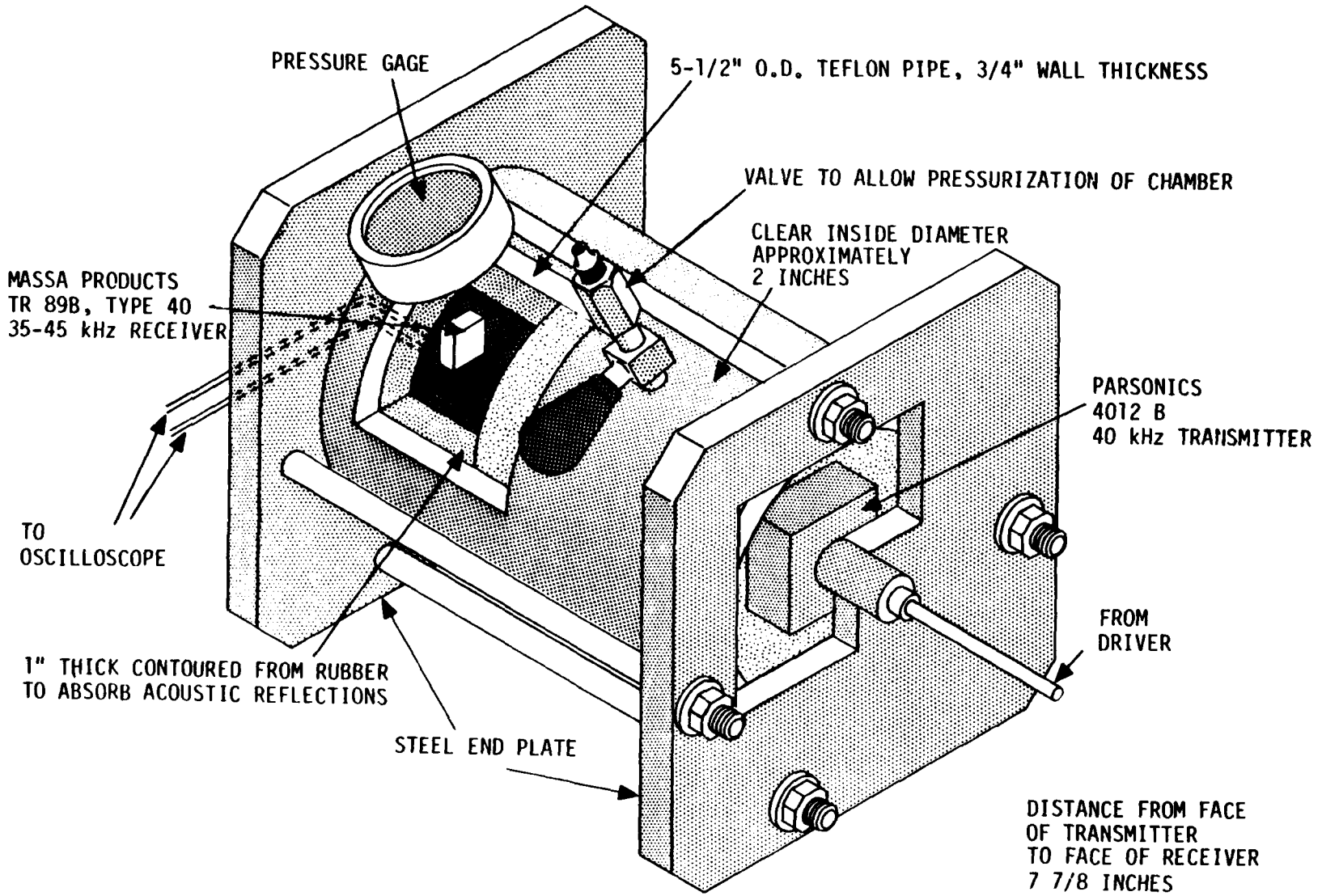

Figure 13. Anechoic chamber used for sensitivity tests.

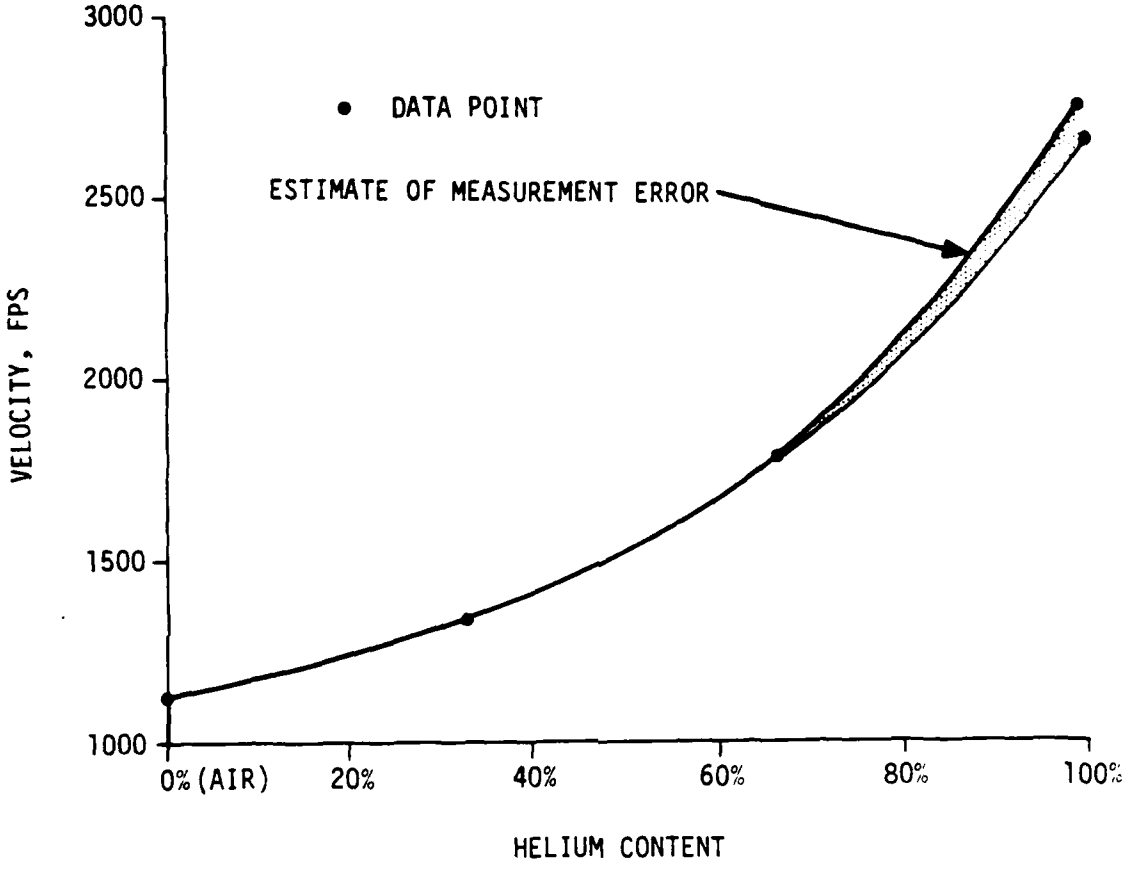

Figure 14. Sound velocity versus helium content of atmosphere.

Table 1. Pressurized anechoic chamber measurements*.

% He	GAGE PRESSURE, PSI				
	0	5	10	20	30
100**	0.8 mV Δt = 0.246 msec	0.9 mV Δt = 0.245 msec	1.1 mV Δt = 0.244 msec	1.3 mV Δt = 0.242 msec	1.7 mV Δt = 0.240 msec
67	1.6 mV Δt = 0.380 msec	2.4 mV Δt = 0.379 msec	3.0 mV Δt = 0.378 msec	4.4 mV Δt = 0.373 msec	5.6 mV Δt = 0.370 msec
33	2.2 mV Δt = 0.497 msec	3.0 mV Δt = 0.495 msec	3.6 mV Δt = 0.494 msec	5.5 mV Δt = 0.492 msec	6.8 mV Δt = 0.490 msec
0	7.0 mV Δt = 0.580 msec	11 mV Δt = 0.579 msec	15 mV Δt = 0.578 msec	18 mV Δt = 0.577 msec	23 mV Δt = 0.575 msec

* Voltage refers to received signal at 20 cm separation $\pm$ 0.01 mV
** Later calculations showed actual percentage to be 96%

Under ambient conditions, the pressure transmitted through the gas should decrease substantially in going from 100% air to 96% helium since both E and ρ are decreasing. This effect is borne out by the observed decrease by a factor of 8.75 in the anechoic chamber tests. This effect is displayed graphically in Figure 15 as a plot of received signal amplitude versus gage pressure for the four air-helium mixes.

The effect of pressure on received signal amplitude is more or less independent of helium concentration. This was born out by replotting Figure 15 to show the effects of pressure on received signal amplitude normalized by the amplitude at zero gage pressure as shown in Figure 16. It appears that the data for 100% helium are inconsistent, but this is most likely attributable to the very low signal levels associated with the mixture and the potentially large percentage changes that result from very small experimental variations measured signal.

The primary reason for the reduction of received signal amplitude at high helium concentrations is the greater impedence mismatch between the less dense mixture and the surfaces of the transmitter and receiver. This characteristic can be used to provide a means to check the concentration of helium used in the anechoic chamber tests. To quantitatively examine the effect of gas density on transmission and reception characteristics, measured received signal levels were expressed as a fraction of the maximum signal received with 100% air. Table 2 summarizes the results of this calculation for the five different pressures tested.

As can be seen in Table 2, each gas mixture has a particular range of signal ratios. The ratios corresponding to 100% helium again show the greatest percentage variation due to the experimental variations at the smaller signal levels. However, closer examination of the values calculated for the 100% helium mixture indicated that actual helium concentration was probably 95% to 97%. This is not too surprising considering that in order to reduce reflected signals the interior of the anechoic chamber was lined with porous foam that may have trapped air from previous tests. The slow release of this trapped air, combined with the possibility of very small leaks could easily have caused the small deviation in helium concentration.

2.4 LOW VELOCITY FLOW MEASUREMENTS.

After the investigation of transmission and reception characteristics had been completed, a test fixture was constructed to evaluate the performance of the trans-

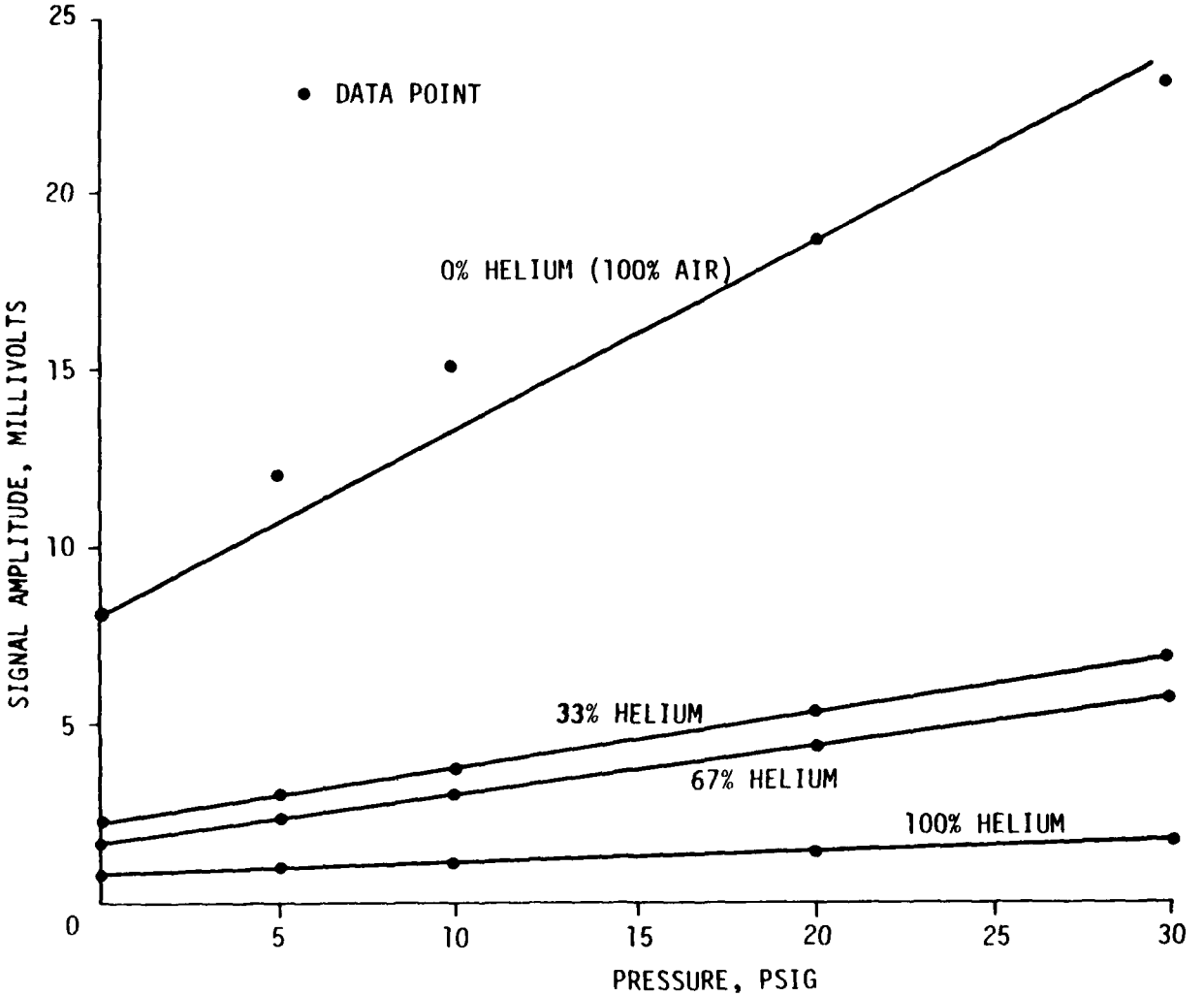

Figure 15. Signal strength versus ambient pressure.

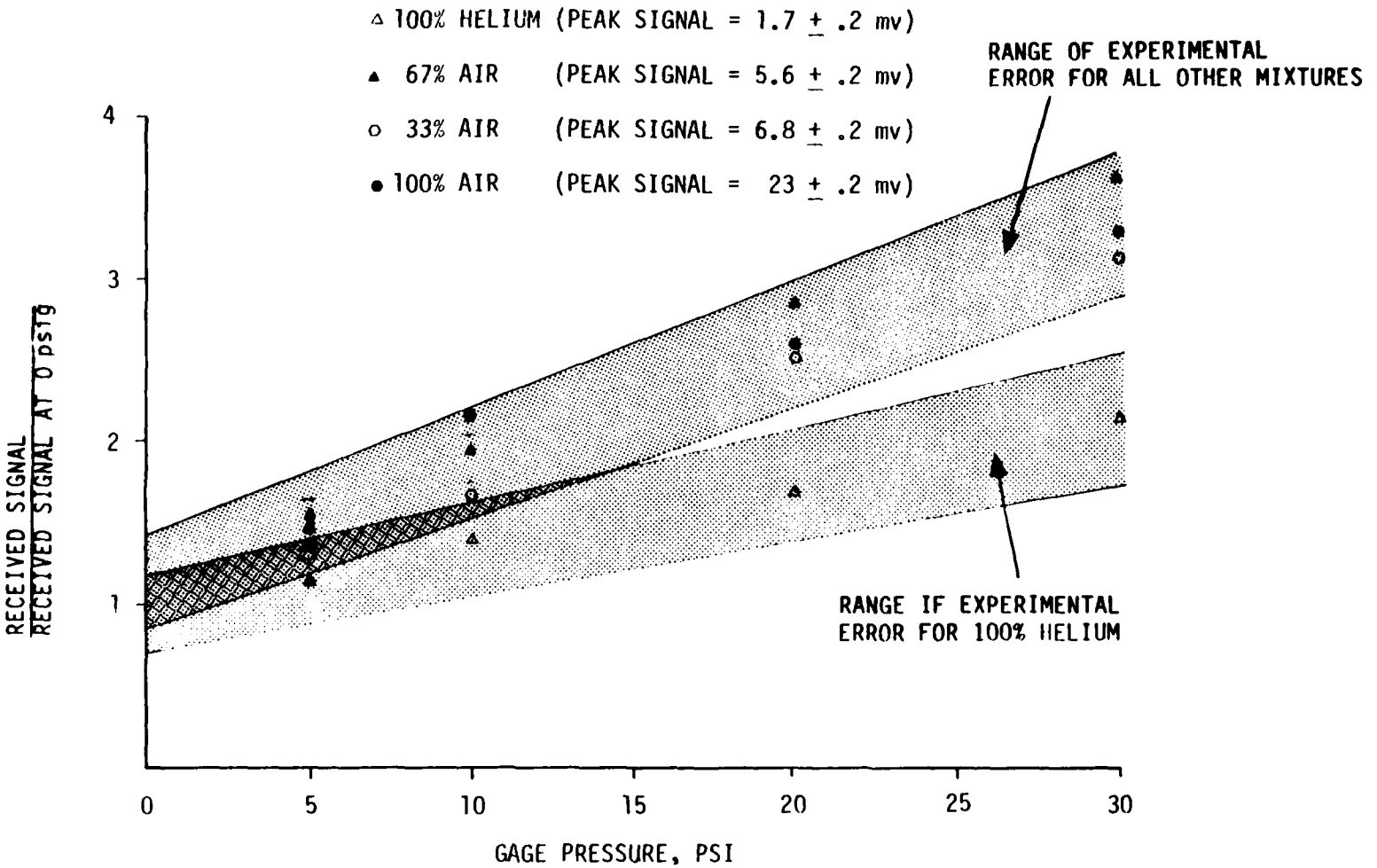

Figure 16. Relative signal strength versus air density and pressure.

Table 2. Ratio of received signal voltages for varying air mixtures and pressures.

MOLECULAR WEIGHT RATIO	PRESSURE, psia				
	14.7	19.7	24.7	34.7	44.7
0.14 (100% He)*	0.11	0.08	0.07	0.07	0.07
0.42 (67% He)	0.22	0.22	0.20	0.24	0.24
0.72 (67% AIR)	0.31	0.27	0.24	0.30	0.30
1.00 (100% AIR)	1.00	1.00	1.00	1.00	1.00

*ACTUAL He CONCENTRATION CALCULATED TO BE 96%

mitters and receivers in clean and dusty flow. The test section fabricated for these tests consisted of a 6-inch square aluminum tube with nominal wall thicknesses of 0.25 inches and a 0.5 inch wall thickness near the point of flow entry into the test section. Airflow through the tube was provided by a 1700 cfm axial-flow blower. A sketch of the test section is shown in Figure 17.

The flow fixture is shown in Figure 17 with a nominal 2-inch pipe section extending from the back end. It was originally thought that this modification would allow easy connection to a high pressure source for the conduction of venting tests. However, schedule and funding restrictions limited the tests to those conducted with the blower. For the blower tests, the back plate was completely removed to reduce the flow losses caused by the abrupt change in cross section between the blower and the test fixture.

The tests performed in the low velocity flow fixture were designed to evaluate several key aspects of the proposed ultrasonic system:

1) ability of turbulent flow to cause perceptible downstream deflection of the ultrasonic pulse;

2) potential adverse effects related to the presence of mechanical vibrations in the receiver mountings;

3) the accuracy of using the ultrasonic system to estimate flow velocities; and

4) what effects the addition of particulates to the flow will have on the operation of the system.

2.4.1 Clean Flow Tests

Initial tests in the low-velocity flow apparatus were conducted without introducing particulates into the flow. Of particular concern during these tests was the potentially adverse effects of mechanical vibration on the performance of the receivers. The blower was connected to the test fixture in such a way as to transmit any vibrational motions resulting from the operation of the blower directly into the walls of the test fixture and into the receivers. The installation of the receivers into the

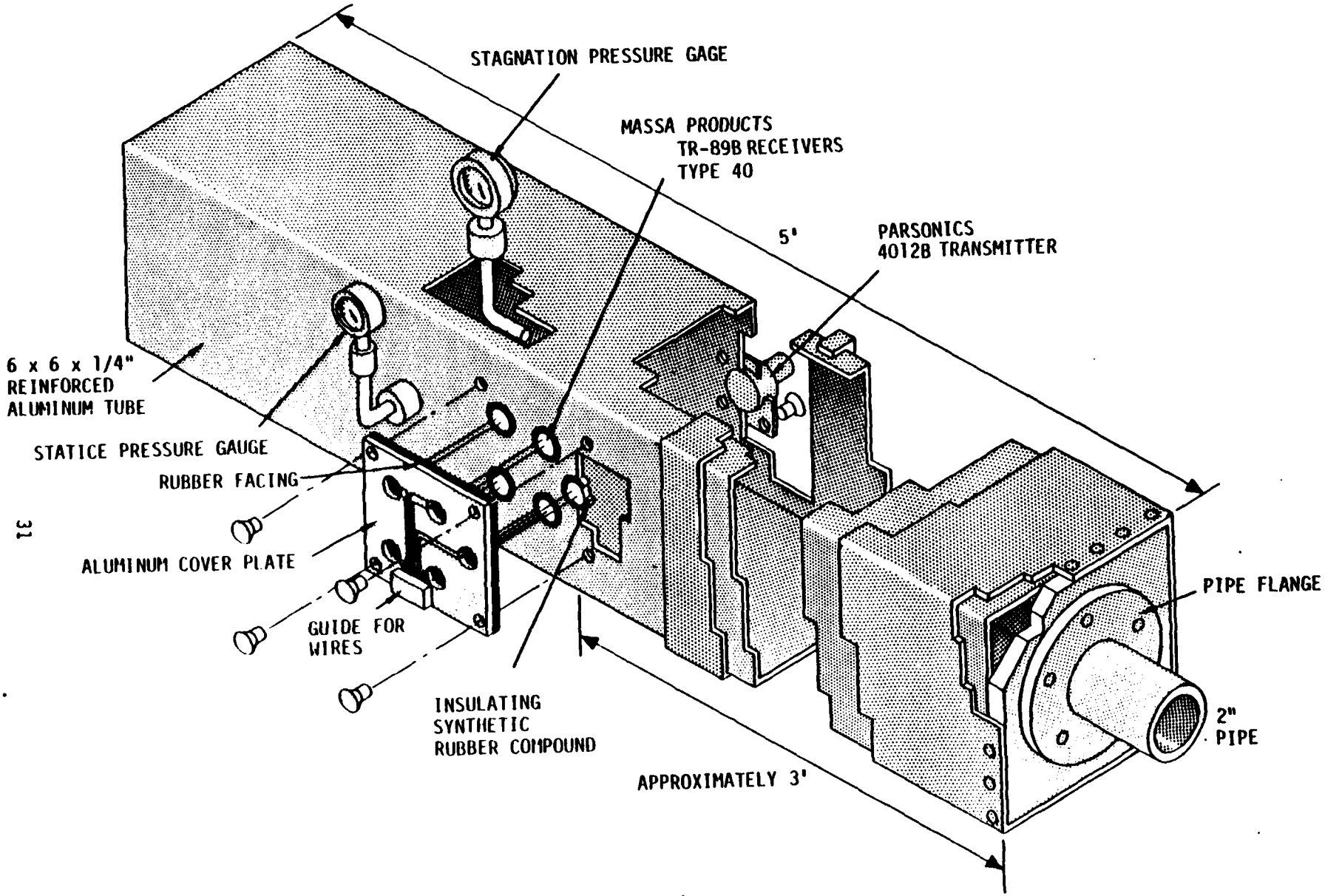

Figure 17. Low velocity flow test fixture.

wall of the test fixture was performed with special attention given to isolating the receivers from direct mechanical vibration in a manner that could be easily implemented in future tests. Vibration isolation was provided by casting a 0.13-inch thick layer of synthetic rubber around the receiver.

Initial check-out of the ultrasonic system in the test fixture revealed a serious problem with reflections. The bare aluminum walls proved to be an efficient reflective surface. This problem was easily eliminated by reducing the pulse repetition rate such that reflections had a chance to die out between pulses. Limitations imposed by the presence of reflections was a problem that became more apparent as testing progressed.

Some received pulses for the cases of no flow and full flow are shown in Figure 18a and 18b, respectively. The maximum effect of mechanical vibration on the received signal is seen to be limited to approximately $\pm$ 13 mV or approximately $\pm$ 7% of the full scale measurement. Estimates of flow velocity were calculated based upon observed changes in received signal amplitude and the earlier test data on transmitted signal power profile. These measurements were then compared with flow velocities measured directly at the exhaust end of the test fixture with a calibrated vane device.

Measurements of the exhaust flow indicated a maximum clean-air flow velocity of 70 fps $\pm$ 4 fps. This indicated that the system was encountering losses in flow energy of approximately 48% based upon calculations of flow velocity required to pass the maximum volume rate of the blower through a 0.21 ft^2 area. An evaluation of potential causes of the inefficiency revealed that nearly all of the losses could be attributed to the blower not meeting its specifications and large abrupt cross-sectional variation at the interface between the blower and the test fixture. No methods were available to alleviate these problems. However, measurements were made to test the ability of the ultrasonic system to measure flow velocity even through the flow much lower than desired. Based upon amplitude shifts under maximum flow, flow velocity was estimated to be 64 fps $\pm$ 4 fps. One explanation of the large error is related to post-test investigations that revealed a possible uncertainty of 0.06 inches in receiver location.

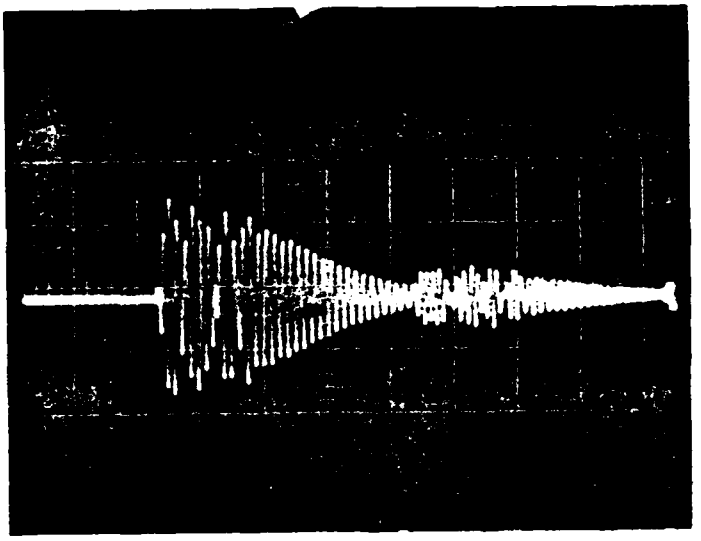

a. BLOWER OFF

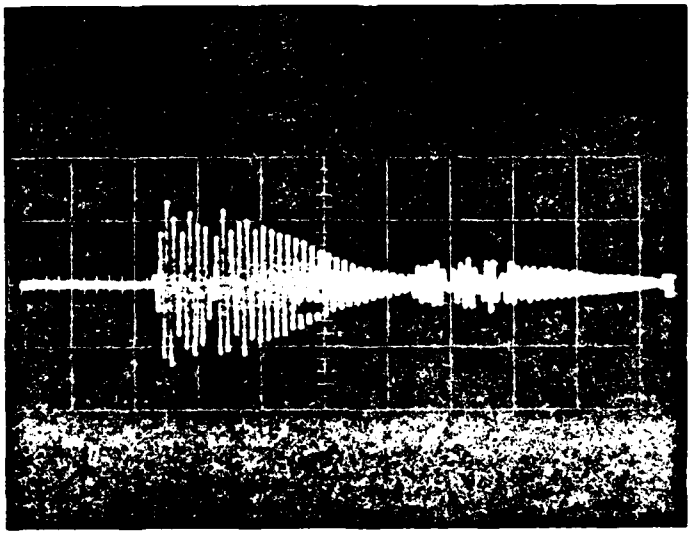

b. BLOWER ON

Figure 18. Comparison of received pulse with and without blower running.

2.4.2 Dusty Flow Tests.

The goals of the dusty flow test were to determine the effect of dust on received signal amplitude, verify the ability of the system to measure flow velocity in a dust-laden mixture and to estimate the errors to be expected from the increase in signal noise levels due to particulates impacting the receiver face.

Because of the method in which particulates were introduced, sand or sand-like particles were not considered because of their highly abrasive nature. Also, sand-like material immediately available was felt to be too large a size (average diameters greater than 200)m) for the type of dust-related effects being investigated. The particulates used in the tests were wheat flour particles. Flour is a fairly uniform material with approximately 90% by weight having a mean average diameter of about 60)m. Flour was introduced into the flow at the intake of the 1700 cfm blower so that any relatively large blocks of flour could be broken up by the blades of the blower.

There was no signal loss observed as the result of the introduction of flour into the flow mixture. This can be seen by examining the photographs in Figure 18 of oscillograph records of the signal received by the cross-flow receivers between signal initiation and signal arrival. This was the expected result considering the small size of the average particle diameter relative to the wavelength of the pulsed signal (60)m versus 8,600)m). The fact that the signal wavelength is approximately 150 times the average particle diameter makes the ultrasonic pulse insensitive to the presence of particulates as large as those in the flour for all but extremely high concentrations of particles. Signal loss at very high particle concentrations is related to reduction in clear pathways between the transmitter and receiver.

Difficulties in obtaining a well-controlled addition of flour into the test section prohibited accurate correlation between measured noise levels and the mass flow rate of flour. However, examination of several portions of the recorded data was done to see if any general trends could be observed. As expected, the level of noise picked up by the ultrasonic receiver increased wth increasing flour density and the related increase in particle impacts. This trend is depicted graphically in Figure 19.

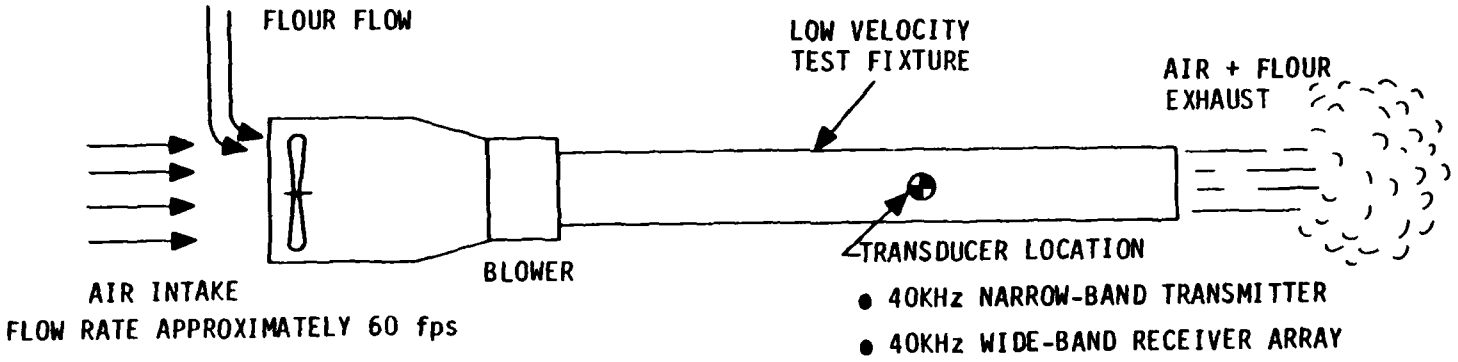

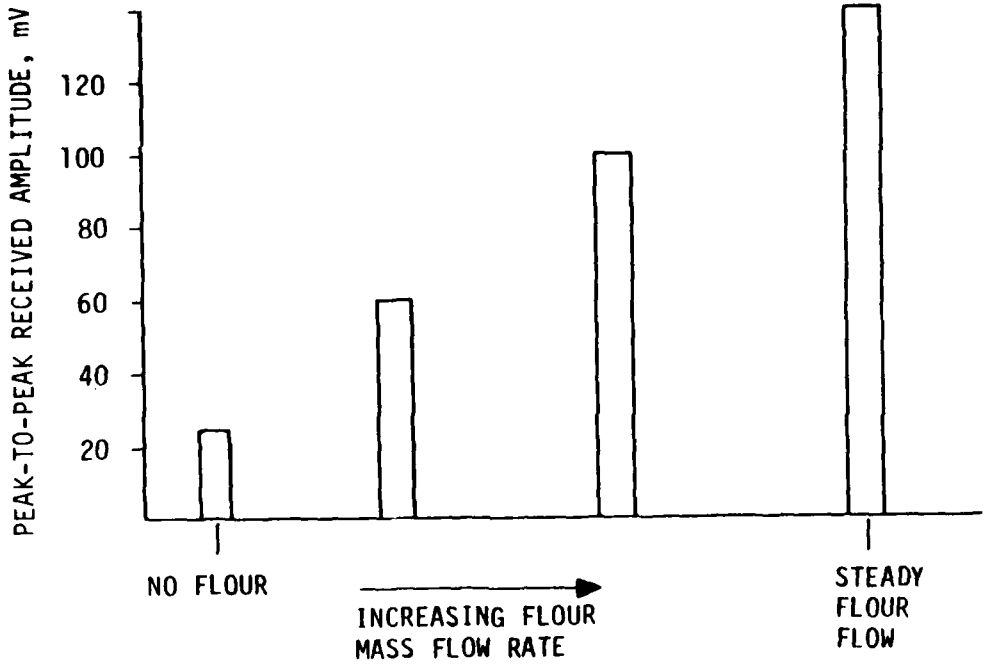

Figure 19. Increasing noise amplitude with increasing flour mass flow data.

The amplitude of the noise levels observed during the flow tests was quite large. The maximum measured noise signal of $\pm$ 80 mV was approximately 46% of the maximum signal received from the ultrasonic transmitter. This amount of noise under conditions that were relatively benign compared to those anticipated in the field caused some concerns. A signal-to-noise ratio of only 2 to 1 for dusty air flow could drop to approximately 1 to 4 in a 100% helium atmosphere based upon the results of the sensitivity tests. To try to minimize the chances of losing the signal in the noise, particular attention was given to increasing the power of the transmitted signal to its maximum practical value and to fabricating a blast-wing housing that would promote flow parallel to the face of the receiver in order to minimize particle impacts.

2.5 TESTS IN THE TRW 4-INCH SHOCK TUBE.

Tests performed in the low velocity flow fixture provided some valuable insights into the performance characteristics of the ultrasonic transducers. However, tests were desired under shocked, dusty flow conditions in order that the operation of the system could be ascertained under conditions approaching those expected in an actual high-explosive simulation. Arrangements were made with TRW personnel to conduct tests in their 4-inch shock tube facility in conjunction with the other dusty flow test programs being supported by that facility. The goals of the testing program were primarily oriented toward evaluating the survivability of the transducers and the potential for shock-generated noise. The shock tube provided a means to expose the ultrasonic system to shock an environment characterized by wave passage, dusty, transonic flow and fluctuating pressures.

2.5.1 Arrangement of Experiment.

Several restrictions were imposed by the small size of the shock tube. First, the transmitter and receiver separation was governed by the 3.5-inch clear space of the shock tube. This close spacing increased the strength of the reflected signals that were very noticeable during the low-velocity flow tests. A range of pulse rates from approximately 50 to 500 pulses per second were planned for the series of tests. Post-test evaluation of the data would be used to determine the highest rate that was practical. The rate of ultrasonic pulse transmission selected as optimal was reduced to approximately 200 pulses/sec. The location available for installation of the ultrasonic station was near the end of the test section and was likely subjected

to reflected signals resulting from passage of the shock wave from the test section into the dump tank approximately 12 inches downstream. Third, the duration of a typical shock pulse was approximately 5 msec, as shown by the oscilloscope trace in Figure 20. This limited the number of data points attainable in a specific test to only 1 or 2 in the shocked flow. For these reasons, the collection of actual measurements was only considered as a possible bonus to the evaluation of survivability.

The test configuration of the ultrasonic system for the TRW shock tube tests is shown in Figure 21. The shock tube test section had a cross-section approximately 3.5 inches square with the dust bed in place. Eight 10-inch diameter ports are located along the test section at four equally spaced stations that have a port on each side. Testing in the shock tube required the fabrication of two special port cover plates capable of supporting installation of the ultrasonic transducers as indicated in Figure 21. The installation of the receivers incorporated the same synthetic rubber compound around their periphery to isolate the receivers from mechanical vibration.

A total of 5 receivers and 1 transmitter were used in the TRW shock tube tests as shown in Figure 22. Four receivers, spaced two inches between centerlines, were used to attempt to track the transmitted pulse. The remaining receiver was located in the same port covering that housed the transmitter and was used to measure the shock-generated noise only. The transmitted beam centerline was set to be between the first two upstream receivers. Placement in this configuration was chosen to allow beam deflections to be more readily noticed. The maximum anticipated downstream deflection of the ultrasonic pulse was estimated, using normal shock relations, as 4.0 inches which corresponds to Mach 1.15 flow. In this position, the second downstream receiver (R2 in Figure 22) could monitor beam movement over 2 inches whereas it would only be able to monitor beam movement for 1 inch in a configuration in which it was lined up directly opposite the transmitter.

The driver used for these experiments was also intended for use in the MINI SCALE 2 field test. The instrument was capable of being powered by batteries or by a 120V A.C., 60Hz power supply. The amplifier was powered by batteries and was also intended for dual use in the MINI SCALE 2 field test and the TRW shock tube tests. Circuit diagrams for the driver and amplifier are provided in Figures 23 and 24. The amplifier could only support 5 channels of output. Therefore, receiver R4 was

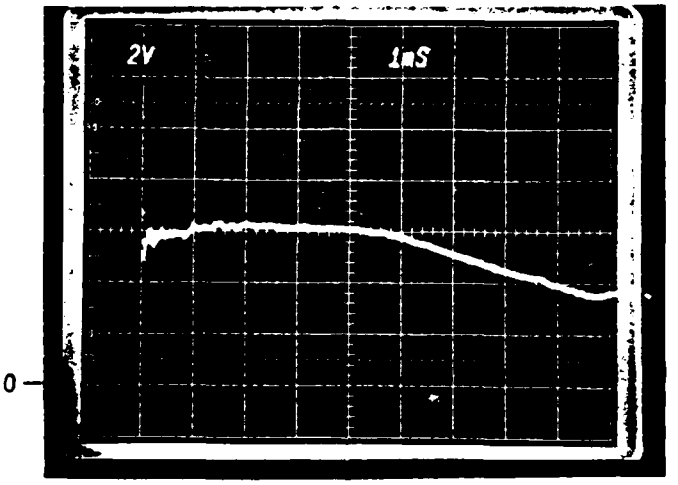

VERTICAL SCALE APPROX. 6.6 PSI/CM

HORIZONTAL SCALE = 0.001 SEC/CM

Figure 20. Typical 4-inch TRW shock tube pressure history.

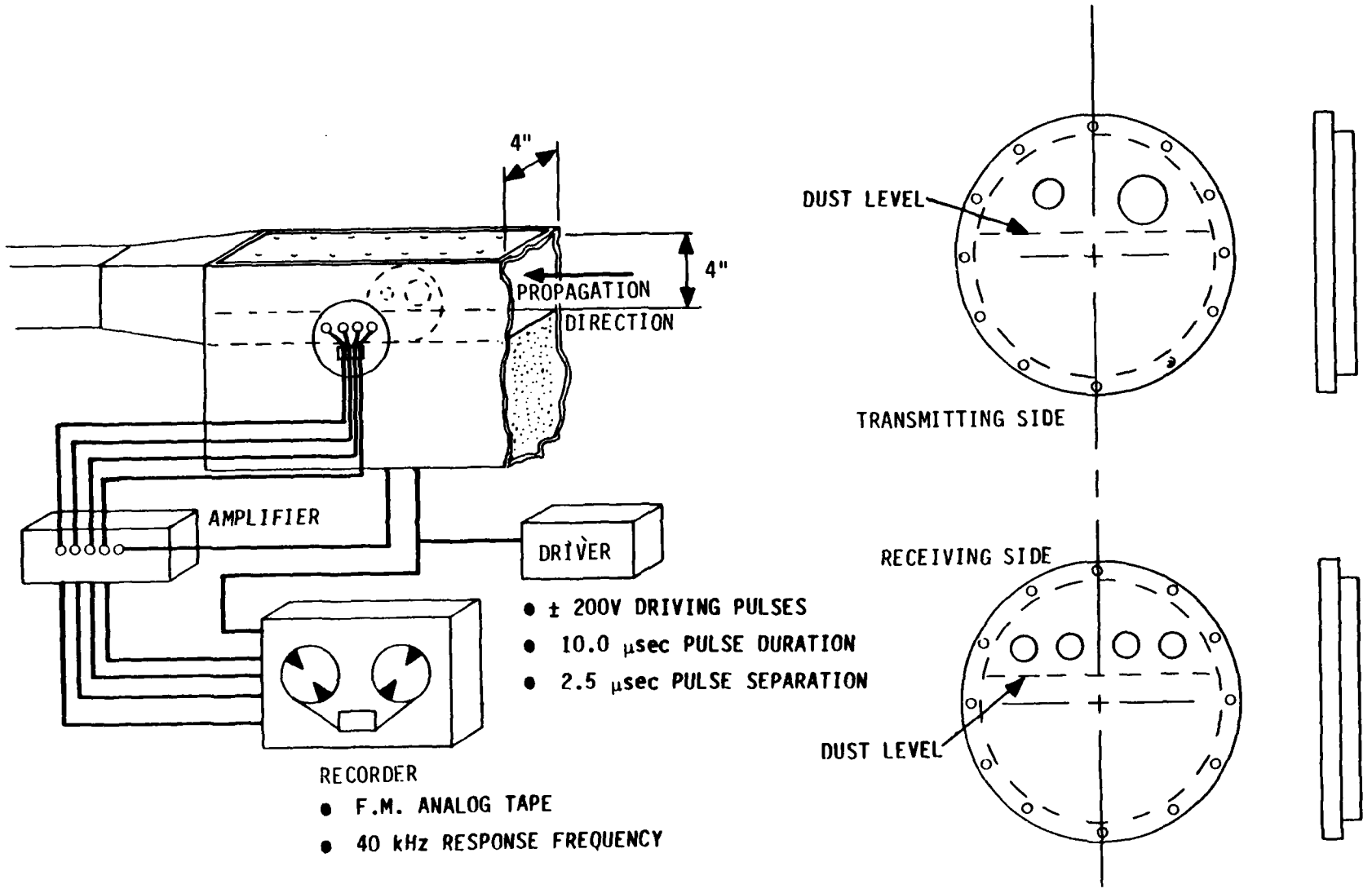

Figure 21. TRW shock tube test fixture.

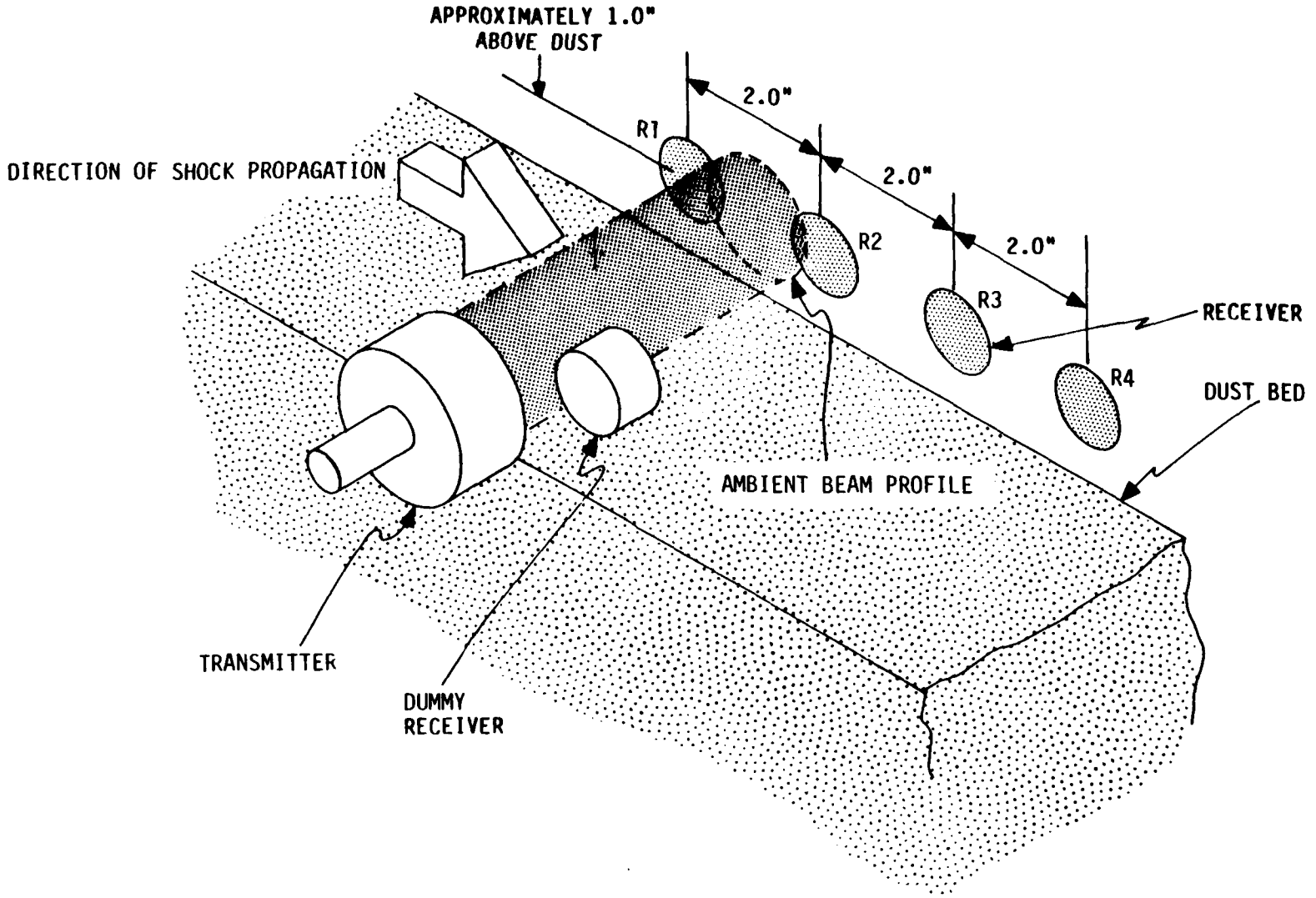

Figure 22. Arrangement of test fixture used in TRW 4" shock tube.

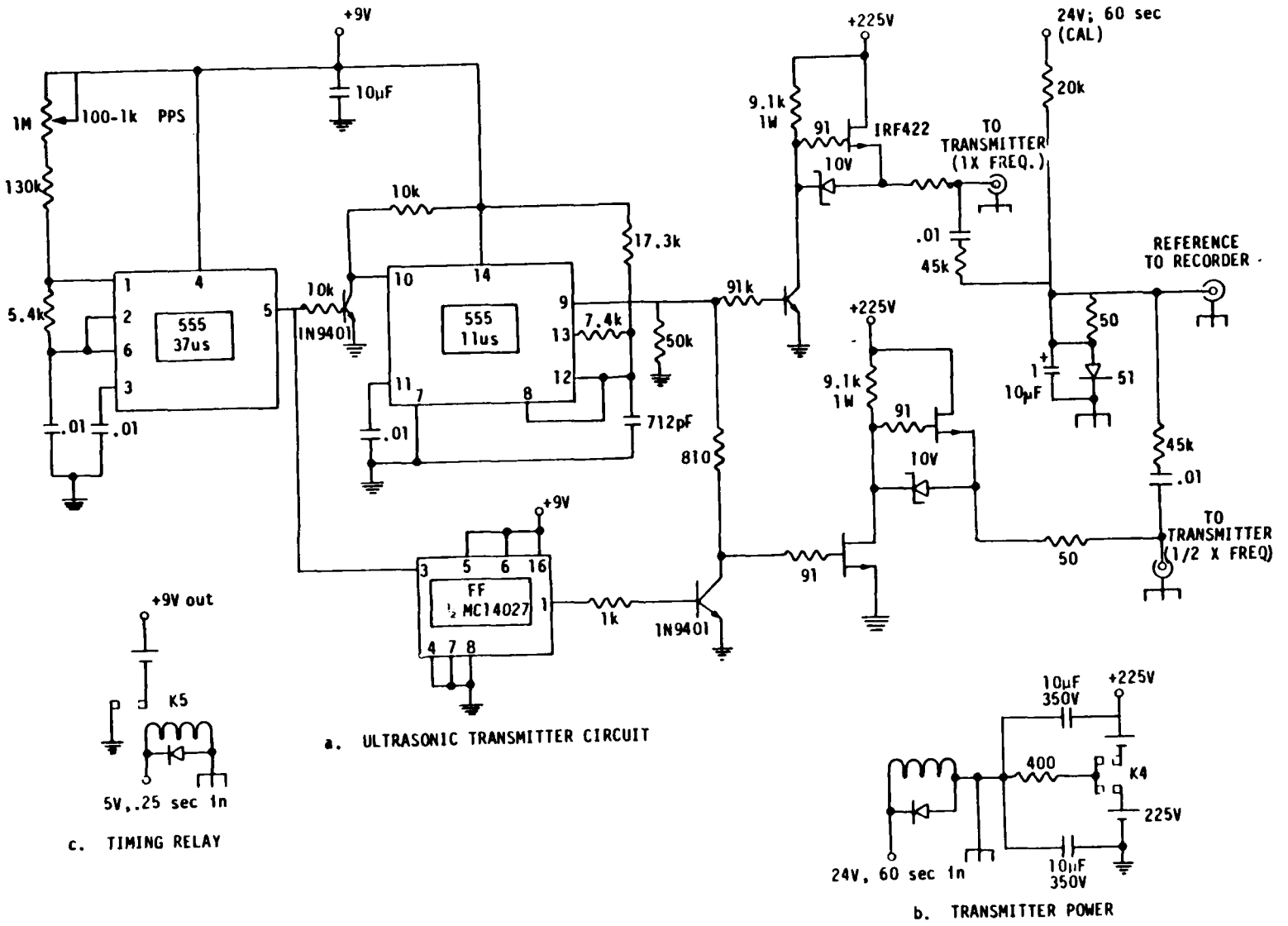

Figure 23. Ultrasonic transmitter circuitry.

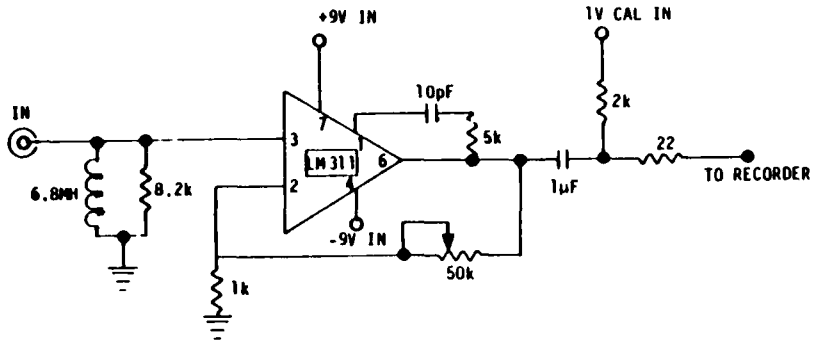

a. TYPICAL ULTRASONIC RECEIVER AMPLIFIER CIRCUIT

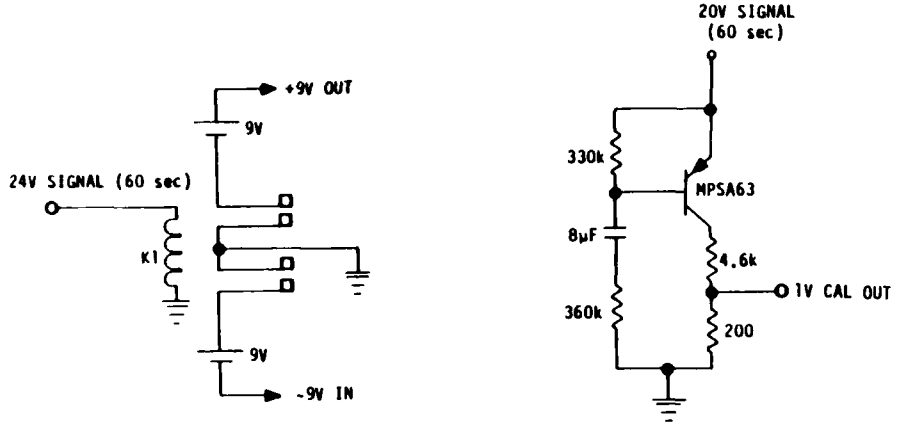

b. RECEIVER AMPLIFIER POWER CIRCUIT

c. RECEIVER AMPLIFIER CALIBRATION CIRCUIT

Figure 24. Ultrasonic receiver circuitry.

not monitored during the test. Output from the amplifier was recorded on a SANGAMO, 14-channel, F.M. analog tape recorder with a response frequency of 40,000 Hz (tape speed of 120 inches per second). The analog data was digitized using a NORLAND 3001A data acquisition system. Preliminary digitization was performed using intervals of 1)sec, 2)sec, and 5)sec. to investigate the potential impact on data reduction. A digitization interval of 2)sec was selected based on this investigation.

2.5.2 Experimental Results.

The shock tube tests yielded two very important results. First, it was made clear that the transducers were not subject to failure as a result of pressure loading attributable to the 20 psig shock passage. Post-test recovery indicated that all but one of the transducers survived. The transducers were not only in place during the five active tests for which data was recorded, but were also subjected to five to ten additional tests prior to their removal by TRW personnel. Investigation into the failure of the one receiver led to the conclusion that the failure was most likely due to mishandling during removal and transport from TRW.

Examination of the data revealed a problem in the sensitivity of the receivers to shock and dust induced noise. All tests indicated a loss of coherent signal immediately following shock arrival. Only at very late times (greater than approximately 25 msec) did the noise level decrease to a point that pulses could again be distinguished.

Several explanations were hypothesized for the poor data return. A possible reason for the poor performance was based upon the location of the ultrasonic sensors in the shock tube. Lab tests of receiver ring-down had shown that noise produced by striking the face of the receiver dissipated after approximately 2 or 3 msec. This was true even for impacts sufficient to cause permanent deformation of the receiver face. The fact that meaningful signal was being lost in the shock tube tests for such a long period of time was an indication that some other phenomenon may have been occurring. The proximity of the test ports to the end of the test section supported the possibility that the receivers could have been exposed to multiple reflected shocks that may have increased the duration of noise signals. Observations of dust flow in the shock tube along with post-test examination of the receiver face indicated that dust particle impacts were probably not the primary cause of the extended noise. The dust bed transition construction itself could also have been

responsible for the generation of some reflected shock structure near the end of the test section. The other conclusion that could have been drawn was that the receivers were too sensitive to the combination of pressure fluctuations and particle impacts to be useful in receiving the transmitted signal.

After the evaluation of all of the test data and possible explanations of why the received signals were so noisy, there was a great deal of uncertainty regarding field performance of the system that had been used in the TRW tests. This result was very disappointing as the shock tube tests were being performed at the same time that final preparations were being made for the system to be installed in the MINI SCALE 2 test. However, limitations in the schedule of MINI SCALE 2 prevented the investigation of receiver hardening designs in time to be of use in their field test. A decision was made to proceed as planned with the MINI SCALE 2 fielding effort and to simultaneously undertake laboratory tests of possible modifications to the receivers that would minimize their sensitivity to noise assumed to be produced by shocked, dusty flow. In this way, if the results of MINI SCALE 2 confirmed that problems observed in the TRW tests were not only shock tube related, a means would be available to modify the sensors for evaluation in future tests.

2.6 EXPERIMENT DESIGN FOR MINI SCALE 2 FIELD TEST.

The ultrasonic sound speed and flow velocity experiment fielded in MINI SCALE 2 consisted of an aluminum dual blast wing structure housing the ultrasonic transducers and an adjacent below ground instrumentation bunker to house the electronic components of the experiment. Details of the blast wing and instrumentation bunker are provided in Figure 25 and 26. The arrangement of the transducers on opposite blast wing faces was very similar to the same as that used in the TRW shock tube tests.

Predictions of expected flow velocities were as high as Mach 2.0. This indicated the possibility of having the transmitted pulse being displaced downstream a distance equal to twice the 6-inch blast wing separation distance or 12 inches. A possible solution would have been to use 13 receivers with 2-inch center-to-center spacing to cover the expected beam displacement. An alternate solution using two transmitters was chosen. As with the TRW tests, one transmitter would transmit to four receivers, spaced 2 inches center-to-center. The initial transmitter alignment, however, corresponded to the first downstream receiver rather than between the

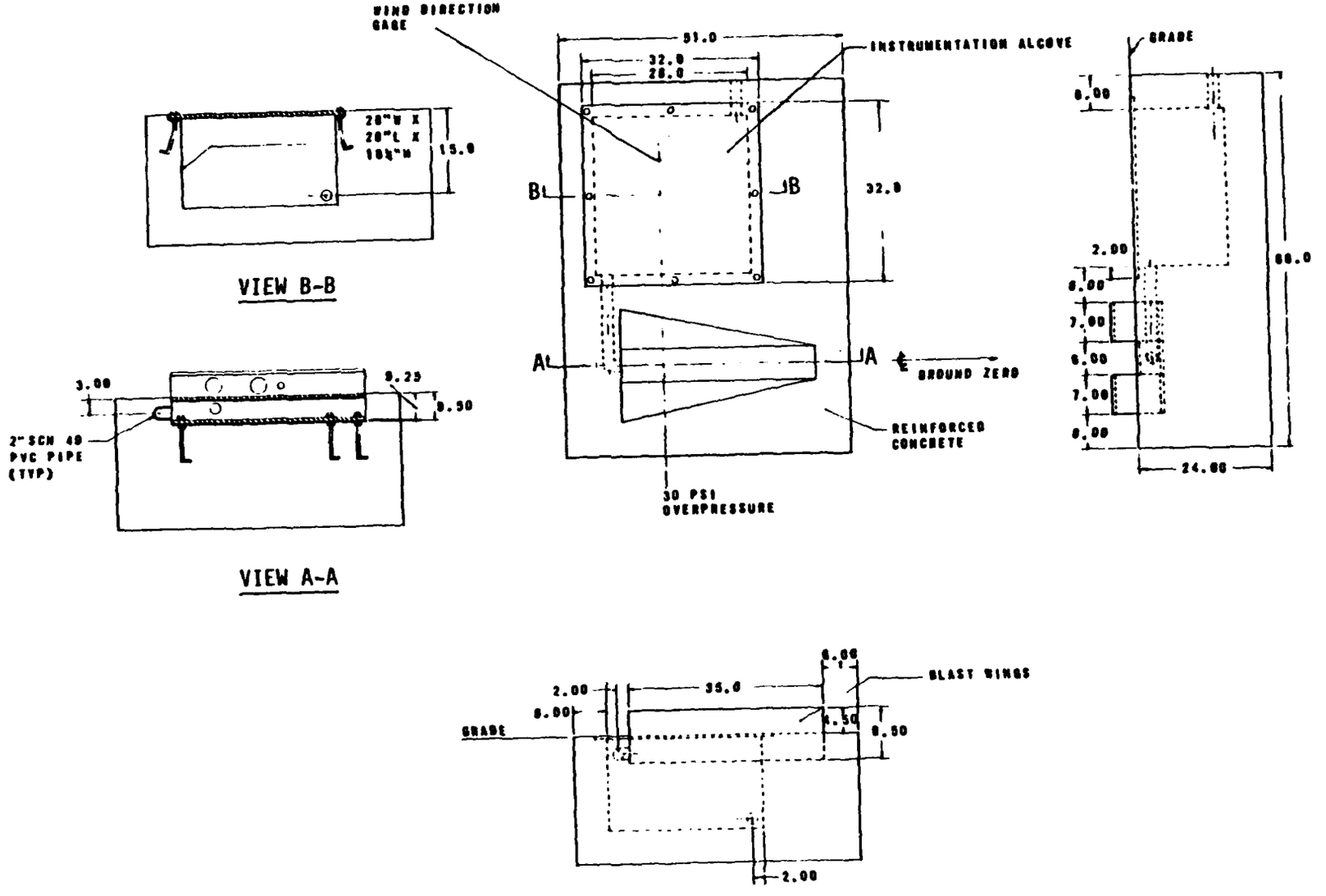

Figure 25. Engineering drawings of blast wings - general.

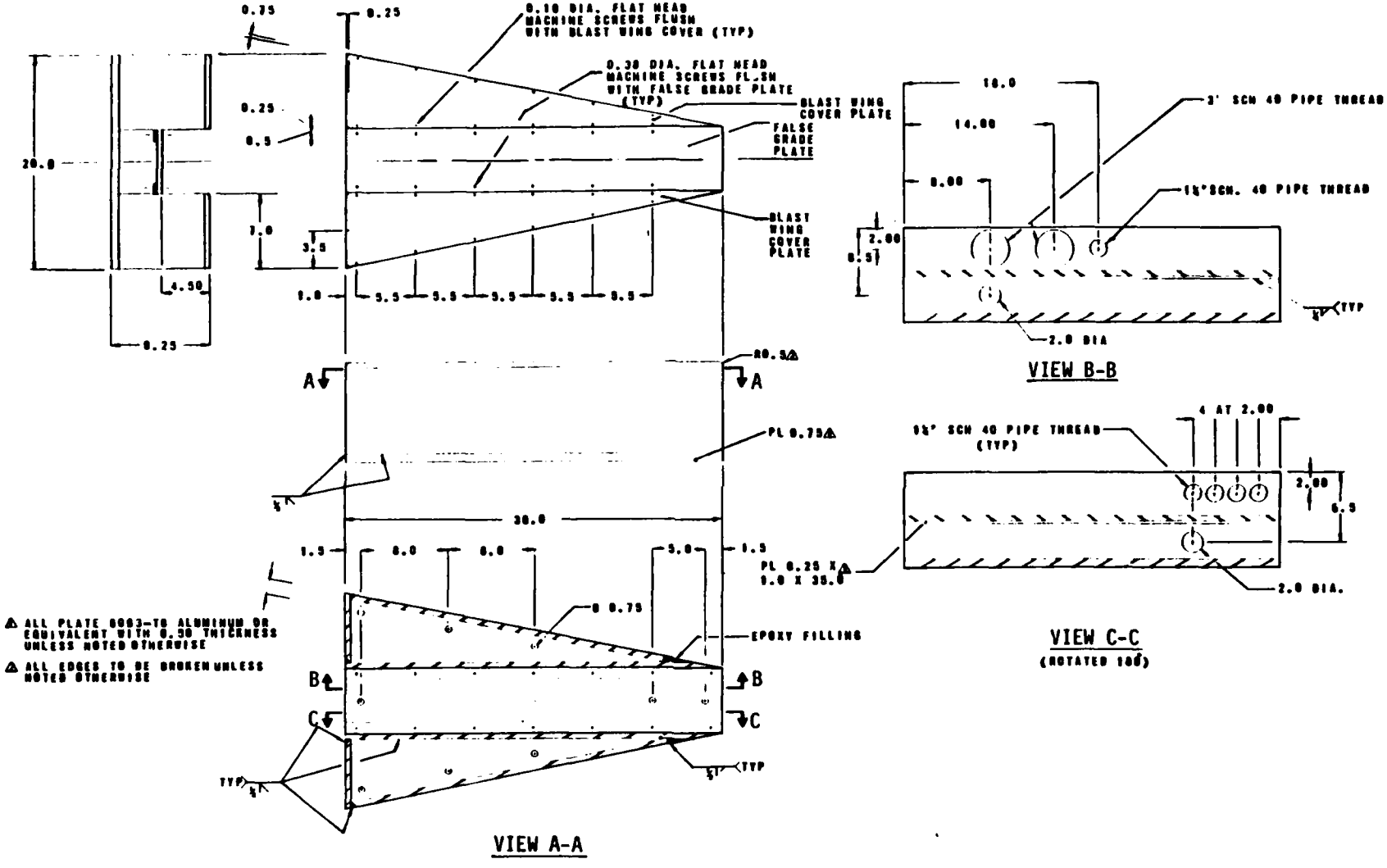

Figure 26. Engineering drawings of blast wings - blast wing structure.

first and second receivers. Signals from this transmitter could be received for flow velocities slightly in excess of Mach 1.0 (see Figure 27). To enable operation at higher flow velocities, a second receiver was placed 6 inches upstream of the first. Signals from the additional transmitter could only be received at flow velocities between approximately Mach 1.0 and Mach 2.0 (see Figure 28). In order to differentiate the signals of the two transmitters, the pulse repetition rate for the sub-sonic flow transmitter was half that of the transmitter active for flows between Mach 1.0 and Mach 2.0. The mounting of the receivers in the blast shields differed slightly from previous tests. As shown in Figure 29, the receivers were cast into place inside a section of PVC pipe with the same synthetic rubber compound used on previous tests. However, in order to broaden the response of the receiver an inductor was attached and shielded as shown in the figure. The use of the PVC pipe facilitated easy installation of the receivers since they only had to be screwed into place.

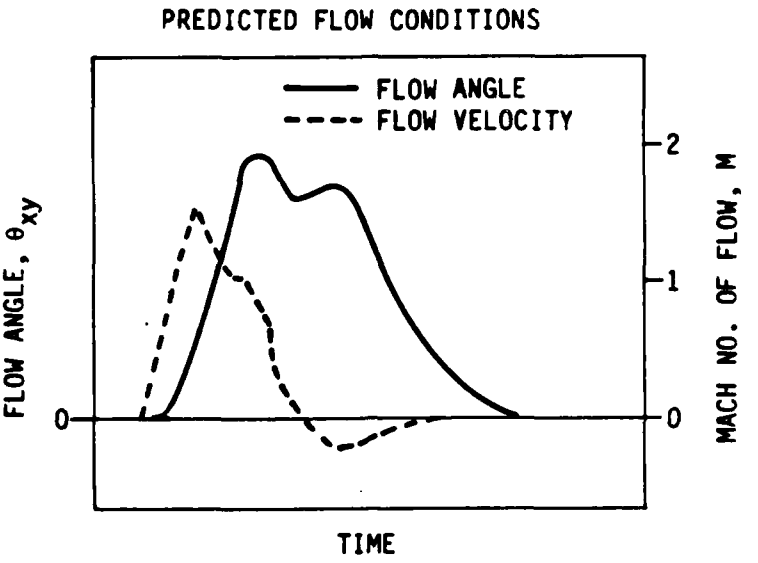

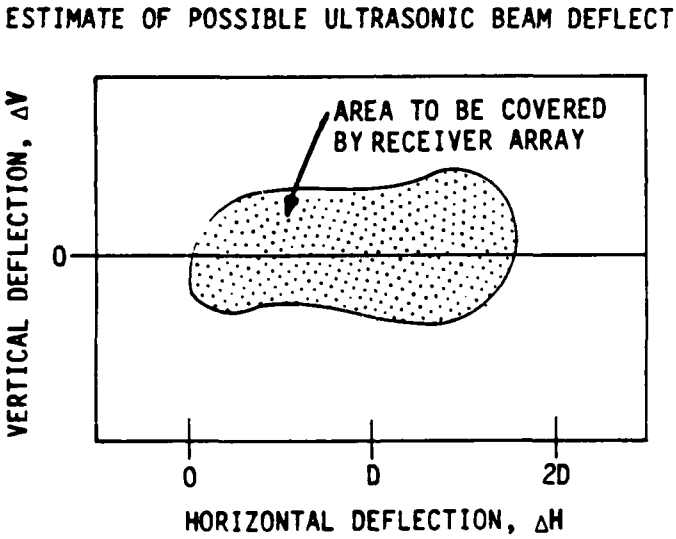

D = BLAST WING SEPARATION

c = ESTIMATE OF SOUND SPEED

$\Delta V = Mc \sin \theta_{xy} \Delta t$

$\Delta H = Mc \cos \theta_{xy} \Delta t$

$\Delta t = \frac{D}{c}$

Figure 27. Rationale for sizing receiver array for one transmitter.

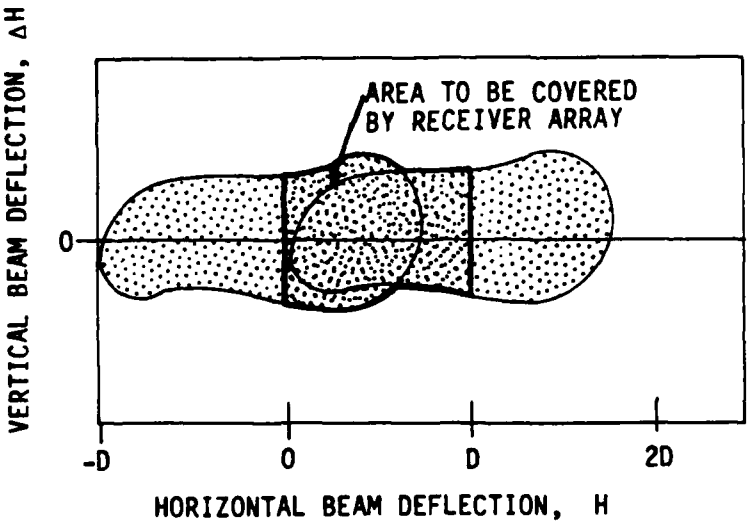

D = BLAST WING SEPARATION

= UPSTREAM SEPARATION OF SECOND TRANSMITTER FROM FIRST TRANSMITTER

c = ESTIMATE OF SOUND SPEED

$\Delta V = Mc \sin \theta_{xy} \Delta t$ FOR BOTH TRANSMITTERS

$\Delta H = Mc \cos \theta_{xy} \Delta t$ FOR FIRST TRANSMITTER

$\Delta H = Mc \cos \theta_{xy} \Delta t - D$ FOR SECOND UPSTREAM TRANSMITTER

$\Delta t = \frac{D}{c}$

Figure 28. Rationale for sizing receiver array with two transmitters.

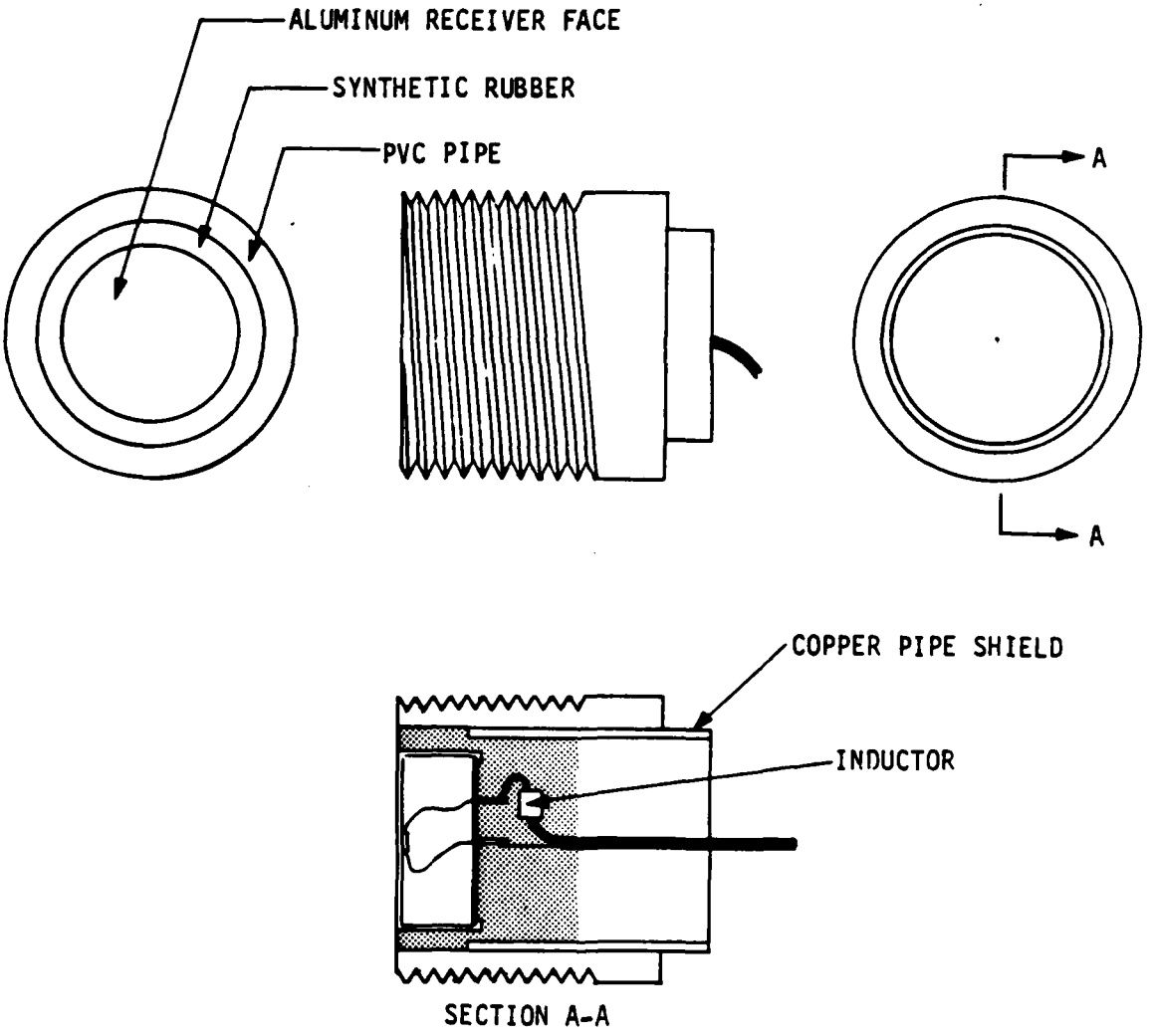

Figure 29. Modified ultrasonic receiver housing for MINI SCALE 2.

SECTION 3
FLOW DIRECTION GAGE

In addition to the ultrasonic sound speed and flow velocity gage experiment, NTS fielded a prototype three dimensional flow direction gage. The goals of this effort were to test the survivability of the gage design, evaluate quality of the data returned from the gage and make a general evaluation of potential gage development.

3.1 THEORY OF GAGE OPERATION.

The design of the three dimensional flow direction gage was based upon the idealized response of a sphere immersed in the dusty precursed flow field. A non-lifting spherical body placed in a flow field is subject to aerodynamic and viscous drag forces as well as load transferred by particle impacts. The magnitude of these combinations of forces is dependent upon many variables (e.g., flow velocity, dust density, gas density, and particle size distribution), most of which are not known for an actual field test. The direction of the various forces, for the most part, is coincident with the direction of flow. Loading in other directions arises as a result of vortex formation in the wake of the sphere, skew particle impacts and slight imperfections in the sphere geometry. Of these, vortex formation has the greatest potential for leading the significant forces that are not aligned with the flow. However, vortex-induced forces are generally normal to the flow direction and periodic in nature. Also, the build-up of vortices requires some finite interval of time which is likely to be greater than the length of record of interest in small-scale high explosive experiments (50 to 60 msec). For these reasons, the design of a flow-direction gage based upon the use of a sphere as a nonlifting body immersed in the flow field.

The configuration of the flow direction gage fielded in MINI SCALE 2, shown in Figure 30, utilized a 1-inch diameter brass sphere to which four wire strands were attached to facilitate measurement of flow-related loads. The wires were located such that they all passed through the center of the sphere. One wire was located in the upper hemisphere and was parallel to vertical. The remaining wires protruded at equal intervals around the lower hemisphere, exiting the sphere at an angle of 30° below the horizontal. If it is assumed that the wires are capable of carrying tension and compression, and the presence of the one vertical wire is ignored, an estimate of the maximum compressive force expected in the three lower wires can be

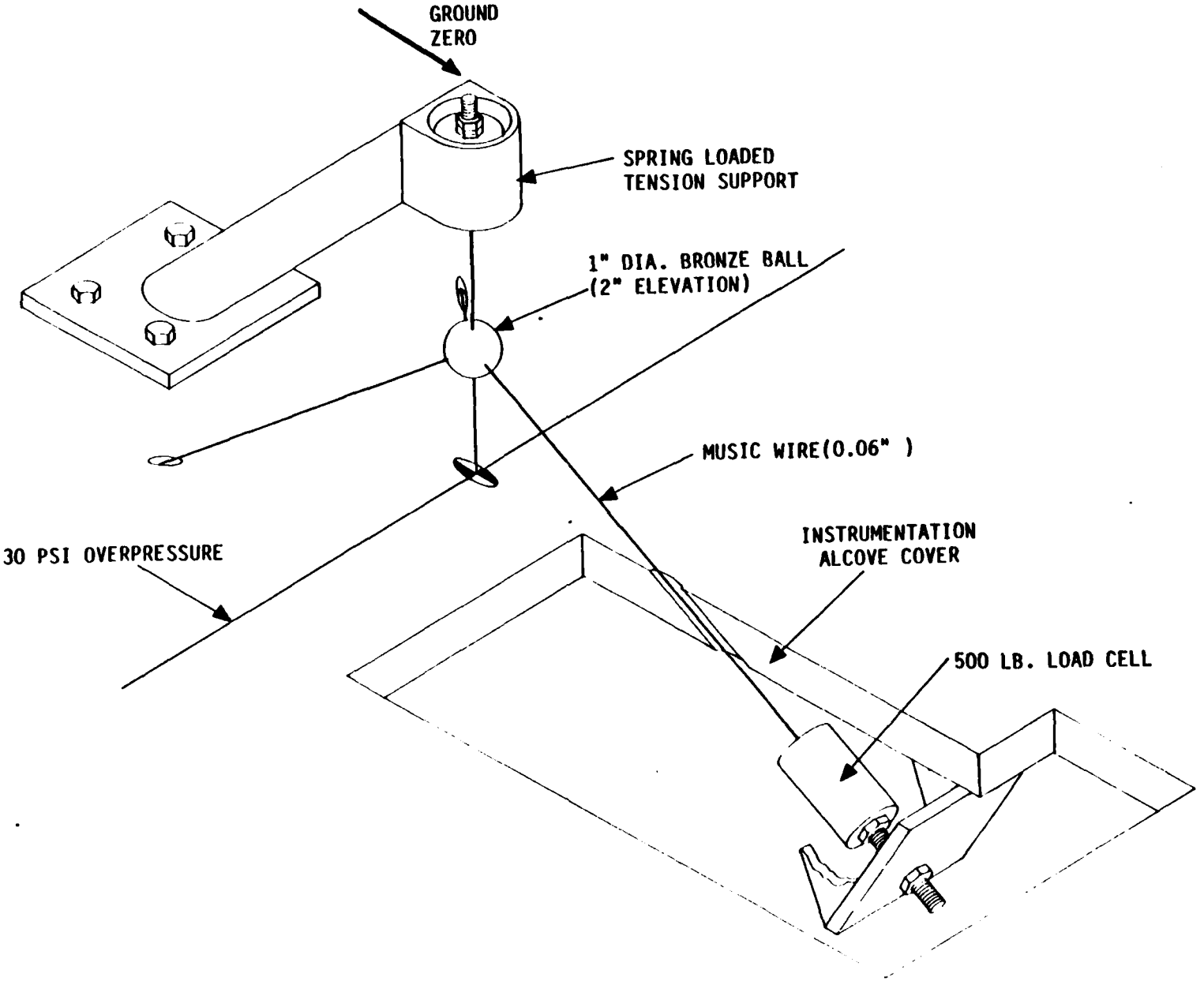

Figure 30. Prototype wind direction gage for MINI-SCALE.

made based upon drag characteristics of the sphere under predicted flow conditions. The need for four wires to make a three-dimensional measurement arises from the inability of a thin wire to carry any appreciable compressive load. The simple geometry of the assemblage of wires is such that a tensile force of T in the vertical wire produces a tensile force of 2/3 T in the remaining three wires. Using this relationship and estimates of drag forces on the sphere, a tensile force, T, can be calculated such that the lower wires will always experience tensile load.

If the tensile force, T, is assumed to be constant and if the displacement of the sphere is assumed to be negligible, formulation of the relative magnitudes of components of the flow can be readily derived from measurements of the change in tensile load of the three lower wires as indicated in Figure 31 for a coordinate system coincident with the radial, tangential and vertical flow components. Knowing the flow components, the angle of flow relative to any plane can be calculated directly. This is also shown in Figure 31 for the same coordinate system.

3.2 DESIGN OF THE FLOW DIRECTION GAGE.

The design of the various components of the flow direction gage involved consideration of the dynamic response characteristics required of the system and the required strength necessary to maintain structural integrity of the system. Conversion of theory into practice typically involves some compromises and this effort was not an exception. Engineering drawings of the gage are provided in Figure 32.

The gage was installed in the aluminum plate used to cover the instrumentation bunker adjacent to the ultrasonic transducers blast shields. Vertical tension was provided by a cam spring rated at 800 lbs. per inch of displacement. A 1-inch diameter aluminum rod, placed behind the brass ball and inclined at 45°, supported the spring assembly. Music wire was used in the gage because its high tensile strength allowed the selection of small diameter wire which helped to minimize flow disturbances near the sphere. The diameter of the pretensioning wire was 0.059 inches and the diameter of the remaining three wires was 0.047 inches. A brass ball was chosen based upon considerations of ease of workability and desirable brazing qualities.

One of the more critical aspects of the gage design concerned the connection of the music wire to the brass ball. Calculations of the ultimate capacity of a soldered

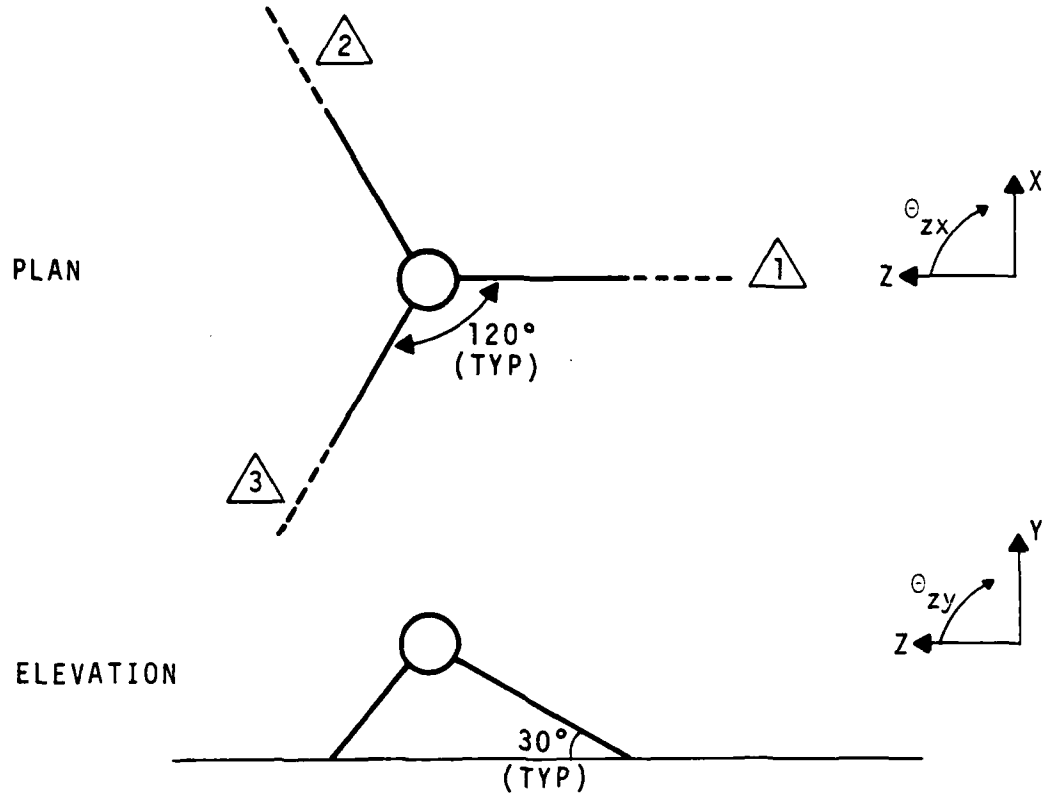

ASSUMING BALL REMAINS STATIONARY:

$$Z = {}_{z} = -(\textcircled{2} + \textcircled{3})\ \cos 30\ \sin 30 + \textcircled{1}\ \cos 30$$

$$X = {}_{x} = (\textcircled{3} - \textcircled{2})\ \cos^2 30$$

$$Y = {}_{y} = (\textcircled{1} + \textcircled{2} + \textcircled{3})\ \sin 30$$

$$\Theta_{xy} = \tan^{-1}\ (Y/X)$$

$$\Theta_{zx} = \tan^{-1}\ (X/Z)$$

$$\Theta_{zy} = \tan^{-1}\ (Y/Z)$$

Figure 31. Wind direction gage data reduction equations.

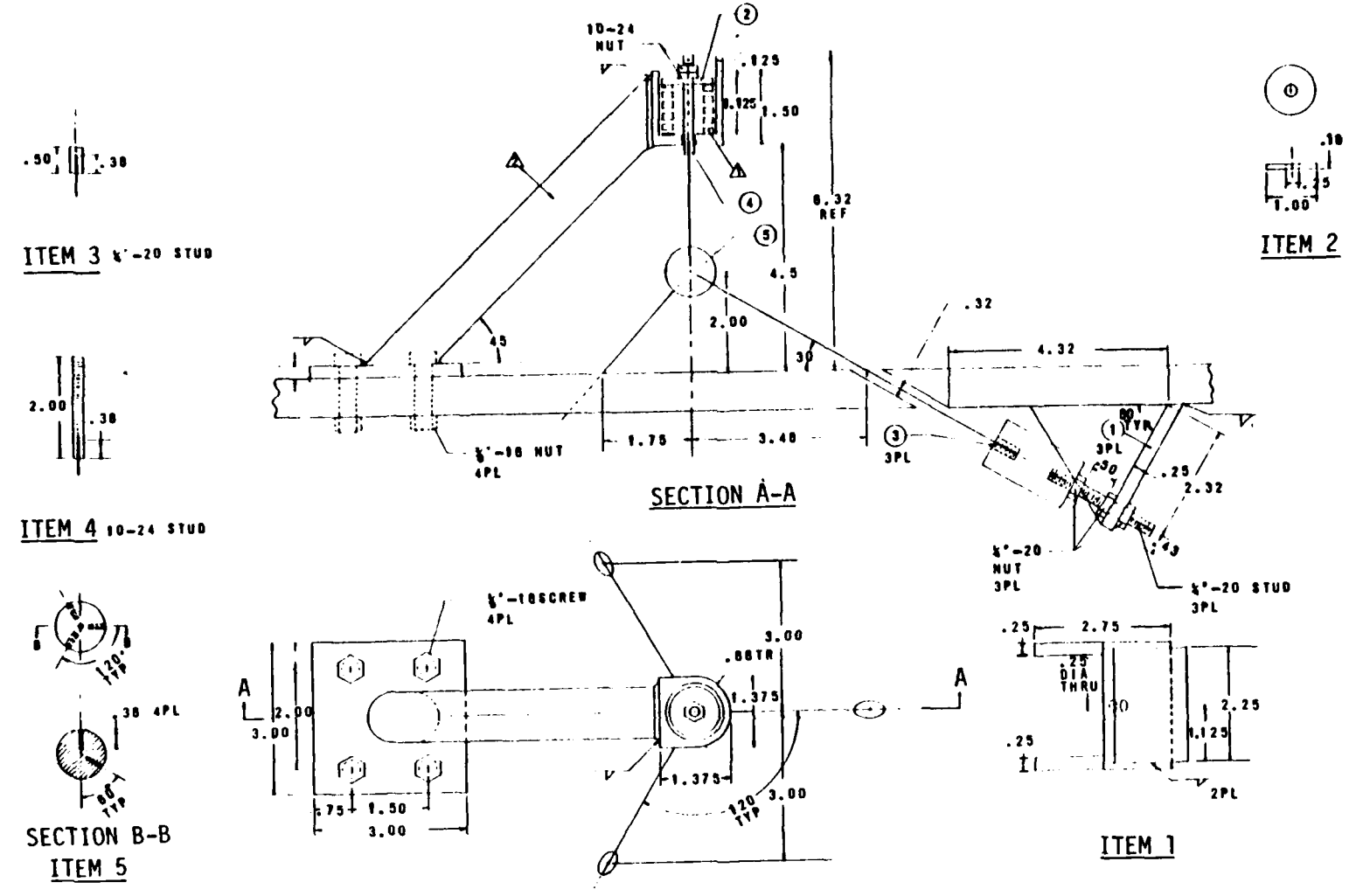

⚠ AL 6061-T6 ROUNDS 1" DIA. MAY BE MADE FROM 8' IN LENGTH

⚠ COMPRESSION DIE SPRINGS 1" HOLE SIZE .1" FREE LENGTH K=800 LB/IN.

Figure 32. Engineering drawing of wind-direction gage.

connection indicated that the strength of the connection was limited by the shear strength of the brass acting on a cylindrical area computed by using the depth of the wire in the brass and the diameter of the hole made to accept the wire and solder compound. Because there was considerable uncertainty regarding the strength characteristics of the brass, the quality of the soldering and the effect of heat applied during soldering on the music wire, several pull-out tests were performed on different combinations of wire size, hole diameter and hole depth. The solder used was All-State No. 430, high-strength solder. This product is a silver-tin alloy solder with a low working temperature of 430°F and a maximum tensile strength of 15,000 psi. The results of these tests indicated a minimum shear strength of 2,800 psi. The maximum design value was taken to be approximately one third of this value of 900 psi. Initial tension required for MINI SCALE 2 was estimated to be 150 lbs.

Knowledge of the natural frequency of the system was an important quantity for evaluation of response frequency and data reduction technique. The vertical vibratory response frequency of the sphere is dependent upon the mass of the sphere and the spring stiffnesses related to the vertical support rod, cam spring, main tensioning wire and load sensing wires. Calculated fundamental frequency was estimated to be 350 to 400 Hz. Periodic forcing related to vortex shedding was estimated to have a maximum frequency of approximately 2,400 to 4,000 Hz (Reference 3). The flow velocity corresponding to a shedding frequency approximately equal to the natural frequency was calculated to be 150 to 200 fps. Since this was in the lower 10% of the range of flow velocities of interest, the effect of substantial vortex-induced oscillations was neglected.

Load variations were measured with three strain gage load cells rated for 0 to 500 lbs. of load. Power for the load cells and amplifiers for the load cell output were provided in the instrumentation bunker. The signal was amplified prior to transmission to the tape recorders to help eliminate potential noise introduced by line noise in the cable runs back to the recording trailor. Recording was done using F.M. analog tape recorders with a response frequency of 40,000 Hz. A schematic of the electronics used for the flow direction gage load cells is provided in Figure 33.

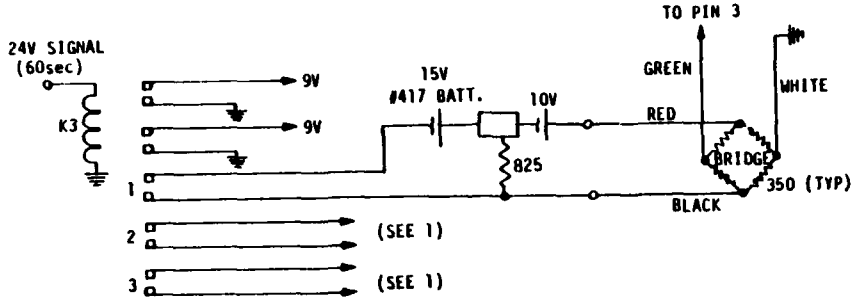

a. LOAD CELL CIRCUIT FOR FLOW DIRECTION GAUGE

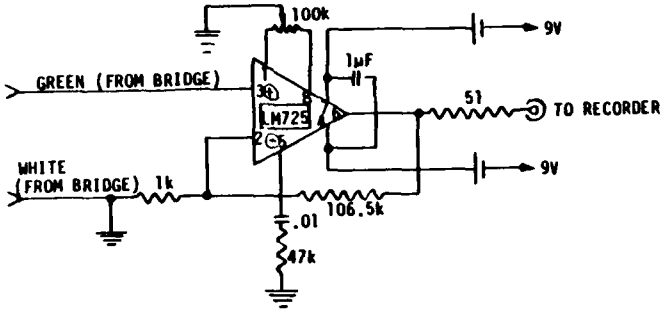

b. TYPICAL STRAIN GAUGE BRIDGE AMPLIFIER IN TO RECORDER

Figure 33. Flow direction gage circuitry.

SECTION 4
ELECTROLYTIC SOIL PRESSURE GAGE

The MINI SCALE 2 test provided an opportunity to test an electrolytic pressure gage design under development at NTS. The goals of the NTS development program are to produce a gage capable of measuring air-blast pressures produced in the cavity of a High Explosive Simulation Technique (HEST) simulator. Use of three gages as soil pressure sensors near the explosives container in MINI SCALE 2 provided a means to test the field operation of the gage electronics and to test the response characteristics of the gage.

The sensing element of the gage consists of a PVC container filled with a 0.1 normal solution of ammonia. A drawing of the canister design is shown in Figure 34. The ammonia solution exhibits piezoresistive characteristics that provide the basis for measurements. Changes in resistance are measured between two spherical platinum electrodes that extend into the container. Prior to field installation, all three gages were calibrated to approximately 19,000 psi. A typical calibration curve is shown in Figure 35. The arrows in the figure indicate the direction of loading. As the curve demonstrates, the gages do not exhibit perfectly linear behavior throughout their total range of loading. However, for the pressures expected for the MINI SCALE 2 test (approximately 1000 psi) the rate of change of resistance can be assumed linear. Significant variance was noticed in the sensitivity of the three gages. Similar variation has been observed in the past and has been found to be related to small inconsistencies in the machining of the platinum electrodes and small deposits of sealant on the surface of the electrodes.

The electronics package used in MINI SCALE 2 was specifically modified to cope with the low pressure levels of the test. A timing closure at -0.200 msec relative to zero FIDU activated the gage and provided sufficient time for the circuit to recover and allow an initial reading of current through the gage, and hence resistance. At approximately zero FIDU an internal timing circuit activated an A.C. amplifier with a gain of 100. In this manner, signal variations of 1% to 3% could easily be detected above the line noise present at the site. This process is shown schematically in Figure 36. A circuit diagram is provided in Figure 37.

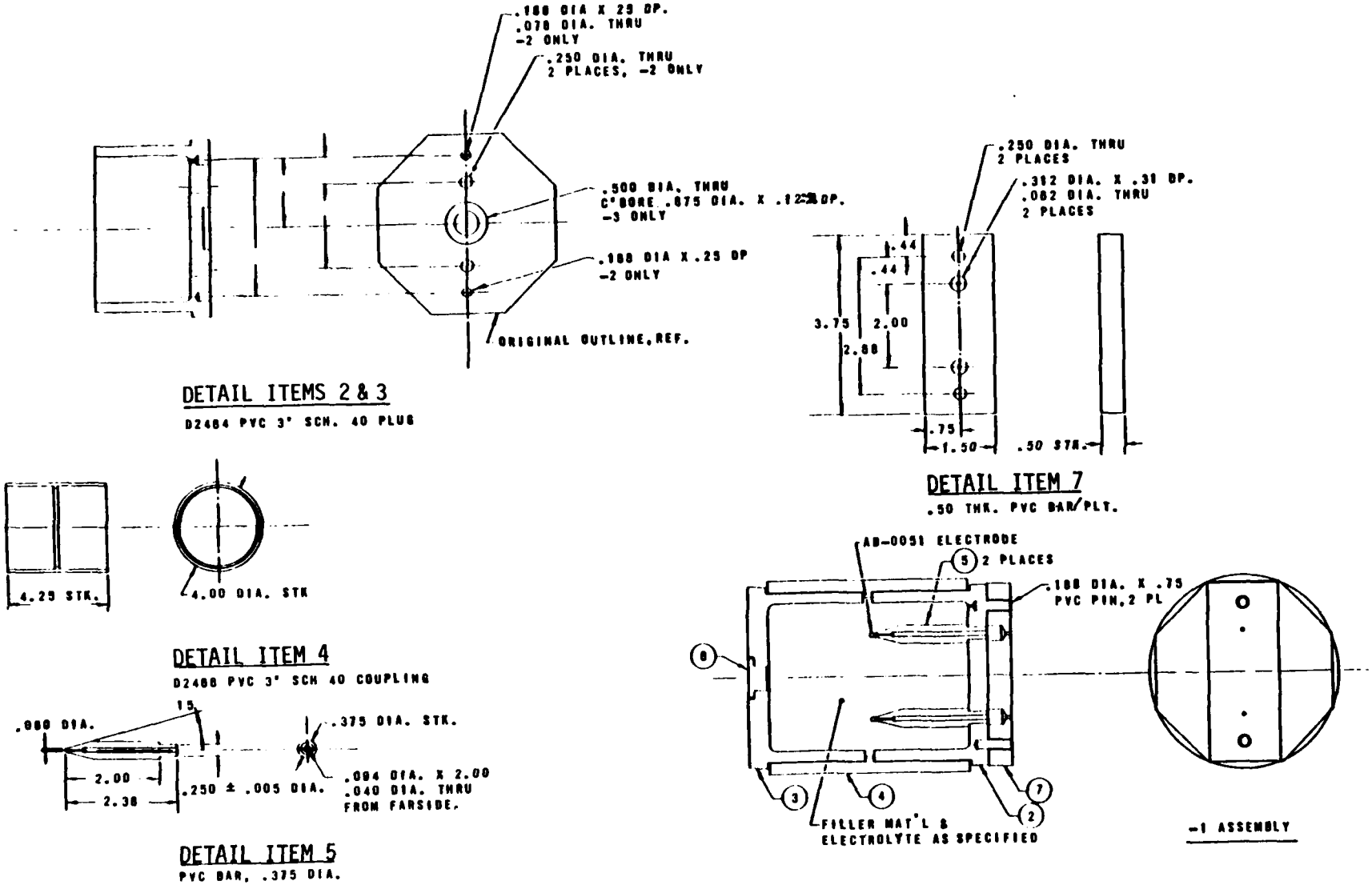

Figure 34. Electrolytic gage cannister design.

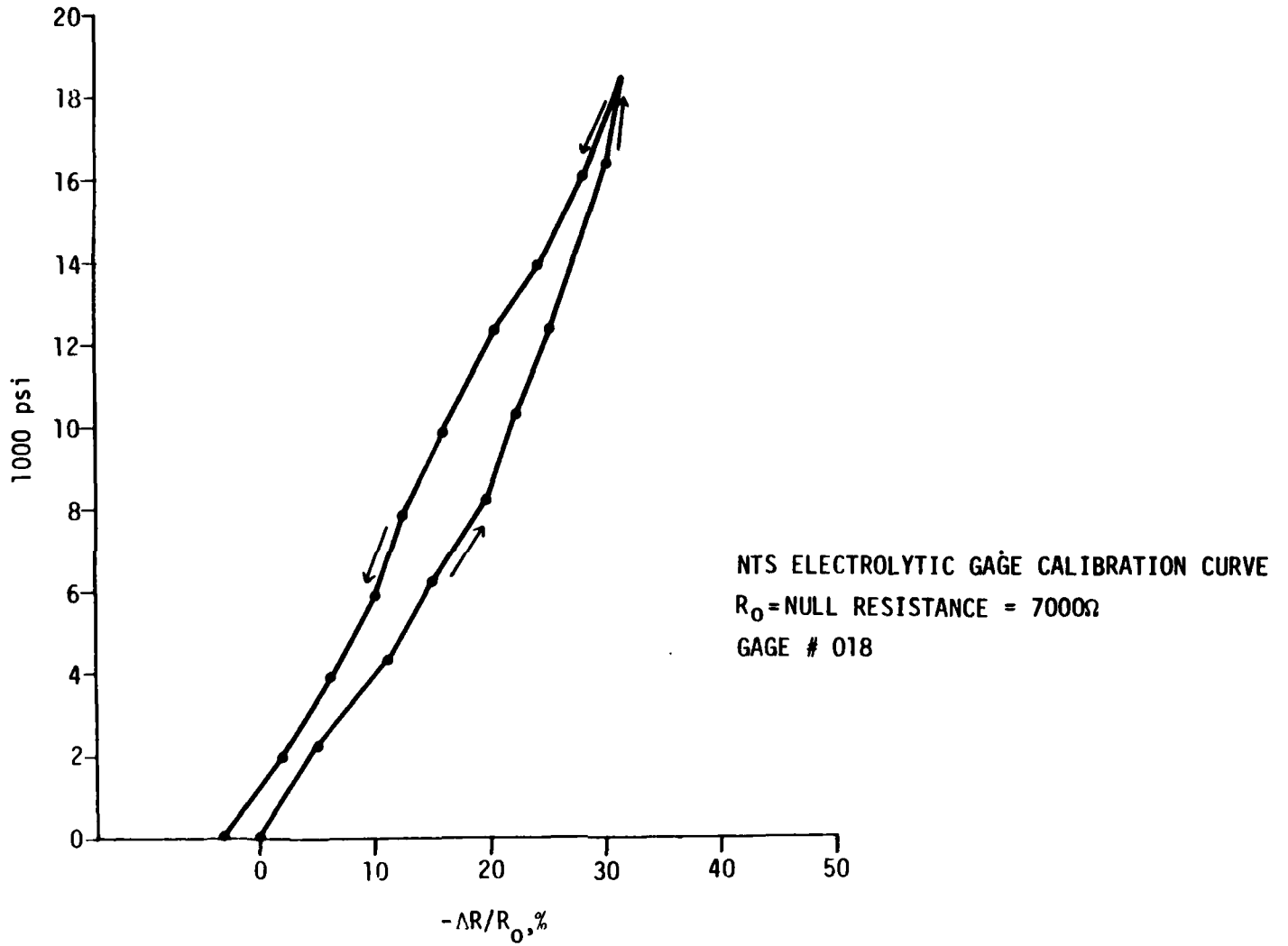

Figure 35. Electrolytic gage calibration curve.

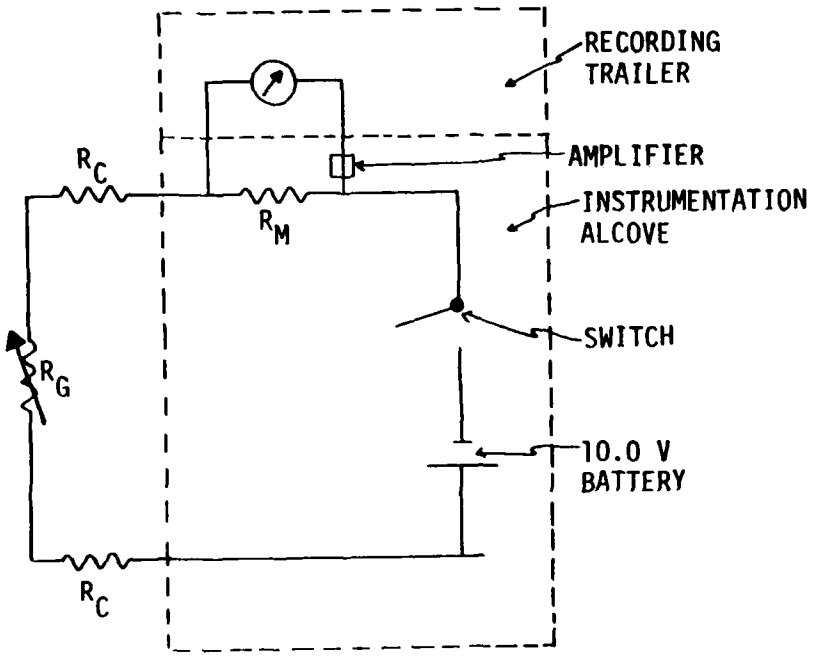

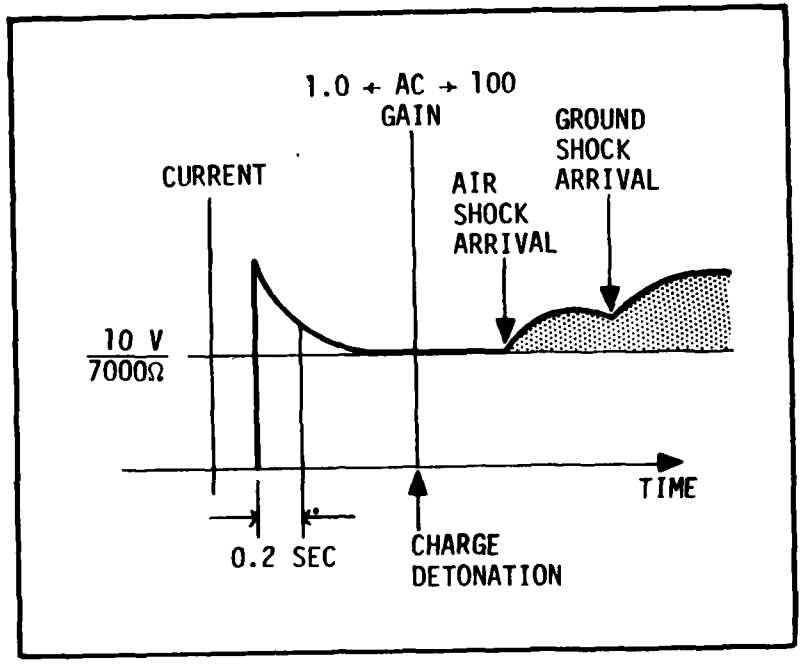

R_G = GAGE RESISTANCE (~7000Ω)

R_M = MEASURING RESISTANCE (~500Ω)

R_C = CABLE RESISTANCE (~1Ω)

Figure 36. Operational scheme of electrolytic gage for MINI-SCALE 2.

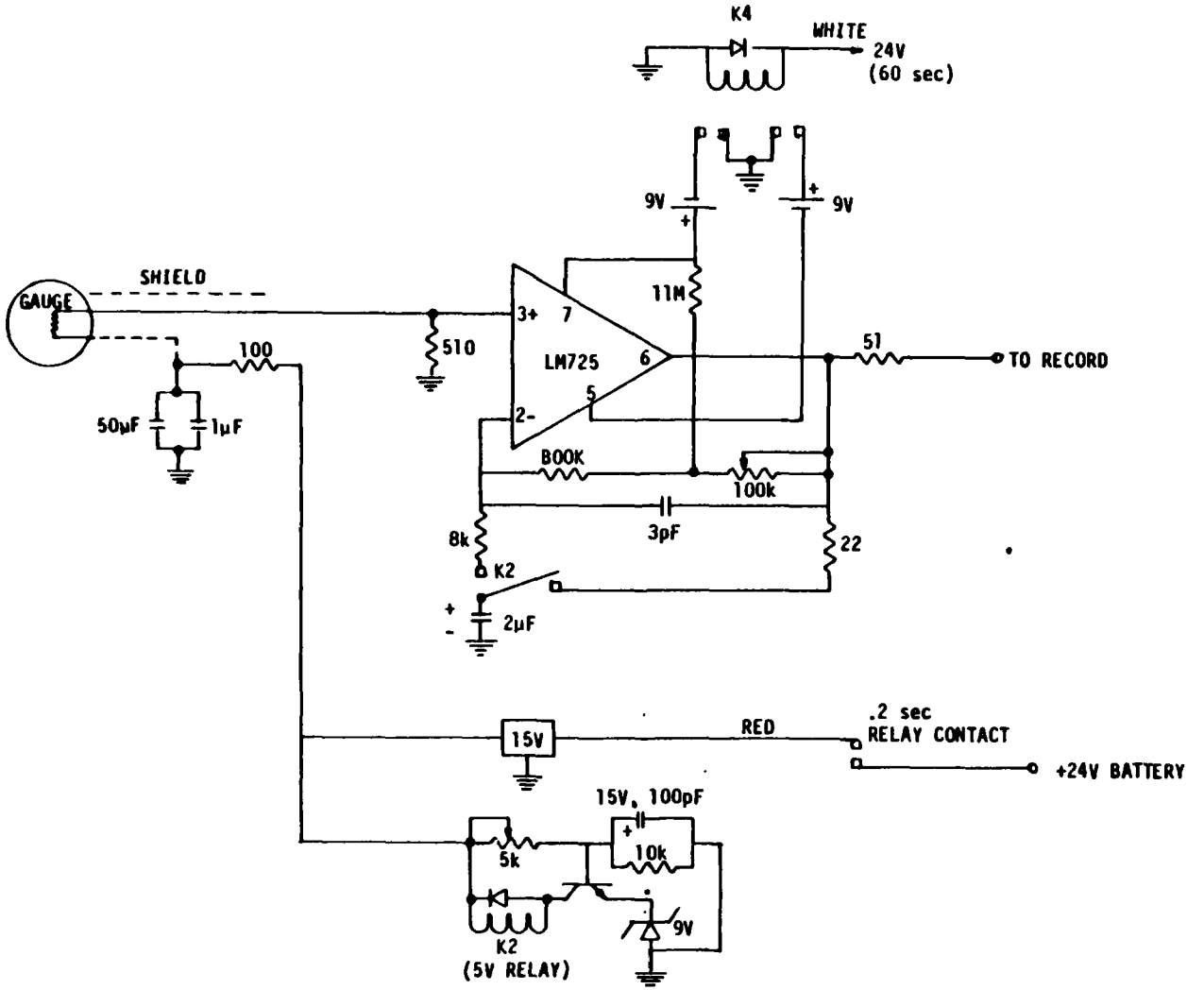

Figure 37. Typical electrolytic gage circuit.

SECTION 5
MINI SCALE 2 FIELD TEST

The MINI SCALE 2 test was a 24-ton high explosive test detonated on February 28, 1985 at the permanent high explosive test site, White Sands Missile Range, New Mexico. This test was the second test performed as a prerequisite to the MINOR SCALE high explosive test. These tests, sponsored by the Defense Nuclear Agency, were directed toward investigations of various aspects of the hardened mobile launchers basing concept.

5.1 PRE-TEST DESCRIPTION.

A plan view of the test bed layout used for MINI SCALE 1 and 2 is shown in Figure 38 with special note given to the location of the instrumentation fielded by NTS. The charge container for the MINI SCALE tests was hemispherical as shown in Figure 39. Outer diameter of the hemisphere was 15.0 feet. The wall of the hemisphere was composed of two 0.188-inch thick layers of fiberglass formed around a 0.50-inch cardboard core.

Placement of the three electrolytic gages is shown in greater detail in Figure 41. The gages were buried to a depth of 2.75 feet at a distance of 30.0 feet from the center of the charge container, 22.5 feet from the edge. During placement of the gages, the epoxy sealant around the wire exiting from one of the gage canisters was observed to be somewhat deteriorated. No leakage of electrolyte was observed and the resistance of the gage appeared to be satisfactory considering the conditions during installation. The three gages were buried to the same depth and spaced in an arc at approximate 1.0 foot intervals. A single coaxial cable ran from each electrolytic gage back to the instrumentation bunker at the ideal 30 psi overpressure range of 197.3 feet.

Installation of the flow direction gage and pretensioning the vertical wire support to 150 pounds was accomplished without incident on February 26. However, difficulties were encountered when attempts were made to correct a zero drift in the load cells. Investigation of the problem revealed that the vertical tensioning wire had suffered a failure in its attachment to the brass ball. The reasons for this were not apparent immediately although it was felt at the time, and still is, that the creep properties of the brazed joint can not cope with even moderately low stress conditions for sustained lengths of time.

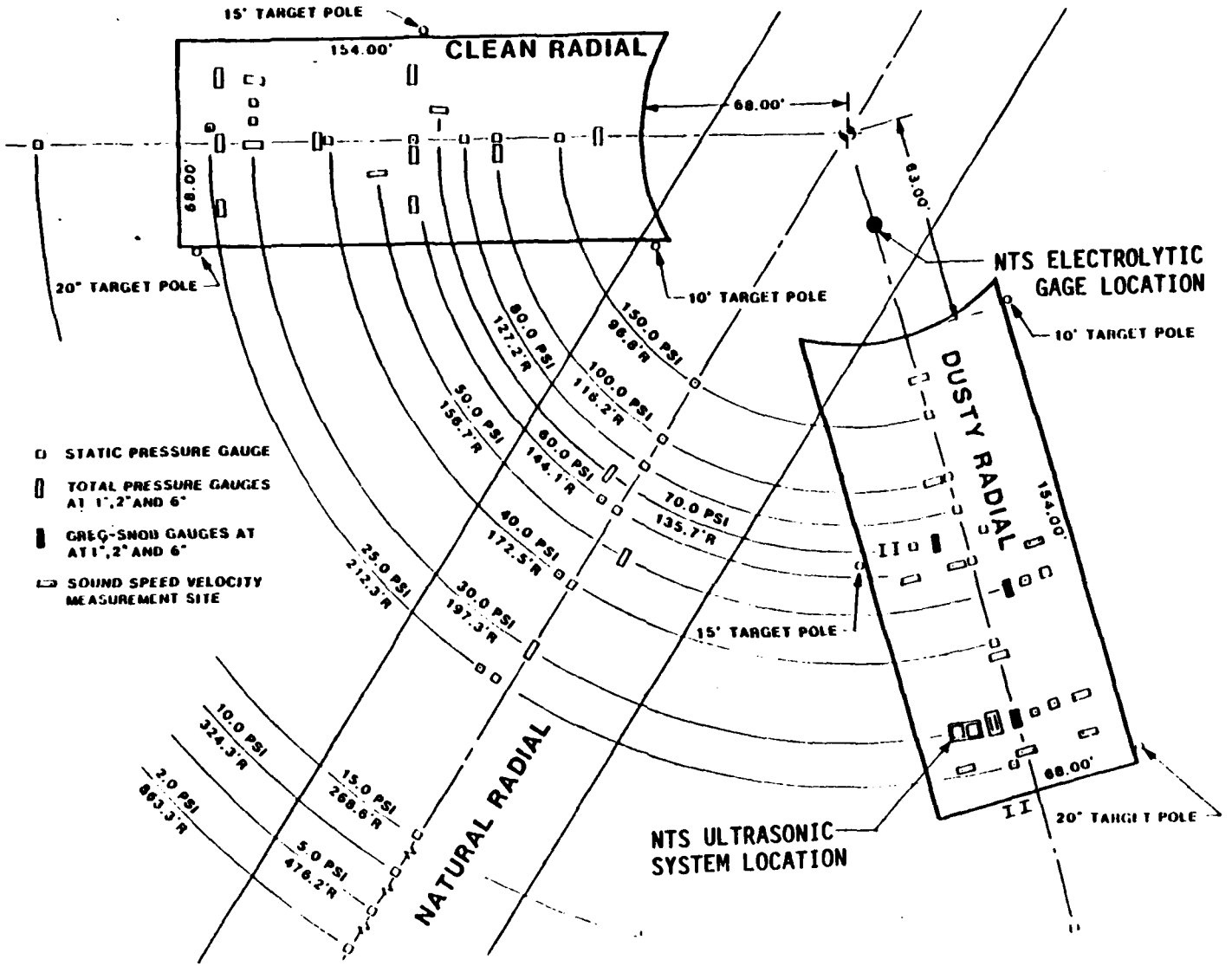

Figure 38. Plan view of MINI-SCALE 2 test area.

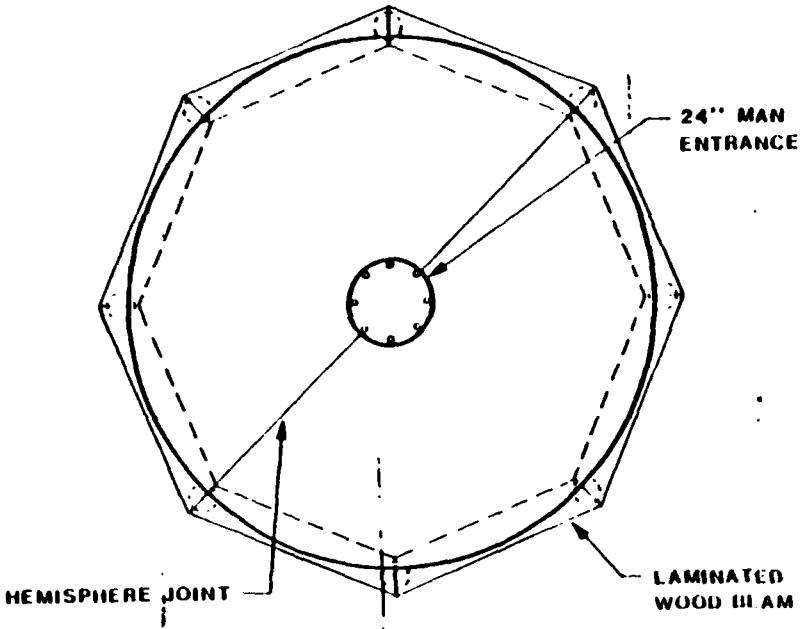

PLAN VIEW

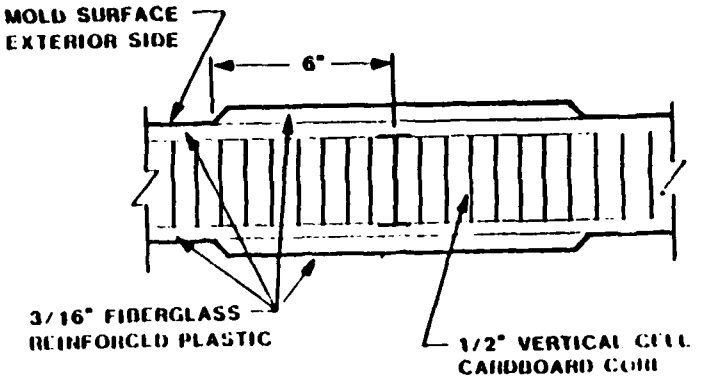

TYPICAL JOINT DETAIL

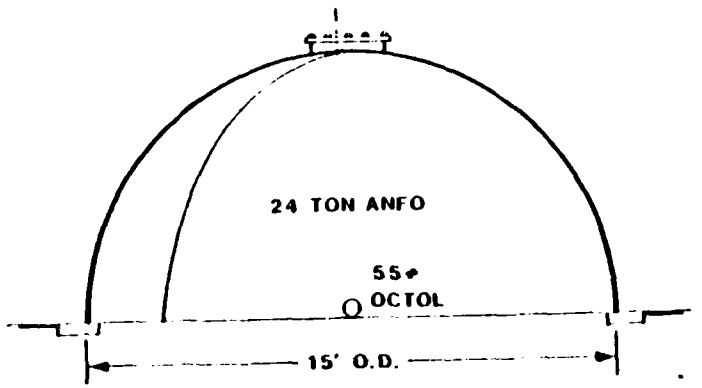

ELEVATION

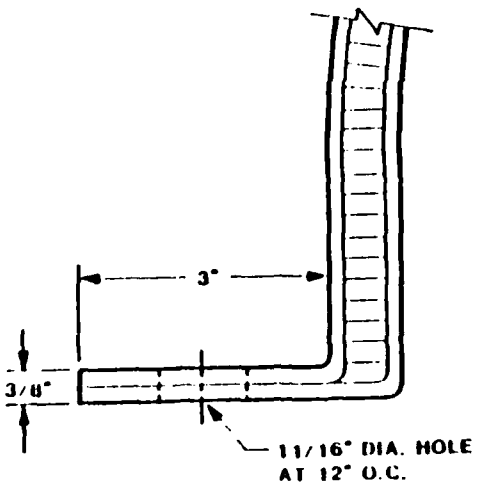

BASE DETAIL

Figure 39. Charge container design for MINI-SCALE tests.

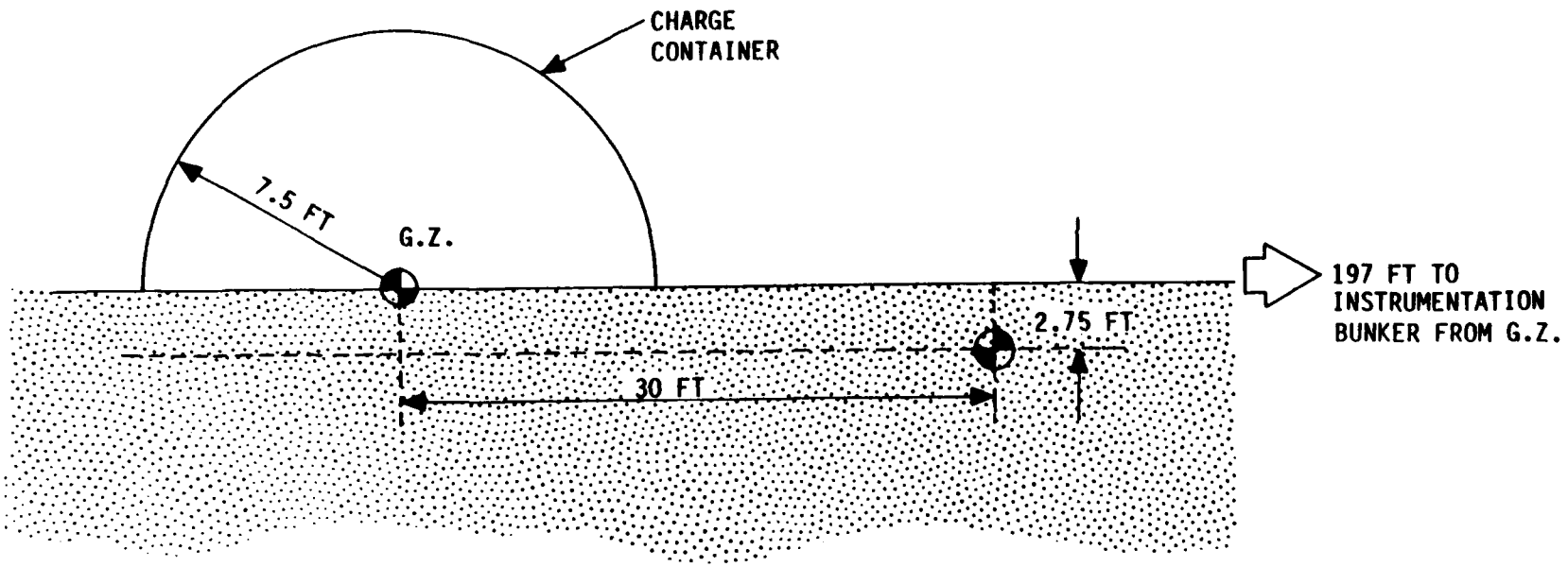

Figure 40. Location of electrolytic gages.

A spare ball and wire assembly had been made in case the original was damaged and was installed. Since the schedule did not allow for a thorough investigation into the nature of the failure of the wire to ball connection, a decision was made to arbitrarily reduce the applied tension to 75 lbs. An inspection of the gage at approximately 7:00 P.M. on February 27 did not reveal any signs of joint failure.

Placement of the blast shields, flow direction gage and instrumentation bunker is shown in Figure 41. All electronics packages (power supplies, timers, amplifiers, signal drivers, etc.) were hardmounted to a 21-inch square 12-gauge steel panel housed in a 24-inch by 24-inch by 12-inch NEMA 4 steel instrumentation enclosure manufactured by Hoffman, Inc. (model A-242412LP with panel A24P24). The enclosure was isolated from ground shock by being surrounded by 2 inches of foam mattress material.

5.2 POST-TEST DESCRIPTION.

MINI SCALE 2 was detonated at approximately 12:07 P.M. local time on February 28, 1985 after a shortened countdown necessitated by the threat of thunder showers. Isolated showers on the test bed interrupted reentry efforts because of concerns over the possibility of lightning strikes.

Reentry into the dusty radial test bed revealed that the flow direction gage was still attached to its vertical support and the load cells. Pieces of mylar tape and bag were wrapped around the vertical support wire. The windward face of the brass ball had a sand-blasted appearance with isolated impact depressions on the order of 0.5 mm to 1.0 mm in diameter. The angled aluminum support behind the brass ball exhibited similar markings with the exception of a region directly behind the ball which lacked any signs of large particle impacts. All brazed connections appeared to be intact and strumming of the wires revealed that they were still under tension. A discoloration of the wires entering the coverplate was observed from their point entry to about a 1.0 inch elevation. The bluish-black color was similar to that observed upon heating of the wire material.

Batteries to power the ultrasonic transmitter were not expected to last more than 10 minutes and so had been drained by the time reentry was made. This made it impossible to make any judgments on performance of the electronics from external observations.

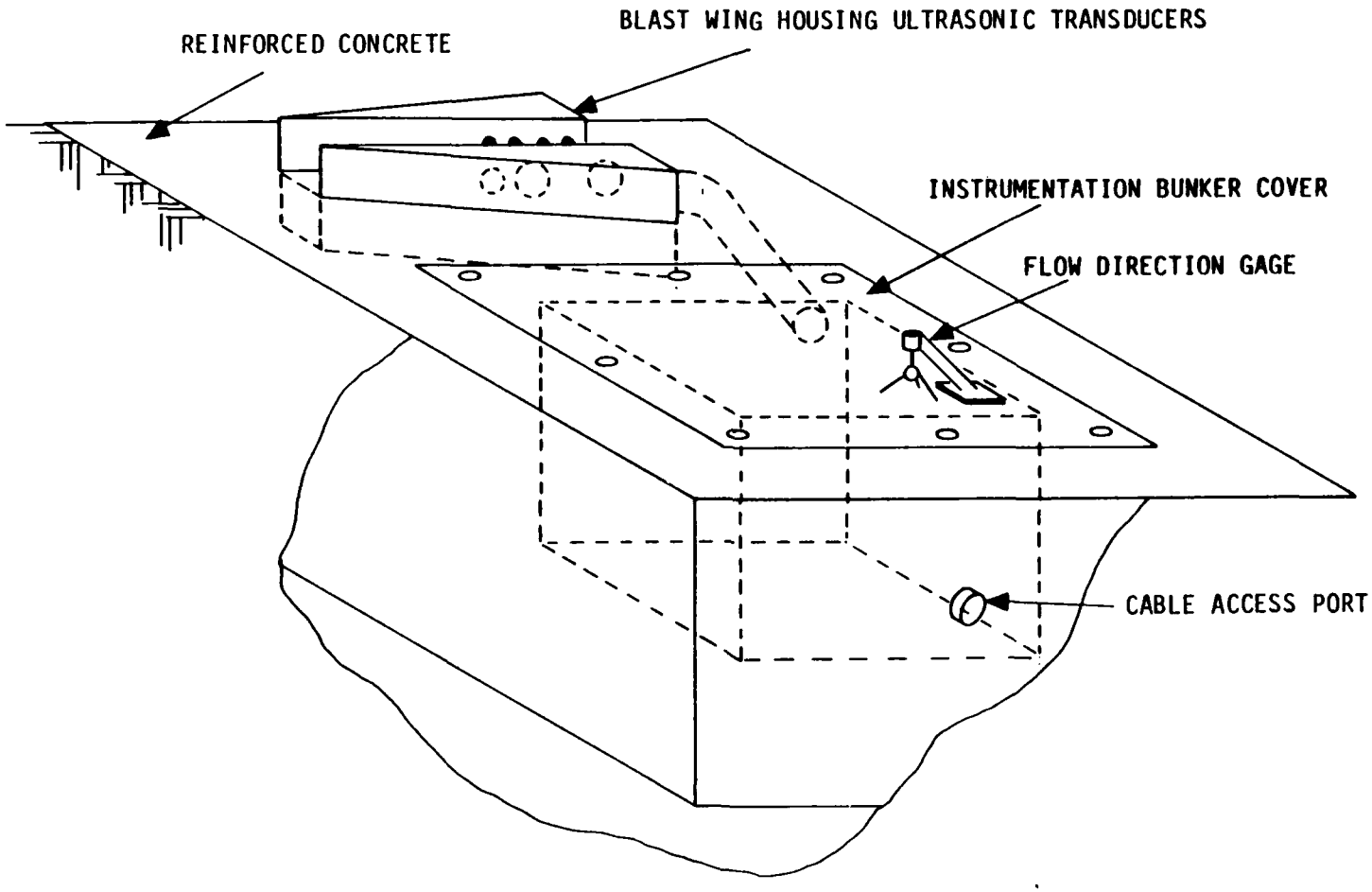

Figure 41. MINI-SCALE 2 experiment configuration.

Examination of the scouring pattern of the blast shields were indicative of a skewed flow pattern with the angle of flow being directed from the centerline of the dusty radial test bed toward the natural radial. This would have tended to direct particles into the face of the transmitters and caused turbulence between the blast shields. No evidence of damage to the rubber-coated transmitter face was observed. However, scratches and evidence of small particulate impacts were observed on the unprotected aluminum faces of the receivers. This was an indication that the 0.11-inch boundary layer, estimated from ideal flow assumptions (Reference 5) may not have been achieved in the test.

5.3 ULTRASONIC MEASUREMENT SYSTEM RESULTS.

Data records from the ultrasonic measurement system were fairly disappointing. The electronics performed as intended and data was obtained for all channels. Examination of the data indicated that the ultrasonic system provided a measurement of sound speed prior to shock arrival and a measure of shock velocity. The portion of the data record related to this information is shown in Figure 42.

Sound speed measured by the ultrasonic gage at a range of 197.2 feet just prior to shock arrival was 2,320 fps. This compares within 5% with the average of the final readings taken by Science Applications, Inc., at stations 7 and 8 (ranges of approximately 173 feet and 212 feet, respectively) of 2,430 fps (Reference 6). Slightly lower readings may actually have been expected considering the many instruments protruding through the bag at the 197.2-foot range. The estimated precision of the ultrasonic measurement is $\pm$ 3%.

Shock propagation velocity was determined to be 3,250 fps by noting the difference in shock arrival time for adjacent receivers. Again, the estimated precision is + 3%. Based upon examination of high-speed photography, Information Science, Inc., (ISI) estimated shock velocities in helium for ranges of 78 feet to 144 feet (Reference 6). This information is presented, along with the NTS measurement at 197.2 feet, in Table 3. Although the NTS measurement seems to agree with the trend exhibited by the ISI measurements, additional information to corroborate this trend was not available.

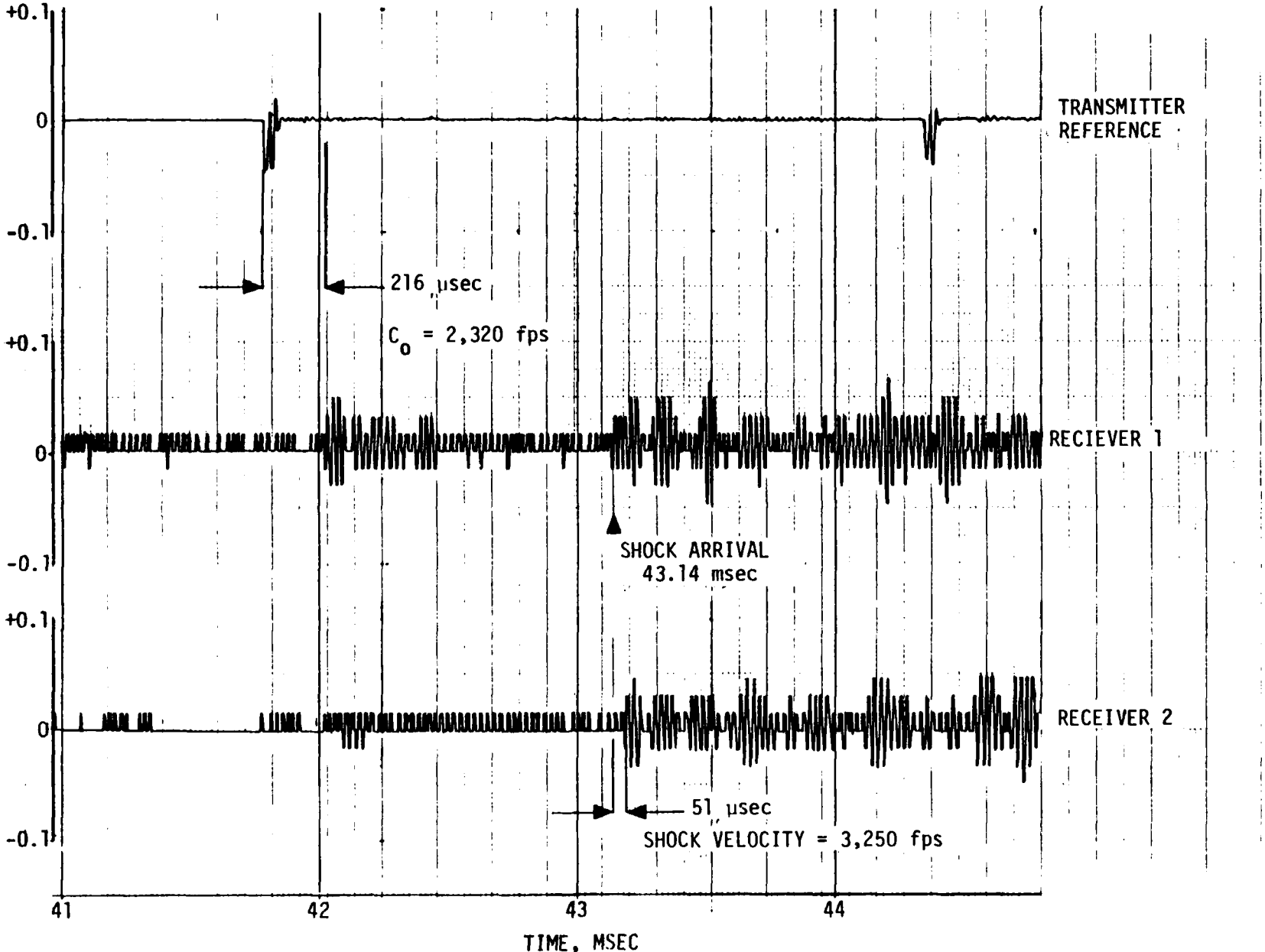

Figure 42. Ultrasonic signal reception prior to shock arrival.

Table 3. Variation in shock propagation velocity with range on dusty radial.

RADIAL DISTANCE FROM G.Z., FT.	SHOCK PROPAGATION VELOCITY IN HELIUM, FPS	OBSERVER
78	5333	ISI
100	4780	ISI
122	3956	ISI
144	3641	ISI
197	3250	NTS

Unfortunately, the noise levels produced by the passage of the shock front combined with the impact of particles prohibited further attempts to gain useful information from the ultrasonic measurements. Attempts to reduce the noise by means of various filtering techniques were not successful primarily due to the similarity in signal frequency and noise frequency picked up by the broad banded receiver. Although the non-ideal flow conditions of the test most likely played a substantial role in the high levels of noise, experience in the 4-inch shock tube tests also indicated a possibility of high noise levels might not have been totally unexpected even under ideal flow conditions.

5.4 FLOW DIRECTION GAGE RESULTS.

Raw analog data from the three load cells used in the flow direction was filtered with a 6,000Hz low pass filter, digitized at intervals of 2μsec and then processed to obtain load variations in the X, Y and Z axis. In this notation, X corresponds to tangential flow, Y corresponds to vertically upward flow and Z corresponds to radially outward flow. The three axes are right handed as shown in Figure 30 in Section 3. The X, Y and Z records, shown in Figure 43 were highly oscillatory indicating an unexpected dynamic response effect.

Several attempts to remove the primary structural response frequencies proved to be ineffective in producing credible records. In an attempt to obtain some useful information from the measurements, 2.13 msec intervals of the records were averaged. This interval was of sufficient length to be approximately equal to the longest period exhibited by the oscillating records. Using this approach it was hoped that insight could be gained into the general flow behavior rather than the detailed characteristics. The X component of the flow was reduced to essentially zero following this procedure. This was in disagreement with physical observations of skewed flow. The resulting Y and Z plots are shown in Figure 44. Also shown in this figure is the magnitude of the flow component in the YZ plane. Knowing some idea of the magnitude of the component is important in evaluating the calculated relative angle of the component. Calculation of large angular changes in flow orientation are valid only if they correspond to significant flow conditions. The 25 mV cut-off level shown in the plot of magnitude was chosen based on comparison with pressure records at the same range. The cut-off leads to a start of credible flow angle measurement that coincides with the start of the pressure records. A comparison of flow angle behavior and pressure records is shown in Figure 45.

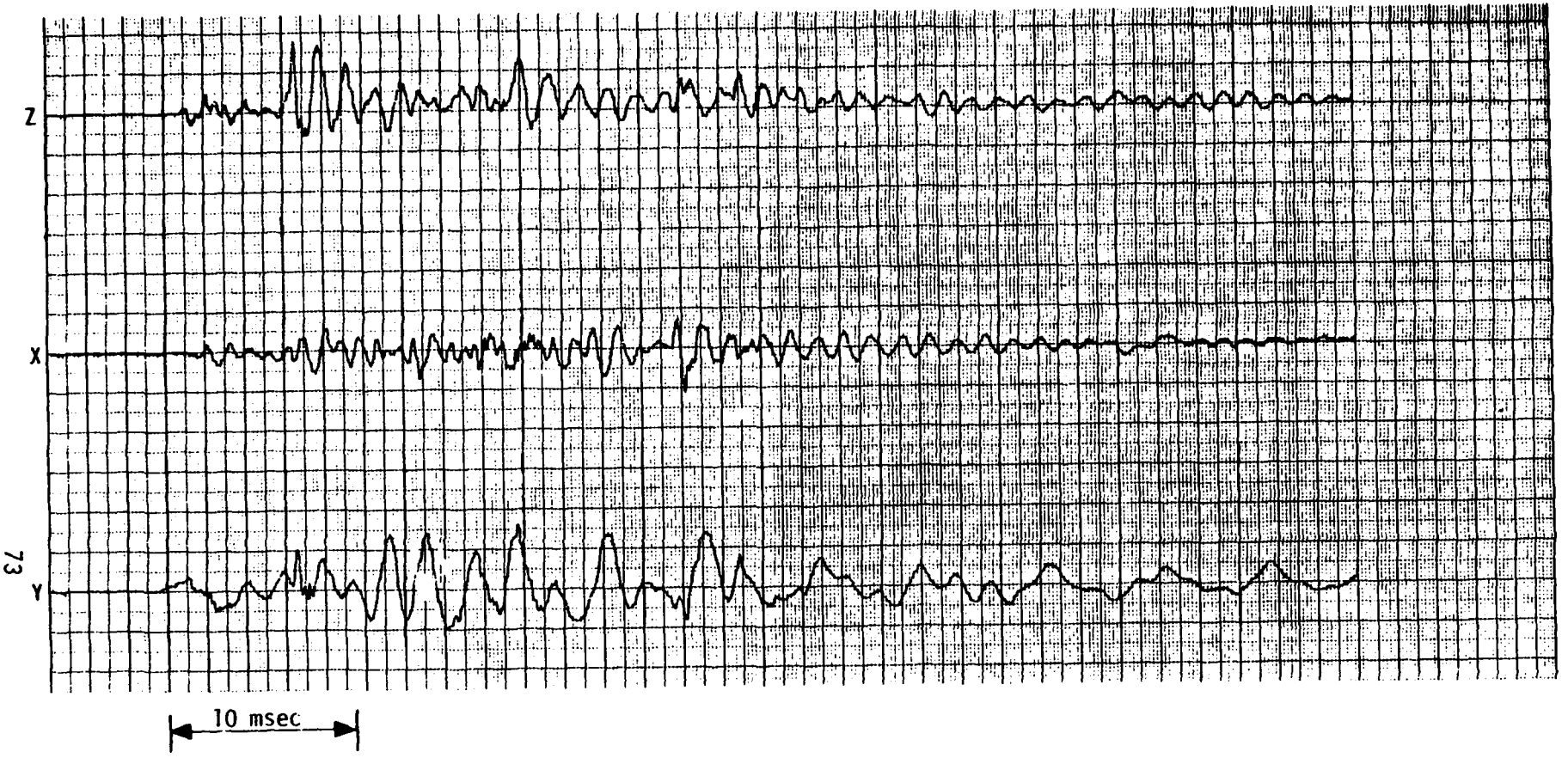

Figure 43. Flow velocity components determined from changes in load cell readings.

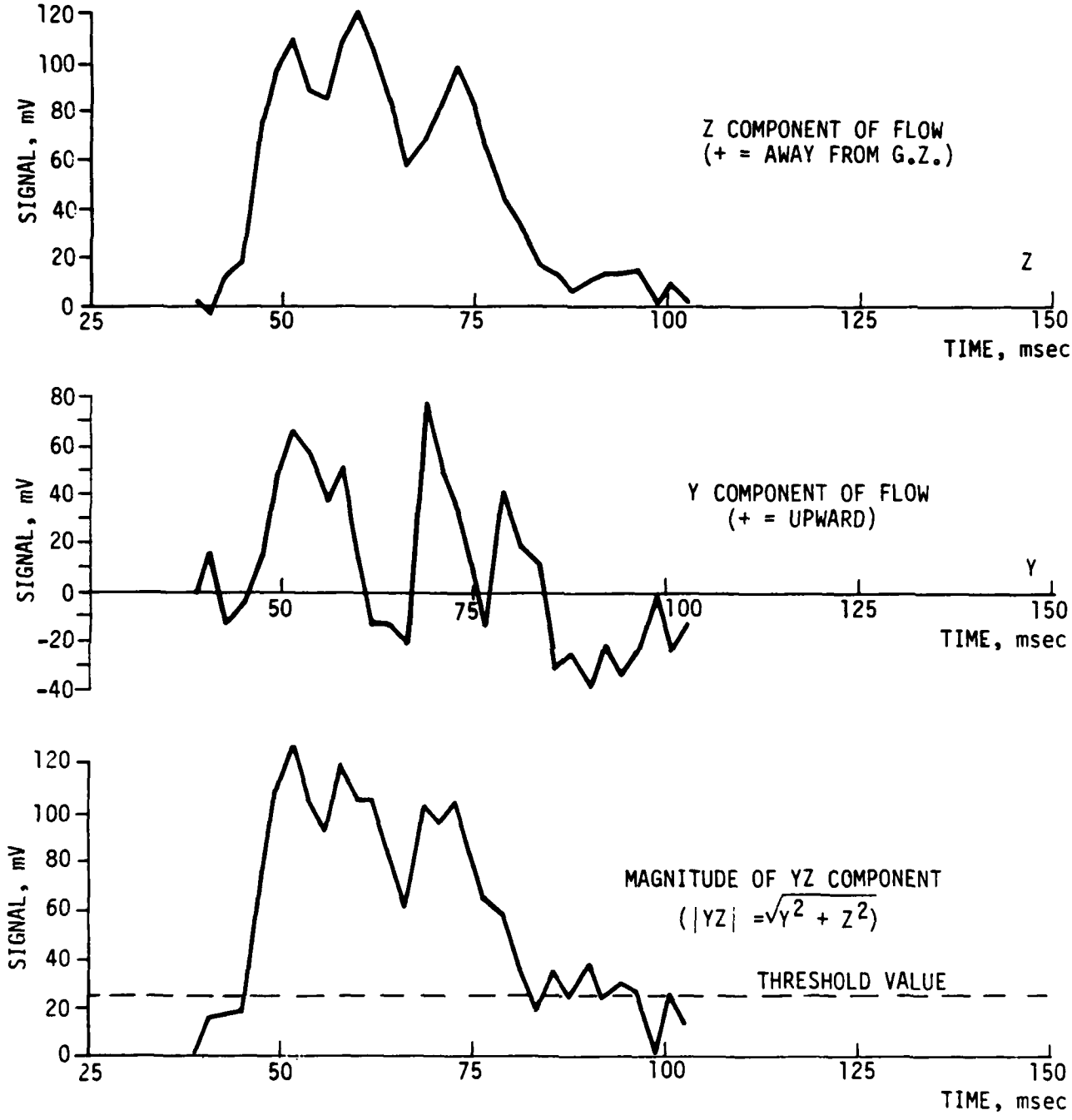

Figure 44. Determination of threshold signal level.

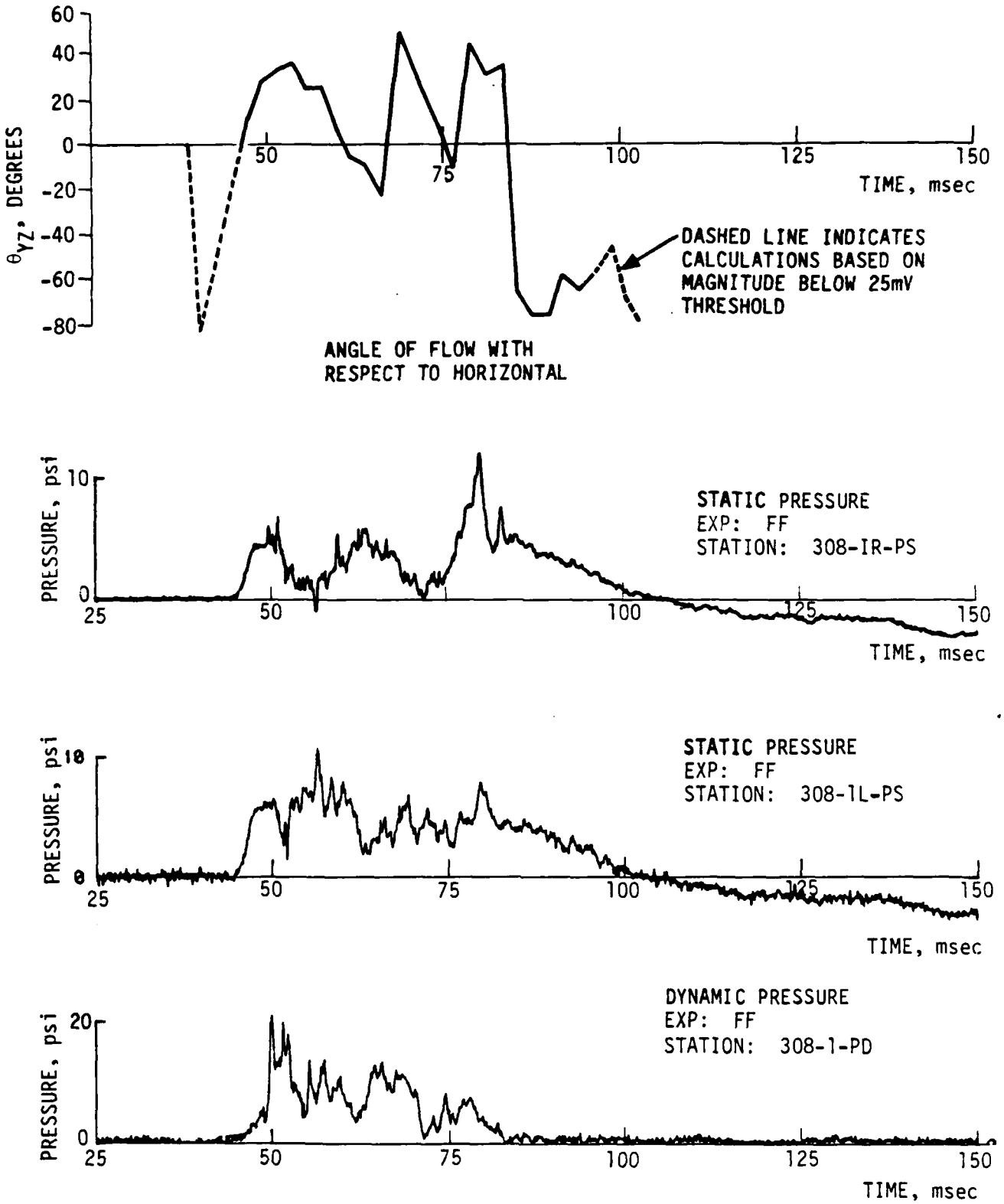

Figure 45. Comparison of measured angle of flow and pressure records.

The flow appears to correlate well with what is occurring during the passage of the precursor. Initially, flow behind the leading edge is expected to be upward as a result of the inclined shock front extending from the leading edge to the triple point. The sharp reversal of flow angle seem near the end of the record corresponds to the peak static pressure from the right static port (station 308-IR-PS), a peak in the record of the left static port (station 308-IL-PS), and to the end of record for the dynamic pressure (station 308-1-PD). This would seem to indicate a sharp flow reversal due to taroidal roll-up. Figure 46 is presented to better illustrate how the flow angle and might correspond to general optical observations of the shock-structure associated with the helium precursor.

The overall behavior of the flow angle measurements seem to correlate well with the more obvious aspects of the flow, i.e., the arrival time, initial flow tendencies and arrival of toroidal roll-up. It should be noted that the measurements differed greatly from the predicted flow angle based upon pre-test calculations. Calculations showed a rapid rise in flow angle at time of arrival to a value of 60° to 70° and then a rapid decrease back to 0° within 5 to 10 msec after time of arrival. Clearly, this was not the type of behavior observed in the measurements.

5.5 ELECTROLYTIC SOIL PRESSURE GAGE RESULTS.

Of the three electrolytic gages fielded in MINI SCALE 2, only one survived to give an interpretable pressure record. One of the gages suffered some form of damage between the time of installation in late December and check-out in late February. The gage appeared to be somewhat unreliable during check-out and did not predict any meaningful record. Another gage failed at shock arrival during the test.

The gage that did produce a pressure record lasted for nearly 30 msec before ground movements caused a failure of the PVC container. This record is shown in Figure 47. The time scale is referenced to FIDU making the spike at approximately 1.5 msec attributable signal contamination by the firing pulse.

An initial increase in pressure to 450 psi is assumed to be related to the airblast loading, the low pressure being caused by the dissipative effects of the unconfined soil. The remainder of the waveform from about 8 msec onward is assumed to be related to direct induced ground shock. The assumptions concerning possible expla-

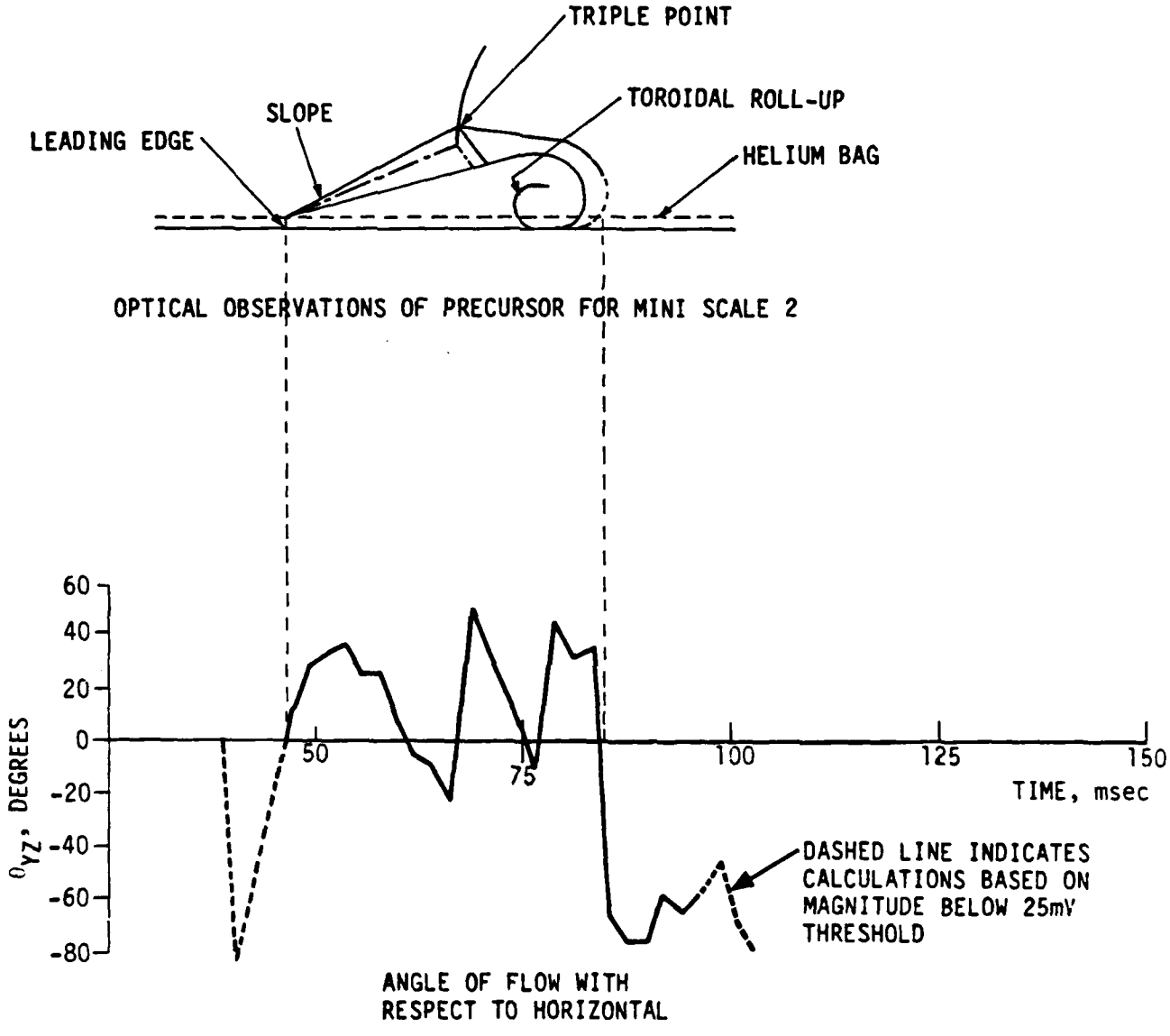

Figure 46. Comparison of flow angle measurements with observed precursor structure for MINI-SCALE 2.

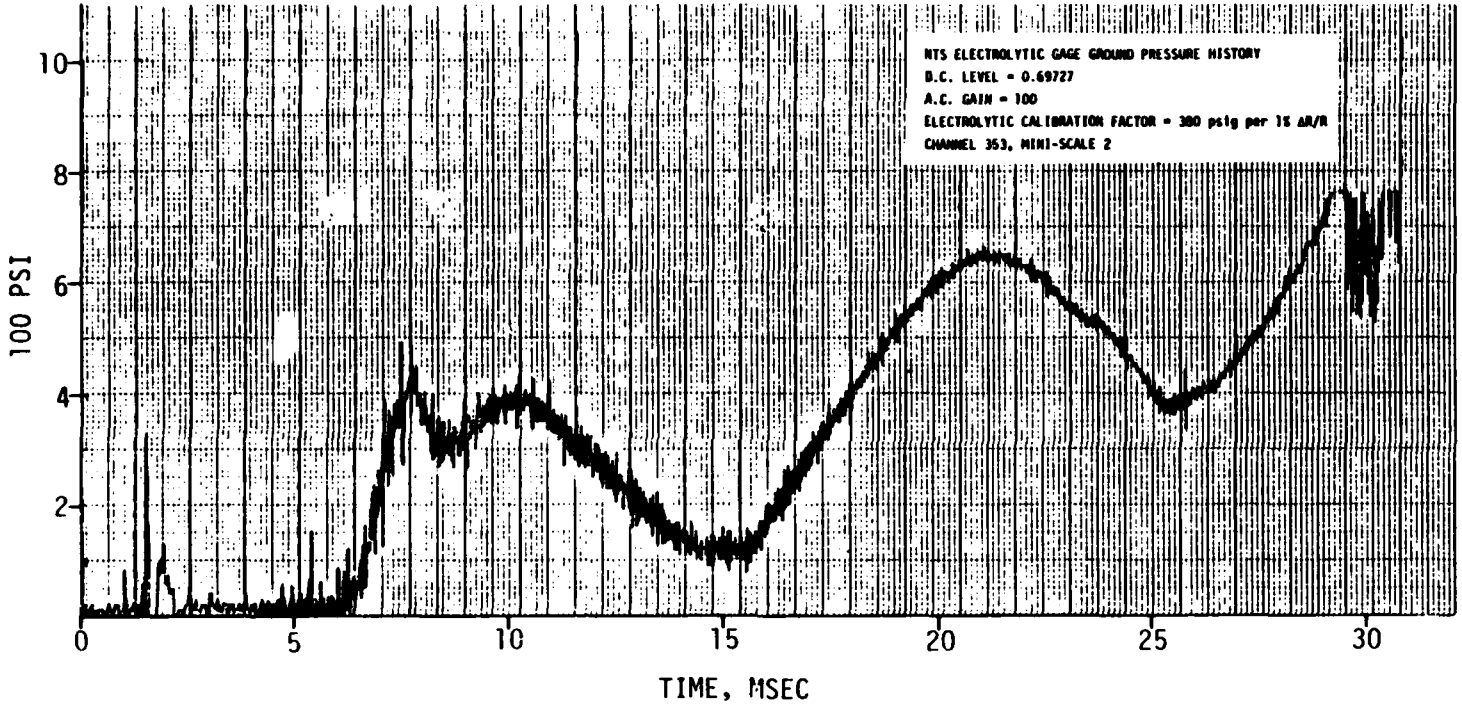

Figure 47. NTS electrolytic gage ground pressure history.

nation of the waveform are quite tentative as no information was available on soil stress histories in the vicinity of a high explosive surface charge.

The location of the electrolytic gages in relation to post-test cratering studies is shown in Figure 48. Given the lack of substantial confining surface pressure during crater formation, the maximum stress to which the gages would be expected to be exposed is on the same order as the failure stress of the compacted soil. If the surface pressure is assumed to be 100 psi and the soil assumed to be similar to McCormick Ranch Sand, the primary stress at failure can be estimated to be about 400 psi to 500 psi (Reference 7). Initial portions of the pressure record measured by the gage (Figure 45) have a maximum value of 300 psi to 400 psi. After 15 msec a second increase in pressure is seen. It is not clear that this increase was caused by the same phenomenon that was responsible for the first portion of the record. The fact that this later increase occurs relatively late in time, when the response of the soil is highly uncertain, makes explanation difficult.

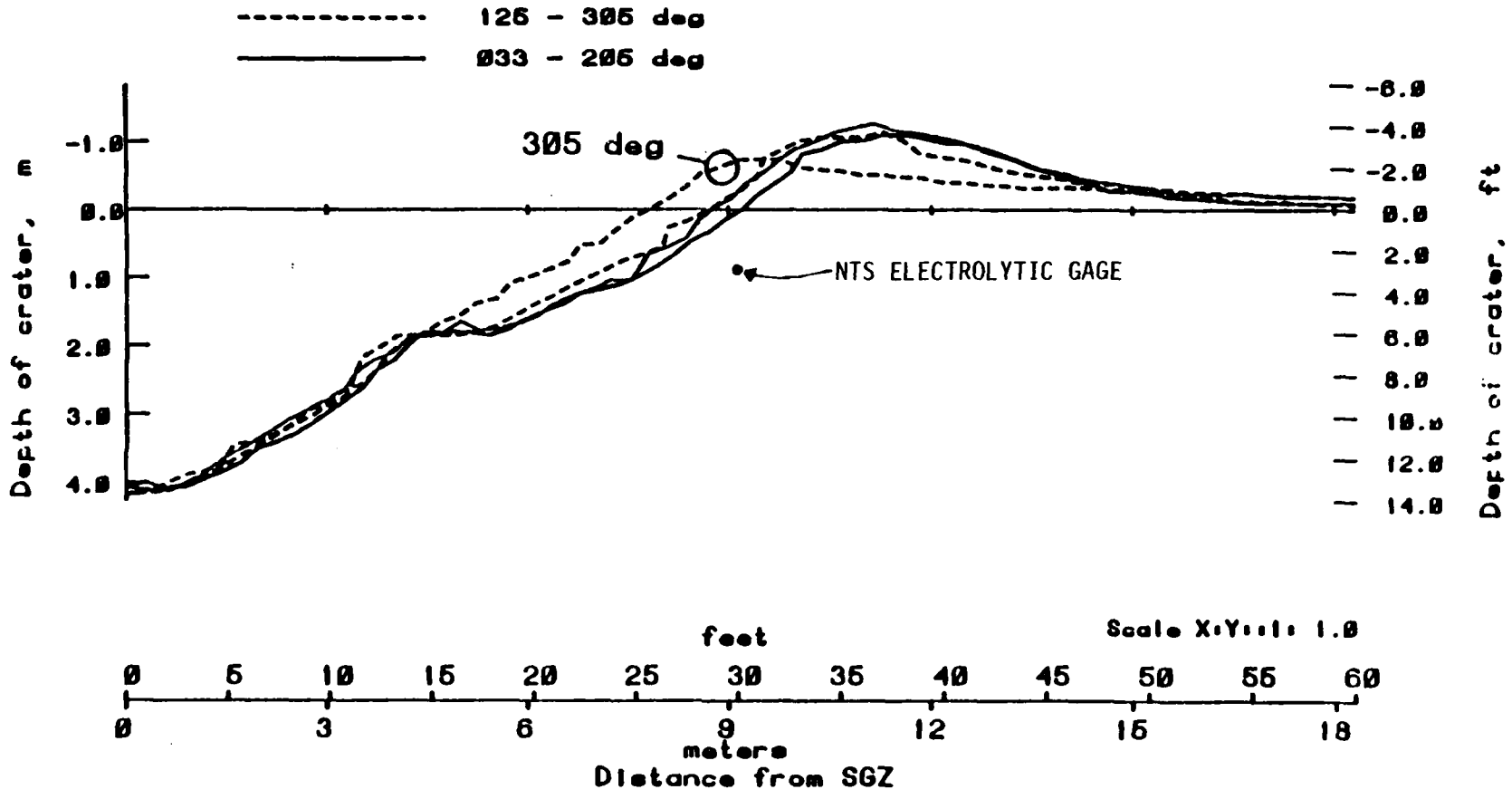

Figure 48. Composite crater profiles for MINI-SCALE 2.

SECTION 6
MODIFICATION AND RETESTING OF ULTRASONIC SYSTEM

Following the evaluation of results from the TRW 4-inch shock tube and MINI SCALE 2, it was apparent that the ultrasonic system needed to be modified to be less sensitive to noise generated by the combination of shock passage and particle impacts.

6.1 HARDENING OF RECEIVER FACE.

Experience with the transmitter had indicated that the rubber facing of the transmitter played an important role in isolating the piezoresistive crystal from particle impacts and in providing a means to aid in the damping of any impact related vibrations of the crystal.

A similar solution was sought for the receivers. In selecting a cover material for the bare aluminum face of the receiver, attention was given to several key requirements:

1) The material selected should have good ultrasonic transmissive properties.

2) The applied thickness of the material to the receiver should be easily controlled to close tolerance.

3) The adhesion of the material to the receiver face should be sufficient to withstand the abrasive effects of particulates.

The BUNA-N covering used on the transmitter had shown to be pervious to ultrasonic signals so initial efforts focussed on other synethetic rubbers.

Experiments with RTV silicone rubber seemed quite promising as indicated in Figure 49. A 0.5 mm coating was applied to the face of a receiver which was then connected to an oscilloscope, along with an uncoated receiver, for monitoring. The noise reduction offered by the coating was tested by comparing the signals produced by the impact of a 4mm diameter, 0.23 gram, steel ball dropped from a height of 1.6 cm. The momentum delivered by this test was roughly equivalent to a 300 micron diameter steel ball travelling approximately 1,300 m/s. This was considered comparable to sizes and velocities often associated with particulates in the precursed flow. As

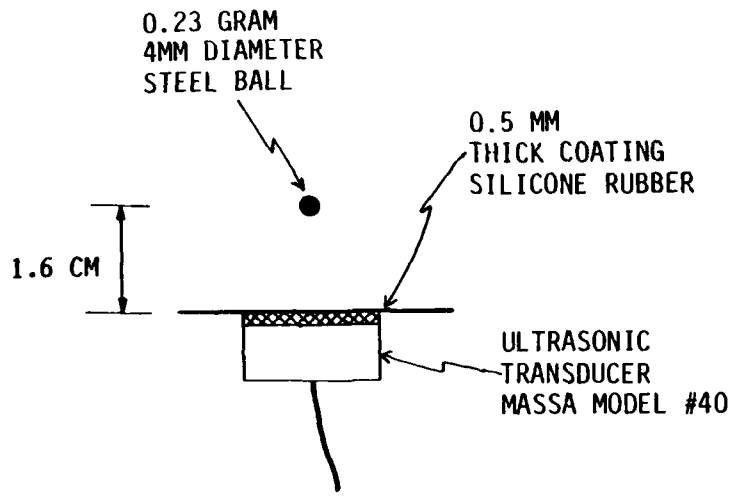

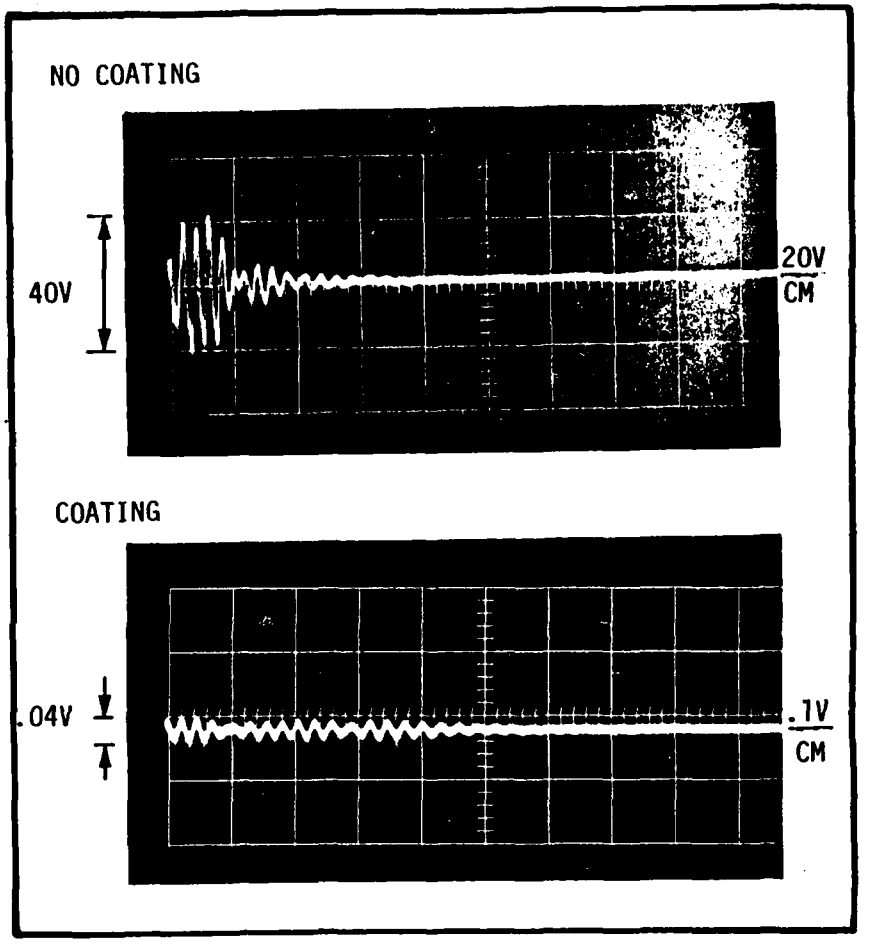

RATIO OF RECEIVED ULTRASONIC SIGNAL WITH COATING TO RECEIVED SIGNAL WITHOUT COATING IS 0.30

Figure 48. Results of impact tests on modified ultrasonic receivers.

indicated by the oscillograph traces in Figure 49, the silicone rubber coating reduced the noise by a factor of about 1000. Comparison of the signal level received by the coated and uncoated receiver indicated a loss of signal sensitivity by a factor of about 3.3 for the coated receiver yielding a net increase in signal to noise ratio by a factor of 330.

6.2 REPEAT OF TRW 4-INCH SHOCK TUBE TESTS.

Initial laboratory testing of the effect of silicone rubber on the receivers was followed by another entry into the TRW 4-inch shock tube facility. The tests were similar to those conducted just prior to MINI SCALE 2. Changes in the second test included applying a 0.5 mm layer of silicone rubber to the faces of the receivers and changing the access port position from the last in the test section to the first in the test section.

Results from the shock tube test were very encouraging. Not only was the severe noise problem eliminated but a transmitted pulse was picked up by the second receiver. Samples of some of the pulses captured by the second receiver are shown in Figure 50. Measured sound speeds for the first 10 msec following shock passage are shown in Figure 51. The sparcity of data points is a direct effect of the restrictive size of the 4-inch shock tube.

Tests in the 4-inch shock tube indicated that a good part of the noise problem has been solved. In addition, the shock tube test verified the ability of a receiver to register a coherentg signal displaced some distance downstream by the air flow. The extent to which the transmitted signal remains coherent for larger displacements remains unknown. Investigation of this characteristic of the ultrasonic system is better suited to wind tunnel tests where there is a relatively high degree of control and repeatability.

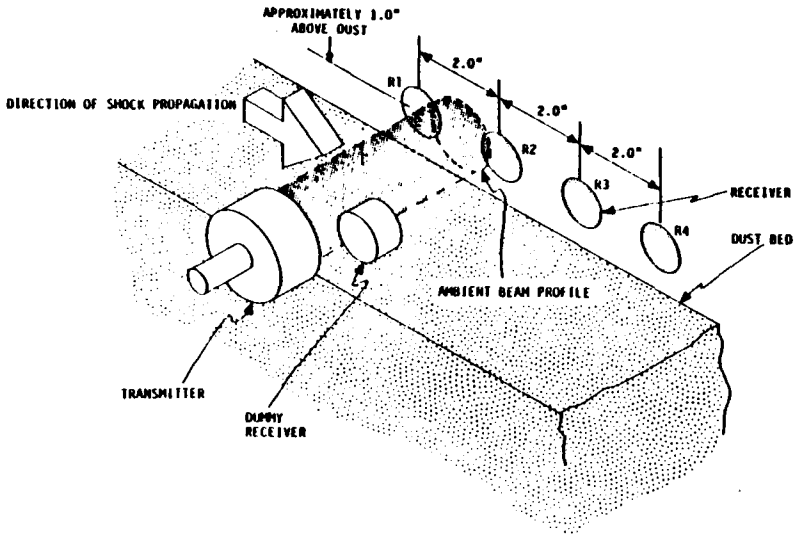

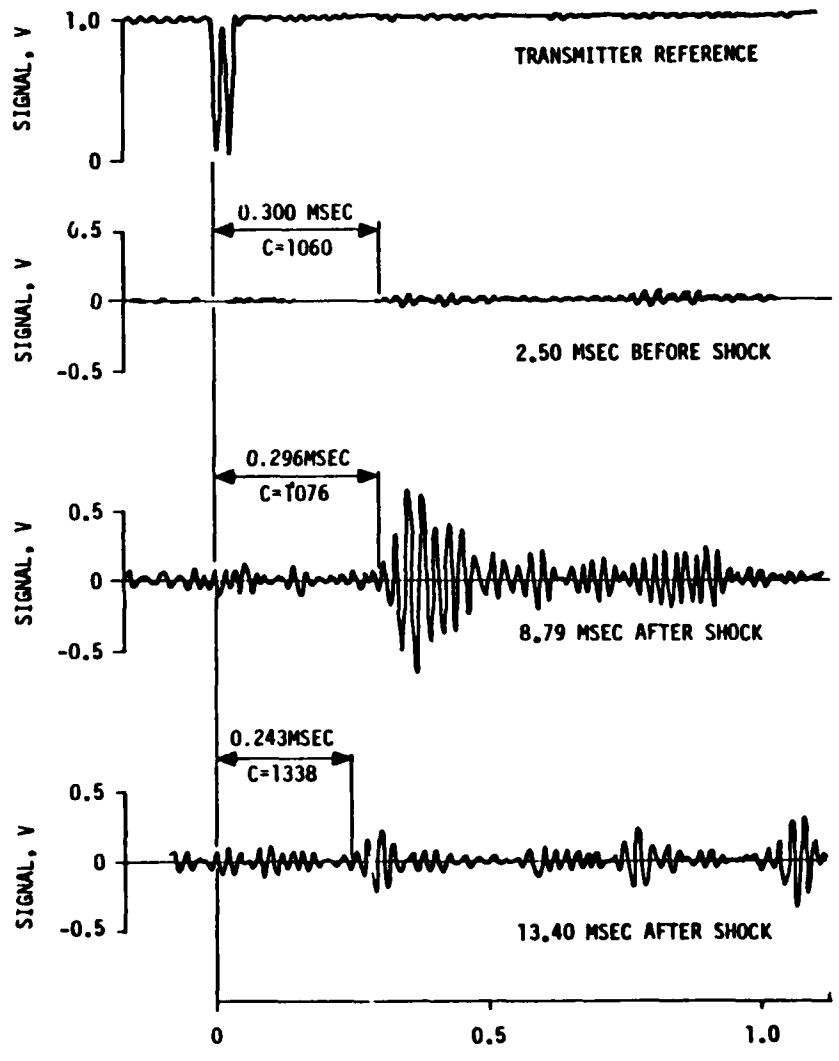

Figure 50. Representative received signals from receiver R2 during dusty shock flow in TRW 4" shock tube.

AD-A171 850 DEVELOPMENT OF INSTRUMENTATION TO MEASURE SOUND SPEED AND FLOW DIRECTION I.. (U) NTS ENGINEERING LONG BEACH CA D G HONEGGER 11 NOV 85 85-1502 DNA-TR-85-369 2/2

UNCLASSIFIED DNA001-84-C-0441 F/G 18/4 NL

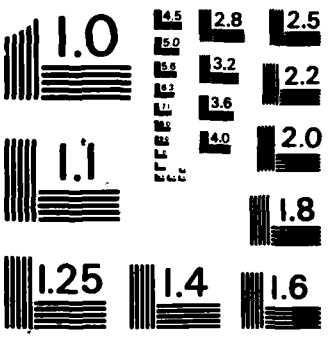

MICROCOPY RESOLUTION TEST CHART

NATIONAL BUREAU OF STANDARDS - 1963 - A

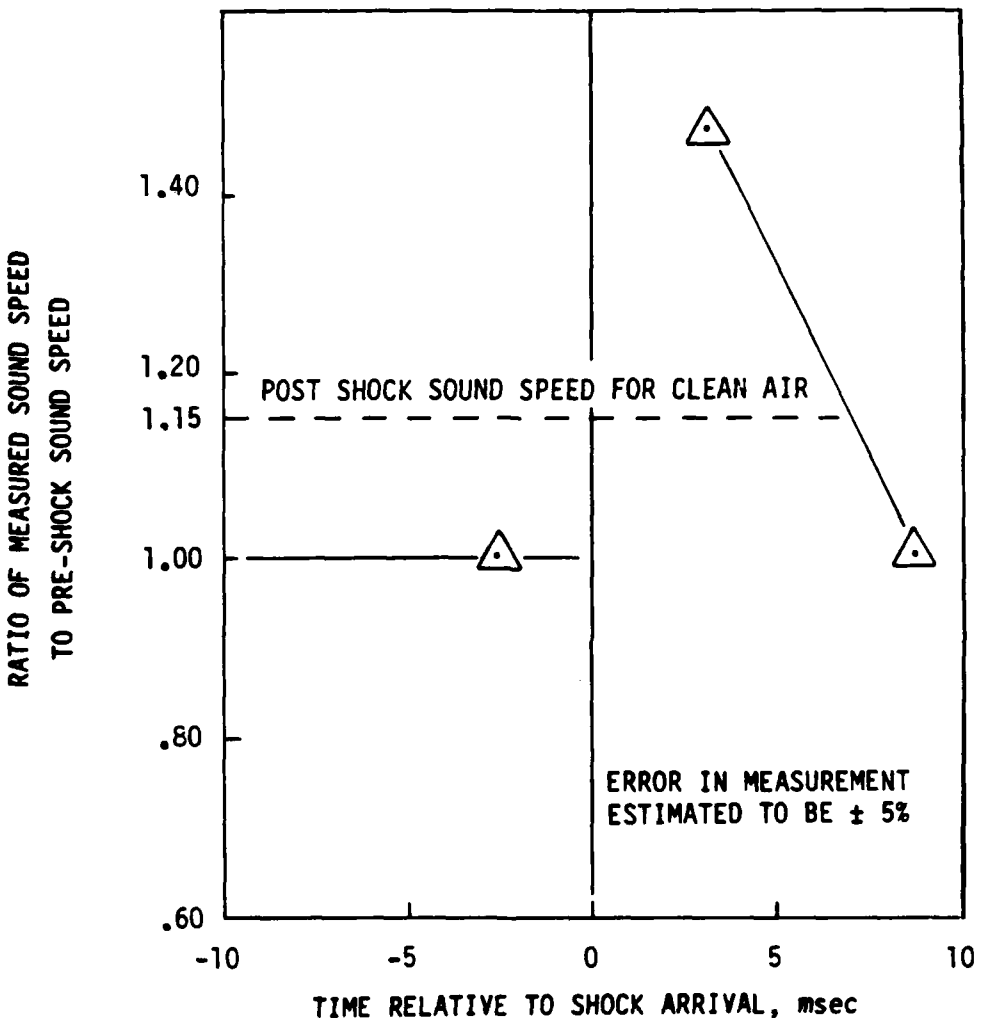

Figure 51. Sound speed measured for dusty flow in TRW 4" shock tube (estimated error ± 5%).

SECTION 7
CONCLUSIONS AND RECOMMENDATIONS

A great deal of experience has been gained during the development, fielding and data processing efforts required for the three instrumentation concepts. Several conclusions and recommendations are presented in the following sections regarding expected performance attainable for the gages and suggested directions for future development efforts.

7.1 ULTRASONIC SYSTEM.

The ultrasonic system for simultaneous measurement of sound speed, flow direction and flow velocity is a concept that requires considerably more effort before it can be fielded reliably. Although the problem of flow-induced noise has been greatly reduced, there still remain a number of unknowns regarding the operation of the system in actual test conditions:

1) The ability of the ultrasonic beam to maintain its integrity while being displaced downstream has only been proven for displacements of less than 1.0 inch. Flow velocities of Mach 2.0 could result in downstream displacements of as much as 12 inches based upon a 6-inch blast shield separation.

2) Providing a system to handle high-speed angular flows requires a large number of receivers to enable accurate tracking of the displaced transmitted beam, thus further complicating an already laborious data reduction process.

3) Recording requirements for the ultrasonic system are more extravagant than most other gages current being fielded. The necessity for five to ten channels of recording for three measurements is a deterrant to the use of the system and is a problem that needs to be addressed if further development is undertaken.

All of the drawbacks pertaining to the ultrasonic system stem from the attempt to make several different kinds of measurements from the same data. While it is desirable to have this capability, experience with this system indicates that it may not be practical at this time.

It should be noted that the use of ultrasonic transducers to obtain sound speed measurements is preferrable to other methods previously employed in the MINI SCALE tests and Minor Scale. With slight modification to the method of housing the ultrasonic transducers, the current system has the capability to measure sound speed prior to detonation, provide an indication of when helium clean-up occurs, and measure sound speed during the test.

The use of parallel blast shields in making only sound speed measurements should probably be abandoned for several reasons. First, for the ultrasonic system, the use of blast shields necessitates using a very complex array of receivers. Second, dependence of parallel blast shields on non-skewed shock front arrival limits their usefulness in field testing situations.

It is important to note that this problem is common to all measurement systems employing parallel blast shields to measure free-field flow conditions. Skew shock front conditions of only 5° to 10° can create serious uncertainties regarding the relationship between conditions measured between the blast shields and those in the free-field.

The use of a simplified ultrasonic system is ideally suited for making reliable measurements of many items of interest for tests using a contained helium layer to develop a precursed blast waveform. Some of the measurements that could be made by such a system include the following:

1) Helium concentration during filling
2) Helium concentration just prior to shock arrival
3) Time of helium clean-up
4) Sound speed variation of the dusty gas

It is recommended that further development of the use of ultrasonic transducers, such as has been discussed above be focussed on the optimization of a simplified system aimed at obtaining only sound speed measurements.

7.2 FLOW DIRECTION GAGE.

The wind direction gage concept fielded in MINI SCALE 2 provided some useful information on the general flow conditions present in the test. In particular, the gage confirmed the initial upward flow related to the precursor and also confirmed the presence of toroidal roll-up on the dusty radial of MINI SCALE 2. The measurements of flow angle obtained by the gage differed substantially from those predicted by pre-test calculations. A major drawback of the gage design is related to its dynamic response to the flow conditions. The predominate oscillation observed in the records was definitely attributable to vibratory response of the spring loaded ball. However, it is felt that the mechanism responsible for driving this oscillation at relatively high amplitude levels requires further investigation before the gage design can be judged to be adequate for reliable field testing.

Simplified calculations have indicated that a modified vane-type gage could possibly provide 1 to 2 msec resolution of flow angle provided a means is available to monitor the vane rotation without increasing the structural response period. The vane approach is more advantageous from a data reduction perspective since the output corresponds directly with flow angle.

It is felt that effort is warranted for the investigation of the potential applications for both the NTS concept and a modified vane design. Specific tasks would address the nature of the response of the NTS flow direction gage and the minimum feasible response interval attainable by a vane-type gage. The measurement of flow angle is critical to judging the quality of a high explosive simulation of precursor effects, the credibility of parallel blast shield measurements and the definition of the flow environment to which structural models are exposed.

7.3 ELECTROLYTIC PRESSURE GAGE.

Electrolytic pressure cells were placed as soil pressure gages in MINI SCALE 2 in order to field-test the electronics package necessary to operate the gages and to examine the response characteristics of the electrolytic cell. The results of MINI SCALE 2 proved the operability of the electronics packages and the response of the gage seemed to be adequate. However, since no other measurement was available for comparison, specific details concerning response frequency will require additional testing.

The use of a electrolytic cell as a piezoresistive pressure transducer is a concept that could be more directly applied to measuring dusty flow field characteristics. The electrolyte canister is a rugged sensor and could be modified for measurements of total pressure, drag body force measurements or other situations in which a sensor must be exposed to a particulate-laden flow environment.

7.4 SUMMARY.

The primary effort of the flow field development program sponsored by DNA was to develop an ultrasonic measurement system that could provide information or sound speed changes within a blast-induced dusty flow. In conjunction with the sound speed measurements it was felt that information as the flow velocity and angle of flow could be ascertained. The work performed as part of this program shows that the use of an ultrasonic system to measure sound speed is feasible. However, experience with the system indicates that the envisioned multiple measurement capability is not practical at this time.

Devoting the ultrasonic technology developed so far to sound speed measurements alone and developing other means to obtain information on flow angle and velocity is recommended based on the simplification of data reduction effort required, a reduction in the number of channels of data to be recorded, and much reduced fielding and construction costs.

A modification of the present ultrasonic technology has been suggested that could provide the needed sound speed information in a straightforward manner and require only one channel of data recording per measurement station. Suggestions for future efforts concerning the further development of the NTS flow direction gage and investigations into possible vane-type gage designs have also been made. Both the NTS flow direction gage and vane-type gage approaches appear to be better suited to flow angle measurements than the use of ultrasonics in terms of number of data channels required, total costs and complexity of data reduction.

SECTION 8
LIST OF REFERENCES

1. Operation TEAPOT, Technical Summary of Military Effects, Programs 1-9, WT-1153 (EX), 1958.

2. Operation TEAPOT, Project 1-11, Special Measurements of Dynamic Pressure Versus Time and Distance, WT-1110, 1958.

3. Development of Airblast and Soil Strength Instrumentation, Systems, Science and Software, DNA Report 5225F, 1980.

4. Blevins, R.D., Flow-Induced Vibrations, Van Nostrand Reihold Co., New York, 1977.

5. Keuth, A.M. and C.Y. Chen, Foundations of Aerodynamics: Basis of Aerodynamic Design, Third Edition, John Wiley and Sons, New York, 1976.

6. Minutes of Results Meeting 2 April 1985, Quick Look Report for the MINI SCALE No. 2 Test and Bag Evaluation Test No. 2, Test Directorage, Field Command, Defense Nuclear Agency.

7. Nelson, I., M.L. Baron and I. Sandler, "Mathmatical Models for Geologic Materials for Wave-Propagation Studies," from Mechanical Reports of Solids, J.J. Burke and V. Weis, eds., Syracuse University Press, 1971.

DISTRIBUTION LIST

DEPARTMENT OF DEFENSE

ASST TO THE SECY OF DEFENSE ATOMIC ENERGY
ATTN: EXECUTIVE ASSISTANT

DEFENSE INTELLIGENCE AGENCY
ATTN: DB-4D
ATTN: DT-2
ATTN: RTS-2B

DEFENSE NUCLEAR AGENCY
ATTN: SPAS
ATTN: SPSS
ATTN: SPTD
ATTN: STSP
4 CYS ATTN: STTI-CA

DEFENSE TECHNICAL INFORMATION CENTER
12 CYS ATTN: DD

FIELD COMMAND DNA DET 2
LAWRENCE LIVERMORE NATIONAL LAB
ATTN: FC-1

FIELD COMMAND DEFENSE NUCLEAR AGENCY
ATTN: FCTT W SUMMA
ATTN: FCTXE

JOINT CHIEFS OF STAFF
ATTN: GD50 J-5 FORCE PLNG & PROG DIV
ATTN: J-5 NUC & CHEM DIV
ATTN: JAD/SFD
ATTN: JAD/SSD

UNDER SECY OF DEF FOR RSCH & ENGRG
ATTN: STRAT & SPACE SYS (OS)
ATTN: STRAT & THEATER NUC FOR F VAJDA

DEPARTMENT OF THE ARMY

DEP CH OF STAFF FOR OPS & PLANS
ATTN: DAMO-NCZ

HARRY DIAMOND LABORATORIES
ATTN: SLCHD-NW-P J GWALTNEY

U S ARMY BALLISTIC RESEARCH LAB
ATTN: SLCBR-SS-T TECH LIB

U S ARMY MATERIAL TECHNOLOGY LABORATORY
ATTN: DRXMR-HH J DIGNAM

U S ARMY NUCLEAR & CHEMICAL AGENCY
ATTN: LIBRARY

U S ARMY TRADOC SYS ANALYSIS ACTVY
ATTN: ATAA-TDC R BENSON

US ARMY MISSILE COMMAND
ATTN: AMSMI-RD-DEP W THOMAS
ATTN: AMSMI-RD-UB H GREENE

DEPARTMENT OF THE NAVY

NAVAL RESEARCH LABORATORY
ATTN: CODE 2627 TECH LIB
ATTN: CODE 4650 A WILLIAMS
ATTN: CODE 4770 G COOPERSTEIN

NAVAL SEA SYSTEMS COMMAND
ATTN: SEA-0352 M KINNA

NAVAL WEAPONS EVALUATION FACILITY
ATTN: CLASSIFIED LIBRARY

OFC OF THE DEPUTY CHIEF OF NAVAL OPS
ATTN: NOP 654 STRAT EVAL & ANAL BR

STRATEGIC SYSTEMS PROGRAMS(PM-1)
ATTN: SP-272

DEPARTMENT OF THE AIR FORCE

AERONAUTICAL SYSTEMS DIVISION, AFSC
ATTN: ASD/ENSSS H GRIFFIS

AIR FORCE ROCKET PROPULSION LAB
ATTN: LKCS G BEALE

AIR FORCE SYSTEMS COMMAND
ATTN: SDM
ATTN: XRTO

AIR FORCE WEAPONS LABORATORY, AFSC
ATTN: HO R DUFFNER
ATTN: NTA A SHARP
ATTN: NTES
ATTN: SUL

AIR FORCE WRIGHT AERONAUTICAL LAB
ATTN: FIMG

AIR FORCE WRIGHT AERONAUTICAL LAB
ATTN: AFWAY MLBT W ANSPACH

AIR UNIVERSITY LIBRARY
ATTN: AUL-LSE

DEPARTMENT OF THE AIR FORCE (CONTINUED)

BALLISTIC MISSILE OFFICE/DAA
ATTN: ENSN
ATTN: ENSR
ATTN: MYE

DEPUTY CHIEF OF STAFF/AF-RDQI
ATTN: AF/RDQI

HEADQUARTERS U S AIR FORCE
ATTN: AFXOOTS

DEPARTMENT OF ENERGY

DEPARTMENT OF ENERGY
ATTN: OMA/DP-225

UNIVERSITY OF CALIFORNIA
LAWRENCE LIVERMORE NATIONAL LAB
ATTN: L-125 J KELLER
ATTN: L-262 J KNOX
ATTN: L-8 P CHRZANOWSKI

LOS ALAMOS NATIONAL LABORATORY
ATTN: E548 R S DINGUS
ATTN: MS670 T T SCOLMAN
ATTN: R S THURSTON
ATTN: R W SELDEN

SANDIA NATIONAL LABORATORIES
ATTN: EDUCATION AND TECH LIB DIV
ATTN: H NORRIS

SANDIA NATIONAL LABORATORIES
ATTN: M B COWAN
ATTN: ORG 7112 A CHABAI

OTHER GOVERNMENT

CENTRAL INTELLIGENCE AGENCY
ATTN: OSWR/NED

DEPARTMENT OF DEFENSE CONTRACTORS

ACUREX CORP
ATTN: C NARDO

AEROJET GENERAL CORP
ATTN: A COLLINS

AEROSPACE CORP
ATTN: H BLAES

ANALYTIC SERVICES, INC (ANSER)
ATTN: J SELIG

APTEK, INC
ATTN: T MEAGHER

BOEING CO
ATTN: M/S 17-53 R L DYRDHAL
ATTN: M/S 40-03 A DACOSTA
ATTN: M/S 8R/83 E YORK

BOEING MILITARY AIRPLANE CO
ATTN: MS 75-74 D SAWDY

CALIFORNIA RESEARCH & TECHNOLOGY, INC
ATTN: K KREYENHAGEN

CALSPAN CORP
ATTN: M DUNN
ATTN: M HOLDEN

CARPENTER RESEARCH CORP
ATTN: H J CARPENTER

G B LABORATORY, INC
ATTN: G BURGHART

GENERAL ELECTRIC CO
ATTN: A GARBER
ATTN: B MAGUIRE

HERCULES, INC
ATTN: P MCALLISTER

INSTITUTE FOR DEFENSE ANALYSES
ATTN: CLASSIFIED LIBRARY

KAMAN SCIENCES CORP
ATTN: L MENTE
ATTN: R RUETENIK
ATTN: W LEE

KAMAN SCIENCES CORP
ATTN: F SHELTON
ATTN: J HOFFMAN
ATTN: J KEITH

KAMAN TEMPO
ATTN: DASIAC

KAMAN TEMPO
ATTN: DASIAC

LOCKHEED MISSILES & SPACE CO, INC
ATTN: F BORGARDT

LOCKHEED MISSILES & SPACE CO, INC
ATTN: R WALZ

MARTIN MARIETTA DENVER AEROSPACE
ATTN: E STRAUSS

MCDONNELL DOUGLAS CORP
ATTN: J KIRBY
ATTN: J PECK
ATTN: L COHEN

MCDONNELL DOUGLAS CORP
ATTN: M POTTER

DEPT OF DEFENSE CONTRACTORS (CONTINUED)

MORTON THIOKOL, INC
ATTN: K HESS

NTS ENGINEERING
2 CYS ATTN: D G HONEGGER

PACIFIC-SIERRA RESEARCH CORP
ATTN: H BRODE, CHAIRMAN SAGE

PHYSICS INTERNATIONAL CO
ATTN: J SHEA

R & D ASSOCIATES
ATTN: F A FIELD
ATTN: P RAUSCH

RAND CORP
ATTN: P DAVIS

RAND CORP
ATTN: B BENNETT

S-CUBED
ATTN: G GURTMAN
ATTN: R DUFF

SCIENCE APPLICATIONS INTL CORP
ATTN: J WARNER
ATTN: W PLOWS
ATTN: W YENGST

SCIENCE APPLICATIONS INTL CORP
ATTN: J COCKAYNE
ATTN: W LAYSON

SCIENCE APPLICATIONS INTL CORP
ATTN: A MARTELLUCCI

SCIENCE APPLICATIONS INTL CORP
ATTN: J MANSHIP

SOUTHERN RESEARCH INSTITUTE
ATTN: C PEARS

SRI INTERNATIONAL
ATTN: D CURRAN

TECHNOLOGY DEVELOPMENT ASSOCIATES
ATTN: C HARRELL
ATTN: N DISPENSIERE

TOYON RESEARCH CORP
ATTN: B GRAGG
ATTN: J CUNNINGHAM

TRW ELECTRONICS & DEFENSE SECTOR
ATTN: A ZIMMERMAN
ATTN: D BAER
ATTN: M SEIZEW
ATTN: N LIPNER
ATTN: P BRANDT
ATTN: R BACHARACH
ATTN: R PLEBUCH HARD & SURV LAB
ATTN: W WOOD

TRW ELECTRONICS & DEFENSE SECTOR
ATTN: D KENNEDY
ATTN: E ALLEN
ATTN: E WONG
ATTN: L BERGER
ATTN: N GUILES
ATTN: P DAI
ATTN: V BLANKINSHIP
ATTN: W POLICH

END

DTIC

9-86